

Unveiling the Pathway for the Nuclear Translocation of the Large Mitochondrial Enzyme Pyruvate Dehydrogenase Complex (PDC)

by

Sotirios Zervopoulos

A thesis submitted in partial fulfillment of the requirements for the degree of

Doctor of Philosophy

In

Experimental Medicine

Department of Medicine

University of Alberta

Abstract

Pyruvate dehydrogenase complex (PDC) is a mitochondrial enzyme that links glycolysis to oxidative phosphorylation by decarboxylating glucose-derived pyruvate to produce acetyl-CoA that is used in the Krebs cycle. PDC was initially thought to reside only in the mitochondrial matrix but we recently showed that proliferative stimuli induce its nuclear translocation, where it facilitates cell proliferation by providing acetyl-CoA towards histone acetylation. The mechanism that allows PDC to navigate throughout the cytoplasm and finally enter the nucleus is currently unknown. Protein import into the nucleus occurs through the nuclear pores (NPs) that allow the free diffusion of proteins and small metabolites of molecular weights up to 40 kDa and diameters of ~5 nm. Larger proteins require a nuclear localization sequence (NLS) that is recognized by cargo carriers before crossing the NP. PDC does not have a known NLS and its multimer size and diameter varies from small complexes that could pass through the NP to very large complexes that would not be able to cross the NP. We propose that while smaller PDC can travel (with the help of chaperones) on microtubules and reach the nucleus, entering through the NPs, larger complexes follow a novel (non-canonical) pathway that does not include NPs. Rather, it involves close contact of the mitochondria to the nucleus, allowing entrance, particularly during mitosis, in a manner similar to what is known for large viruses.

Intracellular protein trafficking is carried out by protein carriers, including molecular chaperones, that move along the microtubules and it is facilitated by acetylation of α -tubulin. Organelles like mitochondria also move along acetylated microtubules, and tubulin acetylation may affect their trafficking. Here we show that

stimuli inducing the nuclear translocation of PDC increase its colocalization with Hsp70 and acetyl-tubulin. Increased levels of tubulin acetylation facilitate the nuclear translocation of PDC. PDC can directly associate with acetylated microtubules through its E2 subunit in a manner irrespective of microtubule stability. We also found that loss of PDC but not of the main acetyl-CoA producer in the cytoplasm, ATP citrate lyase (ACLY), decreases tubulin acetylation suggesting that extramitochondrial PDC might also act as a novel tubulin acetyltransferase.

Mitochondria are highly dynamic organelles that constantly span the cytoplasm and tether to the endoplasmic reticulum (ER) via contact points rich in mitofusin 2 (MFN2). The nuclear envelope (NE) is a continuation of the ER sharing many similarities on their protein profile. Here we show that proliferative stimuli induced a perinuclear clustering of mitochondria before we were able to detect any nuclear PDC. Perinuclear mitochondria under a transmission electron microscope formed electron-dense structures with the NE similar to those between mitochondria and the ER. We detected MFN2 on both the NE and the nucleoplasm, suggesting that it can facilitate mitochondrial tethering to the NE in a manner similar to their tethering on the ER. We also show that loss of MFN2 decreased both nuclear PDC levels and mitochondrial tethering onto the NE.

We found that PDC is released from perinuclear mitochondria and interacts with lamin A (LMNA), which is part of the inner nuclear membrane. Loss of LMNA decreased the levels of nuclear PDC, but had no effect on SIRT6, a protein known to reside into the nucleoplasm. We found that extramitochondrial PDC embedded into the LMNA layer was not associated with the NPs. Inhibition of the trafficking through the

NPs by wheat germ agglutinin (WGA) had no effect on the nuclear PDC levels after exposure to proliferative stimuli, but decreased STAT3, a protein known to enter the nucleus via the NPs. The interaction between PDC and LMNA persisted during mitosis, where LMNA is depolymerized and dispersed throughout the cytoplasm before the formation of the daughter nuclei.

We speculate that the tethering of perinuclear mitochondria on the NE and the interaction of PDC with LMNA provides a novel mechanism for PDC to enter the nucleus in a manner that does not involve the NPs. We believe that this is the predominant mechanism for nuclear entry of PDC under proliferative conditions, without excluding some canonical PDC entrance via the NPs of smaller complexes. Our work enhances the concept of mitochondria to nucleus communication and maybe applicable to the entrance of other large proteins or viruses into the nucleus.

Preface

Chapters 2 and 3 are currently in preparation for submission to peer-reviewed journals.

To Dimitra K. Always in my heart.

The poetry that comes from the squaring off between

And the circling is worth it

Finding beauty in the dissonance

Acknowledgements

I would like to express my great appreciation to my supervisor Dr. Evangelos Michelakis, for giving me the opportunity to carry out this project in his lab. His mentorship and continuous guidance shaped me into the man and scientist that I am today. I also want to express my greatest gratitude to my parents, Dimitrios and Olga Zervopoulos for their love and for always believing in me. I would like to thank my colleagues and friends, Adam Kinnaird, Vikram Gurtu, Areli Lorenzana Carillo, Yongneng Zhang and especially Aristeidis Boukouris; without their help I would not had been able to complete this dissertation. Lastly, I would like to thank Alois Haromy for his friendship and help throughout this project.

Table of Contents

<i>Chapter One: Background</i>	1
<i>1.1 Metabolic enzymes in the nucleus</i>	2
<i>1.2 Pyruvate dehydrogenase complex – composition and regulation</i>	3
<i>1.3 Pyruvate dehydrogenase complex in the nucleus</i>	5
<i>1.4 Involvement of pyruvate dehydrogenase complex in disease</i>	6
<i>1.5 Protein and organelle trafficking within the cell</i>	8
<i>1.6 Nucleocytoplasmic transport of proteins</i>	9
<i>1.7 The nuclear envelope and nuclear lamina</i>	11
<i>1.8 Post-translational modifications of nuclear lamins</i>	13
<i>1.9 Interacting partners of nuclear lamins on the NE and the nucleoplasm</i>	13
<i>1.10 Nuclear lamins in disease</i>	15
<i>Chapter Two: Extramitochondrial PDC translocates into the nucleus via acetylated microtubules and it is involved in the process of tubulin acetylation</i>	40
<i>Abstract</i>	41
<i>2.1 Introduction</i>	43
<i>Results</i>	45
<i>2.2 Proliferative stimuli induce the colocalization of extramitochondrial PDC with Hsp70 and acetylated microtubules</i>	45
<i>2.3 PDC interacts with acetylated tubulin directly via its E2 subunit</i>	47
<i>2.4 Extramitochondrial PDC regulates tubulin acetylation during its nuclear translocation</i>	50
<i>2.5 Loss of tubulin acetylation decreases nuclear PDC levels</i>	51
<i>2.6 Increased tubulin acetylation results in a faster translocation of PDC into the nucleus</i>	52
<i>2.7 Discussion</i>	54
<i>2.8 Materials and methods</i>	59
<i>Chapter three: A non-canonical pathway for the entrance of the large mitochondrial enzyme Pyruvate Dehydrogenase Complex (PDC) into the nucleus</i>	95
<i>Abstract</i>	96
<i>3.1 Introduction</i>	98

<i>Results</i>	<i>100</i>
<i>3.2 Mitochondria cluster around the nucleus and tether on the nuclear envelope, following proliferation stimuli.....</i>	<i>100</i>
<i>3.3 Mitofusin 2 (MFN2) tethers mitochondria onto the nuclear envelope (NE) ..</i>	<i>101</i>
<i>3.4 PDC is released from nucleus-tethered mitochondria and deposited on the lamin layer, before entering the nucleus.....</i>	<i>104</i>
<i>3.5 PDC enters the nucleus independently of nuclear pores (NPs).....</i>	<i>108</i>
<i>3.6 Discussion</i>	<i>110</i>
<i>3.7 Materials and methods.....</i>	<i>115</i>
<i>Chapter four: Final conclusions and future directions</i>	<i>158</i>
<i>4.1 Overall conclusions.....</i>	<i>159</i>
<i>4.2 Future directions.....</i>	<i>162</i>
<i>Bibliography.....</i>	<i>170</i>
<i>Appendix I: Antibodies used in this dissertation</i>	<i>195</i>
<i>Appendix II: Macros for image analysis with FIJI.....</i>	<i>197</i>

Table of Figures and tables

Fig. 1-1 The oxidation of pyruvate to acetyl-CoA by PDC	16
Fig. 1-2 PDC translocates into the nucleus upon exposure to various proliferative stimuli including mitochondrial stress, serum and EGF, where it produces acetyl-CoA that is used towards histone acetylation.....	17
Table 1 Proteins that bind to LMNA through its Ig domain.....	18
Fig. 2-1 PDC can be found outside the mitochondria as a whole complex while translocating into the nucleus	66
Fig. 2-2 Extramitochondrial PDC is localized on acetylated microtubules while translocating into the nucleus	68
Fig. 2-3 Extramitochondrial PDC colocalizes with both acetylated microtubules and Hsp70	69
Fig. 2-4 Proliferative stimuli increase the colocalization of extramitochondrial PDC with acetylated microtubules.....	71
Fig. 2-5 Proliferative stimuli increase the association of extramitochondrial PDC with acetylated microtubules	72
Fig. 2-6 PDC interacts directly with acetylated tubulin via its E2 subunit	74
Fig. 2-7 Binding of PDC onto microtubules is regulated by tubulin acetylation and not the stability of the microtubule network.....	76
Fig. 2-8 Tubulin acetylation peaks after two hours of exposure to serum and EGF	77
Fig. 2-9 Loss of PDC decreases tubulin acetylation.....	79
Fig. 2-10 Loss of tubulin acetylation decreases nuclear PDC and acetyl-histone 3 levels	81
Fig. 2-11 Tubacin increases tubulin acetylation.....	82
Fig. 2-12 Increased tubulin acetylation results in a faster and more efficient nuclear translocation of PDC	84
Fig. 2-13 Proposed model for the nuclear translocation of PDC along acetylated microtubules	85
Fig. 3-1 Mitochondria cluster around the nucleus in response to proliferative stimuli and form electron dense areas with the NE	127
Fig. 3-2 Proliferative stimuli increase nuclear PDC levels and perinuclear mitochondrial clustering	129
Fig. 3-3 MFN2 is between perinuclear mitochondria and the NE.....	131
Fig. 3-4 MFN2 is present on the NE	133
Fig. 3-5 Mitochondria tether to the NE via MFN2-rich contact points	135
Fig. 3-6 Extramitochondrial PDC colocalizes with LMNA on the NE.....	136
Fig. 3-7 PDC interacts with LMNA.....	138
Fig. 3-8 Perinuclear mitochondria release PDC into the nucleoplasm	140

Fig. 3-9 Perinuclear mitochondria release PDC into the nucleoplasm in response to hypoxia 141
Fig. 3-10 All PDC subunits can be found within nuclear invaginations that are increased after exposure to proliferative stimuli 143
Fig. 3-11 LMNA is necessary for the nuclear entrance of PDC 145
Fig. 3-12 PDC does not enter the nucleus through the nuclear pore..... 147
Fig. 3-13 PDC interacts with LMNA during cell division 150

List of Abbreviations

ACLY – ATP citrate lyase
AFU – Arbitrary fluorescent units
ATP – Adenosine triphosphate
BAF – Barrier of autointegration
Cdk1 – Cyclin dependent kinase 1
DNA – Deoxyribonucleic acid
DSS – Disuccinimidyl suberate
E3BP – E3 binding protein
EGF – Epidermal growth factor
EM – Electron microscopy
ER – Endoplasmic reticulum
FADH – Flavin adenine dinucleotide
FG repeats – Phenylalanine glycine repeats
GTP – Guanosine triphosphate
HDAC6 – Histone deacetylase 6
HGPS – Hutchinson’s Gilford progeria syndrome
Hsp70 – Heat shock protein 70
kDa – Kilodalton
LEM domain – LAP2 Emerin MAN1 domain
LMNA – Lamin A
LMNB1 – Lamin B1
LMNB2 – Lamin B2
MDa – Megadalton
MDVs – Mitochondrial-derived vesicles
MFN2 – Mitofusin 2
MLS – Mitochondrial localization sequence
MOF – Ortholog of Drosophila males absent on the first
NADH₂ – Nicotinamide adenine dinucleotide
NE – Nuclear envelope
NLS – Nuclear localization sequence

NP – Nuclear pore
nPDC – Nuclear PDC
PBC – Primary biliary cirrhosis
PCG – Polycomb group of proteins
PDC – Pyruvate dehydrogenase
PDK – Pyruvate dehydrogenase kinase
PDP – Pyruvate dehydrogenase phosphatase
PKM2 – Pyruvate kinase isoform 2
PLA – Proximity ligation assay
SDHB – Succinate dehydrogenase B
Ser – Serine
shRNA – Short hairpin ribonucleic acid
siRNA – Short interfering ribonucleic acid
SIRT2 – Sirtuin 2
SIRT6 – Sirtuin 6
STAT3 – Signal transducer and activator of transcription 3
STAT5 – Signal transducer and activator of transcription 5
TCA cycle – Tricarboxylic acid cycle
TOM20 – Mitochondrial import receptor subunit TOM20 homolog
VDAC – Voltage-dependent anion channel
WGA – Wheat germ agglutinin
WNT – Wingless and Int-1
ZMPSTE24 – Zinc metalloproteinase STE24
 α TAT1 – α -Tubulin N-acetyltransferase 1
 $\Delta\psi_m$ – Mitochondrial membrane potential

Chapter One: Background

1.1 Metabolic enzymes in the nucleus

Metabolism is the summary of chemical and enzymatic reactions that occur in our bodies to provide energy and the necessary building blocks for sustaining life. Most of these reactions occur in distinct cellular compartments, i.e. the cytoplasm (e.g. glycolysis) or the mitochondria (e.g. TCA cycle and oxidative phosphorylation). The majority of these reactions are carried out by specialized enzymes that are collectively known as metabolic enzymes. Nowadays, it is known that a large number of these enzymes can translocate into the nucleus, where they exert either their canonical or non-canonical functions (reviewed in ¹). The nuclear translocation of these enzymes suggests that their role in the cell is far more complex than what we once thought and paves the way for exciting discoveries in the years to come.

All glycolytic enzymes, that once perceived as strictly cytoplasmic, have been found to be present and active in the nucleus since the late 1950s^{2,3} but the purpose and stimuli that induce their nuclear translocation remain unknown for most of them. One exception is pyruvate kinase M2 (PKM2), which plays a major role in cancer progression and tumorigenesis. Nuclear PKM2 can alter gene expression either directly as a transcription factor or indirectly by promoting histone phosphorylation by using phosphoenolpyruvate and producing ATP and pyruvate (canonical function)⁴⁻⁷. Pyruvate can then be converted to various metabolites that affect gene transcription by altering histone post-translational modifications⁸.

Mitochondria are central organelles to metabolism and the energy production process since two of the main metabolic pathways occur in their matrix and inner membrane, i.e. the Krebs cycle and oxidative phosphorylation respectively⁹. Like

glycolytic enzymes, most of the mitochondrial enzymes that translocate into the nucleus participate in various aspects of controlling gene transcription either by acting as members of transcription activating complexes or through their end products that can alter DNA and histone post-translational modifications e.g. histone or DNA methylation via alpha-ketoglutarate and histone acetylation via acetyl-CoA respectively¹. Interestingly enough, one of the largest enzymes of the cell, pyruvate dehydrogenase complex (PDC), has also been found to translocate into the nucleus, where it contributes to the nuclear pool of acetyl-CoA¹⁰.

1.2 Pyruvate dehydrogenase complex – composition and regulation

PDC is a conserved enzymatic complex that can be found in different organisms ranging from prokaryotes to eukaryotes. The prokaryotic form of PDC includes three main subunits, the E1, the E2 and the E3 subunit, while the mammalian PDC includes a fourth subunit known as the E3 binding protein (E3BP)¹¹. In mammals, PDC resides in the mitochondria and is considered to be a gatekeeping enzyme that links glycolysis to the TCA cycle⁹. PDC catalyzes the conversion of glucose-derived pyruvate towards CO₂, acetyl-CoA and NADH (H⁺) (**Fig 1-1**)¹². The E1 subunit is a heterodimer of E1 α and E1 β and is known as pyruvate dehydrogenase. The function of this subunit depends on thiamine phosphate and catalyzes two reactions **a**) the decarboxylation of pyruvate to CO₂ and **b**) the reductive acetylation of the lipoyl groups of the E2 subunit. The E2 subunit is known as dihydrolipoamide acetyltransferase and adds the acetyl-group to a CoA-SH molecule. The E3 subunit is known as dihydrolipoamide dehydrogenase (E3)

and reoxidizes the lipoamide of E2 by generating FADH¹¹. In mammals, the E3BP facilitates the binding of all subunits to E2, which forms the core of the complex¹¹.

The exact organization of the complex in mammals is unknown. There are currently two proposed models trying to describe it: **i)** the addition model, where the core of the complex comprises of 60 copies of E2 binding to 12 copies of E3BP¹³ and **ii)** the substitution model, where the core is comprised of 40 copies of E2 and 12 of E3BP¹⁴ or 40 copies of E2 and 20 of E3BP¹⁵. The stoichiometry and organization of the individual subunits that result in the final form of the complex makes PDC one of the largest complexes within the cell with molecular weights ranging from 1-10^{16,17} and diameters from 25-45 nm¹⁶⁻¹⁸.

The regulation of PDC occurs mainly through phosphorylation of Ser²³², Ser²⁹³ and Ser³⁰⁰ of the E1 subunit^{19,20}. The addition of a phosphate group to these serines is mediated by pyruvate dehydrogenase kinase (PDK) and results in the inhibition of the complex. Mammals express four PDK isoforms that are tissue-specific, except PDK2, which is expressed ubiquitously²¹. Removal of the phosphate group is mediated by the pyruvate dehydrogenase phosphatase (PDP)¹¹. Mammals express only two PDP isoforms. Both PDK and PDP are binding to the lipoyl-domains of the E2 subunits of the complex before they exert their function. Other factors that can also activate PDC is pyruvate, while it can be inhibited by high levels of acetyl-CoA. Moreover, PDC, along with other mitochondrial enzymes, is calcium dependent²².

1.3 Pyruvate dehydrogenase complex in the nucleus

PDC was found to translocate into the nucleus as a whole complex upon exposure to various proliferative stimuli e.g. serum stimulation, exposure to epidermal growth factor (EGF) and mitochondrial stress (e.g. rotenone). Nuclear PDC carries out its canonical function, i.e. producing acetyl-CoA from pyruvate that is used towards histone acetylation affecting the progression of the cell cycle¹⁰ (**Fig. 1-2**). More importantly, PDK, the main inhibitor of PDC, did not translocate into the nucleus along with the whole complex¹⁰, suggesting that nuclear PDC is either constantly active or it is regulated via other mechanisms that might include already known nuclear kinases.

All the subunits of PDC, like all mitochondrial proteins that are transcribed in the nucleus, contain a mitochondrial localization sequence (MLS) that targets them to the mitochondria and are partially folded as precursor proteins²³. Once they enter the mitochondria they are being processed by the mitochondrial protein peptidase that cleaves the MLS and are folded properly by the action of mitochondrial chaperones like the mitochondrial heat shock protein 70, also known as mortalin²³. This suggests that PDC has to first enter the mitochondria and be fully assembled before it translocates into the nucleus as a whole complex. The exact mechanism for PDC's translocation into the nucleus is currently unknown, except that it mediated by the molecular chaperone heat shock protein 70 (Hsp70)¹⁰, which has been previously found to act as a carrier of proteins that enter the nucleus²⁴. Identification of this pathway will expand our current knowledge on how mitochondrial proteins enter the nucleus and how they contribute to the mito-nuclear communication that plays an important role in critical cell decisions, like apoptosis, proliferation and cell differentiation.

Recent work has showed that nuclear PDC can form a complex with PKM2 upon activation of the aryl-hydrocarbon receptor and induces the expression of certain genes. As part of that complex, PKM2 produces pyruvate from phosphoenolpyruvate and PDC produces acetyl-CoA that is used for histone acetylation by the acetyltransferase p300⁷. Another group found that nuclear PDC plays a major role in zygote formation by increasing histone acetylation and facilitating genomic activation of the human embryo²⁵. PDC has also been found to play a role in adipocyte signaling by forming complexes with STAT5 into the nucleus and initiating downstream signaling cascades²⁶ as well as maintaining lipogenesis in renal cancer²⁷. Lastly, nuclear PDCE2 levels have also been found to be elevated and identified as a potential target for therapy of acute liver failure²⁸.

1.4 Involvement of pyruvate dehydrogenase complex in disease

PDC has been shown to be involved in various human diseases with different clinical manifestations but the most prominent of them is a lethal disease known as PDC deficiency, where the whole complex is dysfunctional due to indels or missense mutations in one of its individual subunits. In most cases, patients with this deadly disease have a dysfunctional E1 α subunit due to indels that affect mostly females and occur preferentially in exons 10 and 11 or missense mutations that can be found on all exons²⁹⁻³¹. There are 37 missense mutations that have been documented so far, where some of the most common ones were found in exons 3, 7, 8 and 11²⁹. The symptoms of PDC deficiency range from lactic acidosis to chronic neurologic dysfunction that is not associated with systemic acidosis^{32,33}.

Pulmonary arterial hypertension is a disease that manifests as thickening of the pulmonary artery resulting in increased pulmonary vascular resistance and finally to right ventricular failure³⁴. It has been shown that PDC is inactivated in the endothelial cells of the patients and its activation via inhibition of PDK through treatment with dichloroacetate, a small drug inhibitor, has significantly improved their survival³⁵.

Another deadly disease that PDC plays a central role is cancer. Cancer cells show increased glycolysis and decreased oxidative phosphorylation due to mitochondrial inhibition that is associated with hyperpolarization (i.e. increased mitochondrial membrane potential, $\Delta\psi_m$) due to inhibition of the mitochondrial voltage dependent anion channel (VDAC) by a phosphorylated form of hexokinase 2³⁶. Moreover, cancer cells show decreased mitochondrial PDC activity due to its phosphorylation by PDK, which further contributes to mitochondrial hyperpolarization and the increased glycolytic phenotype³⁷. A small clinical trial showed that activation of PDC by dichloroacetate resulted in mitochondrial depolarization and increased apoptosis in cancer cells; prolonging the survival of patients with glioblastoma, an aggressive type of brain cancer^{38,39}.

Primary biliary cirrhosis (PBC) is a chronic cholestatic liver disease that destroys the small intrahepatic bile ducts and can lead to cirrhosis through various complications⁴⁰. Patients with PBC have high titer of antimitochondrial antibodies in their serum. These antibodies target a specific family of mitochondrial enzymes including the E3BP subunit of PDC and a family of enzymes termed 2-oxo-acid dehydrogenase complexes that include PDCE2^{41,42}. The cause of the disease as well as

why immune cells react to these particular mitochondrial enzymes is currently unknown.

1.5 Protein and organelle trafficking within the cell

A plethora of proteins and organelles are being trafficked or are in constant movement at any given time within the cell. Most of the intracellular trafficking occurs on the cytoskeleton and more importantly on the actin and microtubule networks⁴³. Microtubules are dynamic polymers that consist of heterodimers of α - and β - tubulin and are undergoing several polymerization and depolymerization events during the cell cycle (reviewed in ⁴⁴). The main carrier proteins that are mediating the majority of the cytoplasmic protein and organelle trafficking through microtubules belong to the superfamilies of dyneins (responsible for retrograde trafficking i.e. towards the nucleus)⁴⁵ and kinesins (responsible for anterograde trafficking i.e. away from the nucleus)⁴⁶. These proteins bind to their cargo and propelled along microtubules via a sophisticated cycle that involves GTP hydrolysis⁴⁷.

Even though dyneins and kinesins are the main cargo carriers within the cell, there are other carrier proteins that also use microtubules to reach their destination within the cell. One of them is the heat shock protein (Hsp) family, the members of which play an important role in heat-shock induced stress, protein folding and intracellular trafficking⁴⁸. A well-studied example is the nuclear translocation of the glucocorticoid receptor, which upon activation forms a complex with Hsp70 and Hsp90 and enters the nucleus by using the microtubule network^{49,50}. The nuclear translocation of the glucocorticoid receptor has been associated with increased acetylation of α -tubulin on

K40, a post-translational modification that has been shown to facilitate motor protein binding on the microtubules and enhance intracellular trafficking^{51,52}.

Microtubules mediate the intracellular trafficking of various organelles, like mitochondria and the endoplasmic reticulum⁵³⁻⁵⁵, and proteins. One example is HIF-1 α , the master regulator of hypoxic response, which translocates into the nucleus upon establishment of hypoxia via acetylated microtubules⁵⁶. Another example is the tumour suppressor p53 that translocates into the nucleus upon induction of DNA damage also in a microtubule-dependent manner⁵⁷. Moreover, the microtubule network is also exploited by certain viruses as a means to reach the nucleus before they start replicating themselves^{58,59}. All these examples highlight the importance of an intact microtubule network in intracellular trafficking.

The recent discovery of mitochondrial-derived vesicles (MDVs) offers a novel pathway for intracellular protein trafficking that is exclusive to mitochondria⁶⁰. In this work, the authors showed that oxidized mitochondrial proteins can be encapsulated into double membrane vesicles budding off from the mitochondria and translocate into the late endosome, where they are degraded^{60,61}. Among these proteins the authors detected PDC⁶¹ but they were not able to detect its final destination or if the MDVs use microtubules to navigate through the cytoplasm.

1.6 Nucleocytoplasmic transport of proteins

The nuclear import and export of proteins occurs mainly through the nuclear pore complexes (NPs)⁶². NPs are highly conserved megacomplexes that penetrate the nuclear envelope with a total mass that can reach up to 120 MDa in mammals^{63,64}. The

NPs consist of more than one hundred proteins and are comprised of three distinct components: **a)** the cytoplasmic ring, **b)** the central ring and **c)** the nucleoplasmic basket. The central ring consists of various nucleoporins that contain phenylalanine-glycine (FG) repeats that play a central role in trafficking of proteins through the central channel of the NP^{65,66}. The assembly and proper positioning of the NPs has been found to be regulated by nuclear lamins⁶⁷.

NPs allow for the passive diffusion of small proteins and metabolites with molecular weights of up to 40 kDa or a diameter around 5 nm⁶⁸. Proteins with larger diameters (of up to 39 nm⁶⁹) and molecular weights (more than 40 kDa) are crossing the NP via assisted transport through association with specialized protein carriers known as importins⁷⁰. Importins recognize and bind to certain amino acid sequences of proteins that are destined to enter the nucleus known as nuclear localization sequences (NLS)⁷¹. Except from nuclear import, importins are also facilitating the exit of proteins from the nucleus through a sophisticated mechanism, where the small GTPase Ran-GTPase binds to them and facilitates their nuclear export in the expense of a GTP molecule. Once outside of the nucleus, Ran-GTPase dissociates from the importin that releases its cargo into the cytoplasm⁷².

Not all proteins that enter the nucleus contain a known NLS. One example is beta-catenin that upon activation of the WNT signaling pathway enters the nucleus in an NLS-independent manner⁷³. This also applies to the majority of the metabolic enzymes that translocate into the nucleus, including PDC. Moreover, the large molecular weight and diameter of PDC further prohibits it from entering the nucleus through the nuclear

pore due to size exclusion. This suggests that it might be another yet undiscovered mechanism that PDC uses to enter the nucleus.

1.7 The nuclear envelope and nuclear lamina

The nucleus is surrounded by two lipid double membranes known as the nuclear envelope (NE)⁷⁴ that separate the cytoplasm from the nucleoplasm. The NE consists of the outer and inner nuclear membranes and shares many similarities with the rough ER, since its outer membrane is a continuation of it⁷⁵. The proteins attached to the NE are involved in diverse cellular functions, including mechanotransduction, initiation of various signaling cascades, nuclear positioning and genomic organization⁷⁶. The NE also hosts the NPs that are scattered on its surface and are formed on areas where the outer and inner nuclear membranes merge⁶⁴.

Underneath the NE lies a layer known as nuclear lamina consisting of lamins that are classified as type V intermediate filaments^{77,78}. Mammals have two types of lamins known as A- and B-type. A-type lamins consist of lamin A and C that are produced from alternative splicing of the LMNA gene and are expressed on differentiated cells. Some vertebrates express two less abundant isoforms of A-type lamins known as A Δ 10 and C2 that are also products of alternative splicing of the same gene^{79,80}. B-type lamins consist of lamin B1 and lamin B2 that are transcribed from the LMNB1 and LMNB2 genes respectively and are ubiquitously expressed in all cells (reviewed in ⁸¹). The LMNB2 gene also encodes for a testis-specific isotype known as lamin B3, which is a product of alternative splicing⁸².

All nuclear lamins, except lamin C, undergo farnesylation and carboxymethylation shortly after their synthesis. These modifications are thought to facilitate targeting to the inner nuclear membrane⁸³⁻⁸⁶. The farnesylated site of lamins A, B1 and B2 is the CaaX domain of their C terminus, where C is a cysteine, a is any aliphatic residue and X is generally methionine. After incorporation into the nuclear lamina, lamin A undergoes further processing by the zinc metalloproteinase Ste 24 homolog (ZMPSTE24)⁸⁷ that cleaves the last 15 amino acids including the farnesylated C terminus. This second modification occurs only on lamin A and is part of its maturation process.

All nuclear lamins consist of a small stretch of amino acids known as the head domain, which is followed by a central rod domain that contains four coiled-coil regions (1A, 1B, 2A and 2B)^{88,89}. This domain increases the stability of the lamin network by facilitating lateral interactions between lamin polymers. Downstream of the rod-domain lies a nuclear localization sequence (NLS) and a beta immunoglobulin-like (Ig-like) domain⁹⁰. Ig-like domains have been described to facilitate protein - protein interactions⁹¹ and it is now known that many of the interacting partners of lamins bind to that domain (**Table 1**)⁹².

The stoichiometry of lamins on the nuclear lamina has been suggested to affect nuclear rigidity. In fact, it was shown recently that migrating cells have low lamin A to B ratio, which was associated with softer nuclei that were able to fit through narrow openings during cell migration⁹³. On the contrary, an increased lamin A to B ratio was associated with more rigid nuclei, highlighting the importance of lamin A on nuclear stability.

1.8 Post-translational modifications of nuclear lamins

Lamins undergo various post-translational modifications during the cell cycle, including phosphorylation, methylation, acetylation and SUMOylation⁹⁴. The most important among them is the cell cycle dependent phosphorylation of Ser-22 (lamin A/C), Ser-23 (lamin B1) and Ser-37 (lamin B2) by cyclin dependent kinase 1 (cdk1). The phosphorylation of these serines promotes the depolymerization of nuclear lamins and eventually the disassembly of the nuclear envelope that precedes cell division⁹⁵⁻⁹⁷. Upon depolymerization, lamin A/C is dispersed throughout the cytoplasm and remains there until its dephosphorylation that promotes its reassembly on the nuclear envelope of the daughter cells.

Lamin A was found to be acetylated in various lysine residues by a mass-spectrometry study but the effect of this post-translational modification remains unknown. Recent evidence suggests that lamin A acetylation is associated with increased stability of the nuclear envelope and it might have implications on various diseases that include defects of the nuclear lamina^{98,99}. MOF is the only acetyltransferase that has been associated with the acetylation of a specific lysine residue of lamin A (K311) to date⁹⁸. However, since more than one lysine residues of lamin A appear to be acetylated it is tempting to speculate that MOF might not be the only lamin A acetyltransferase.

1.9 Interacting partners of nuclear lamins on the NE and the nucleoplasm

Lamins are known to interact with other lamins of the same type in the nuclear periphery that allows them to form the nuclear lamina network underlying the NE.

Moreover, they can also interact with lamins of different types through their rod domain facilitating the positioning of various proteins that reside on the NE, including the NPs^{100,101}. Once the lamin network is fully assembled lamins can interact with a plethora of other proteins and DNA (or histones) either directly or indirectly (reviewed in ⁹²). Indirect binding of lamins with histones is mediated mostly through association with proteins containing a LEM (Lap, Emerin and MAN) domain¹⁰² that can subsequently bind to a conserved metazoan factor known as barrier to autointegration (BAF) that binds directly to histones¹⁰³. Moreover, it has been reported that lamins contain a LEM-like domain on their C terminus that allows them to bind directly to certain DNA sequences^{104,105}.

Lamin A is the only member of the lamin family that has been found in the nucleoplasm, where it interacts with various proteins including retinoblastoma and RNA polymerase II^{106,107} that are known to play an important role in the regulation of the cell cycle¹⁰⁸. It has also been suggested that nucleoplasmic lamin A can form complexes with proteins that can repress gene transcription, like the polycomb group of proteins (PCG) that promotes heterochromatin formation via histone methylation^{109,110}.

Nucleoplasmic lamin A has been suggested to form a network similar to the cytoskeleton in the cytoplasm¹¹¹⁻¹¹³. Even though the function of this network is poorly understood it has been proposed to facilitate the formation of microdomains, where lamin A associates with other proteins that can potentially regulate chromatin organization and gene expression¹¹³. Therefore, it is tempting to speculate that such

nucleoplasmic lamin microdomains might offer a platform where various proteins bind to and regulate different nuclear processes, including histone acetylation.

1.10 Nuclear lamins in disease

Mutations in nuclear lamins or proteins that associate with them result in a wide spectrum of diseases known as laminopathies (reviewed in ¹¹⁴). Laminopathies can be categorized based on their phenotype as **a)** striated muscle diseases (e.g. dilated cardiomyopathy), **b)** lipodystrophy syndromes (e.g. Dunnigan-type familial partial lipodystrophy), **c)** peripheral nerve disorders (e.g. Charcot-Marie-Tooth disease), **d)** bone diseases (e.g. Buschke-Ollendorf syndrome) and **e)** accelerated aging disorders (e.g. Hutchinson-Gilford progeria syndrome).

A well-studied laminopathy is the Hutchinson-Gilford progeria syndrome (HGPS), where a *de novo* silent mutation in the position 608 of lamin A results in a cryptic splicing site and the transcription of progerin¹¹⁵. Progerin, is a truncated form of lamin A that lacks the binding site of ZMPSTE24, resulting in a permanently farnesylated product that eventually leads to NE distortion. Patients affected from HGPS usually die in their second to third decade of life mostly by heart-related issues¹¹⁶.

Alterations in nuclear lamin expression have also been associated with cancer progression due to the highly dysmorphic nuclei that characterize the disease¹¹⁷. Altered lamin ratios between the different types of lamins in cancer have been suggested to participate in genomic instability that is a hallmark of cancer¹¹⁸.

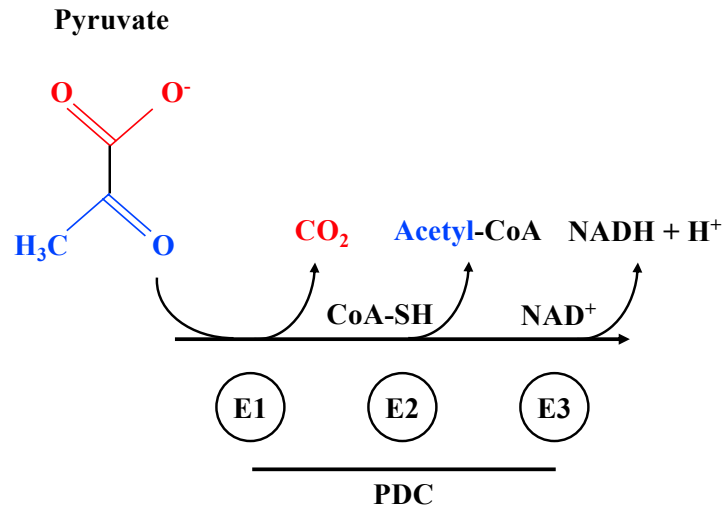


Fig. 1-1 The oxidation of pyruvate to acetyl-CoA by PDC.

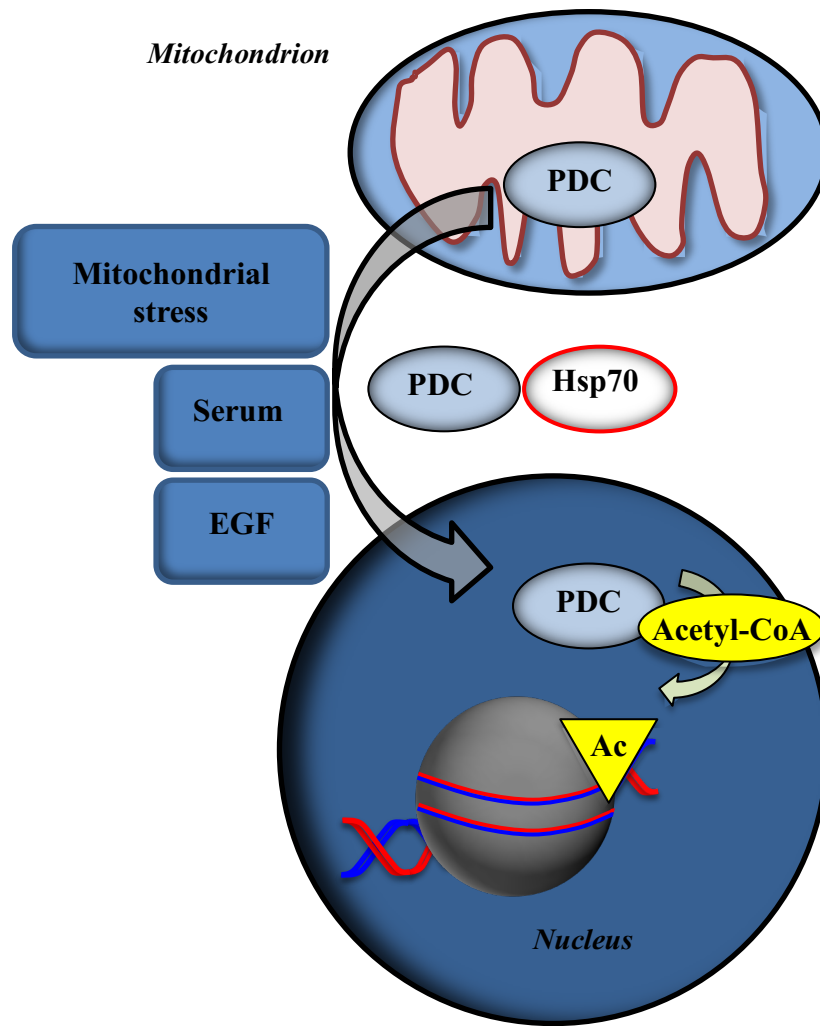


Fig. 1-2 PDC translocates into the nucleus upon exposure to various proliferative stimuli including mitochondrial stress, serum and EGF, where it produces acetyl-CoA that is used towards histone acetylation. PDC's entrance into the nucleus is facilitated by the molecular chaperone Hsp70.

Table 1 Proteins that bind to LMNA through its Ig domain

Protein	Reference
F-Actin	119
Titin	120
Nesprin 2	121,122
LCO1	123
SUN1	124
SUN2	125
Nup153	126
Nup88	127
Lap2 α	128
MAN1	129
LEM2	130
Emerin	131,132
PCNA	133
DNA	134
SREBP1 a/c	135
PKC α	136
NARF	137

References

- 1 Boukouris, A. E., Zervopoulos, S. D. & Michelakis, E. D. Metabolic Enzymes Moonlighting in the Nucleus: Metabolic Regulation of Gene Transcription. *Trends Biochem Sci* **41**, 712-730, doi:10.1016/j.tibs.2016.05.013 (2016).
- 2 McEwen, B. S., Allfrey, V. G. & Mirsky, A. E. Studies on Energy-yielding Reactions in Thymus Nuclei : III. PARTICIPATION OF GLYCOLYSIS AND THE CITRIC ACID CYCLE IN NUCLEAR ADENOSINE TRIPHOSPHATE SYNTHESIS. *J Biol Chem* **238**, 2579-2586 (1963).
- 3 Siebert, G. & Humphrey, G. B. Enzymology of the nucleus. *Adv Enzymol Relat Areas Mol Biol* **27**, 239-288 (1965).
- 4 Yang, W. *et al.* PKM2 phosphorylates histone H3 and promotes gene transcription and tumorigenesis. *Cell* **150**, 685-696, doi:10.1016/j.cell.2012.07.018 (2012).
- 5 Dayton, T. L., Jacks, T. & Vander Heiden, M. G. PKM2, cancer metabolism, and the road ahead. *EMBO Rep* **17**, 1721-1730, doi:10.15252/embr.201643300 (2016).
- 6 Vander Heiden, M. G. *et al.* Evidence for an alternative glycolytic pathway in rapidly proliferating cells. *Science* **329**, 1492-1499, doi:10.1126/science.1188015 (2010).
- 7 Matsuda, S. *et al.* Nuclear pyruvate kinase M2 complex serves as a transcriptional coactivator of arylhydrocarbon receptor. *Nucleic Acids Res* **44**, 636-647, doi:10.1093/nar/gkv967 (2016).

- 8 Fan, J., Krautkramer, K. A., Feldman, J. L. & Denu, J. M. Metabolic regulation of histone post-translational modifications. *ACS Chem Biol* **10**, 95-108, doi:10.1021/cb500846u (2015).
- 9 Berg, J. M., Tymoczko, J. L., Stryer, L., & Stryer, L. *Biochemistry*. 7th edn, (New York: W.H. Freeman, 2002).
- 10 Sutendra, G. *et al.* A nuclear pyruvate dehydrogenase complex is important for the generation of acetyl-CoA and histone acetylation. *Cell* **158**, 84-97, doi:10.1016/j.cell.2014.04.046 (2014).
- 11 Patel, M. S., Nemeria, N. S., Furey, W. & Jordan, F. The pyruvate dehydrogenase complexes: structure-based function and regulation. *J Biol Chem* **289**, 16615-16623, doi:10.1074/jbc.R114.563148 (2014).
- 12 Patel, M. S. & Roche, T. E. Molecular biology and biochemistry of pyruvate dehydrogenase complexes. *FASEB J* **4**, 3224-3233, doi:10.1096/fasebj.4.14.2227213 (1990).
- 13 Sanderson, S. J., Miller, C. & Lindsay, J. G. Stoichiometry, organisation and catalytic function of protein X of the pyruvate dehydrogenase complex from bovine heart. *Eur J Biochem* **236**, 68-77, doi:10.1111/j.1432-1033.1996.00068.x (1996).
- 14 Hiromasa, Y., Fujisawa, T., Aso, Y. & Roche, T. E. Organization of the cores of the mammalian pyruvate dehydrogenase complex formed by E2 and E2 plus the

- E3-binding protein and their capacities to bind the E1 and E3 components. *J Biol Chem* **279**, 6921-6933, doi:10.1074/jbc.M308172200 (2004).
- 15 Brautigam, C. A., Wynn, R. M., Chuang, J. L. & Chuang, D. T. Subunit and catalytic component stoichiometries of an in vitro reconstituted human pyruvate dehydrogenase complex. *J Biol Chem* **284**, 13086-13098, doi:10.1074/jbc.M806563200 (2009).
- 16 Sumegi, B., Liposits, Z., Inman, L., Paull, W. K. & Srere, P. A. Electron microscopic study on the size of pyruvate dehydrogenase complex in situ. *Eur J Biochem* **169**, 223-230, doi:10.1111/j.1432-1033.1987.tb13601.x (1987).
- 17 Zhou, Z. H., McCarthy, D. B., O'Connor, C. M., Reed, L. J. & Stoops, J. K. The remarkable structural and functional organization of the eukaryotic pyruvate dehydrogenase complexes. *Proc Natl Acad Sci U S A* **98**, 14802-14807, doi:10.1073/pnas.011597698 (2001).
- 18 Zhou, Z. H. *et al.* Direct evidence for the size and conformational variability of the pyruvate dehydrogenase complex revealed by three-dimensional electron microscopy. The "breathing" core and its functional relationship to protein dynamics. *J Biol Chem* **276**, 21704-21713, doi:10.1074/jbc.M101765200 (2001).
- 19 Korotchkina, L. G. & Patel, M. S. Site specificity of four pyruvate dehydrogenase kinase isoenzymes toward the three phosphorylation sites of human pyruvate dehydrogenase. *J Biol Chem* **276**, 37223-37229, doi:10.1074/jbc.M103069200 (2001).

- 20 Teague, W. M., Pettit, F. H., Wu, T. L., Silberman, S. R. & Reed, L. J. Purification and properties of pyruvate dehydrogenase phosphatase from bovine heart and kidney. *Biochemistry* **21**, 5585-5592, doi:10.1021/bi00265a031 (1982).
- 21 Bowker-Kinley, M. M., Davis, W. I., Wu, P., Harris, R. A. & Popov, K. M. Evidence for existence of tissue-specific regulation of the mammalian pyruvate dehydrogenase complex. *Biochem J* **329 (Pt 1)**, 191-196, doi:10.1042/bj3290191 (1998).
- 22 Denton, R. M. Regulation of mitochondrial dehydrogenases by calcium ions. *Biochim Biophys Acta* **1787**, 1309-1316, doi:10.1016/j.bbabi.2009.01.005 (2009).
- 23 Schmidt, O., Pfanner, N. & Meisinger, C. Mitochondrial protein import: from proteomics to functional mechanisms. *Nat Rev Mol Cell Biol* **11**, 655-667, doi:10.1038/nrm2959 (2010).
- 24 Shi, Y. & Thomas, J. O. The transport of proteins into the nucleus requires the 70-kilodalton heat shock protein or its cytosolic cognate. *Mol Cell Biol* **12**, 2186-2192, doi:10.1128/mcb.12.5.2186 (1992).
- 25 Nagaraj, R. *et al.* Nuclear Localization of Mitochondrial TCA Cycle Enzymes as a Critical Step in Mammalian Zygotic Genome Activation. *Cell* **168**, 210-223 e211, doi:10.1016/j.cell.2016.12.026 (2017).
- 26 Richard, A. J., Hang, H. & Stephens, J. M. Pyruvate dehydrogenase complex (PDC) subunits moonlight as interaction partners of phosphorylated STAT5 in

- adipocytes and adipose tissue. *J Biol Chem* **292**, 19733-19742,
doi:10.1074/jbc.M117.811794 (2017).
- 27 Chen, J. *et al.* Compartmentalized activities of the pyruvate dehydrogenase complex sustain lipogenesis in prostate cancer. *Nat Genet* **50**, 219-228,
doi:10.1038/s41588-017-0026-3 (2018).
- 28 Ferriero, R. *et al.* Pyruvate dehydrogenase complex and lactate dehydrogenase are targets for therapy of acute liver failure. *J Hepatol* **69**, 325-335,
doi:10.1016/j.jhep.2018.03.016 (2018).
- 29 Lissens, W. *et al.* Mutations in the X-linked pyruvate dehydrogenase (E1) alpha subunit gene (PDHA1) in patients with a pyruvate dehydrogenase complex deficiency. *Hum Mutat* **15**, 209-219, doi:10.1002/(SICI)1098-1004(200003)15:3<209::AID-HUMU1>3.0.CO;2-K (2000).
- 30 Dahl, H. H. *et al.* Mutations and polymorphisms in the pyruvate dehydrogenase E1 alpha gene. *Hum Mutat* **1**, 97-102, doi:10.1002/humu.1380010203 (1992).
- 31 Chun, K. *et al.* Mutations in the X-linked E1 alpha subunit of pyruvate dehydrogenase: exon skipping, insertion of duplicate sequence, and missense mutations leading to the deficiency of the pyruvate dehydrogenase complex. *Am J Hum Genet* **56**, 558-569 (1995).
- 32 Brown, G. K., Otero, L. J., LeGris, M. & Brown, R. M. Pyruvate dehydrogenase deficiency. *J Med Genet* **31**, 875-879, doi:10.1136/jmg.31.11.875 (1994).

- 33 Robinson, B. H., MacMillan, H., Petrova-Benedict, R. & Sherwood, W. G. Variable clinical presentation in patients with defective E1 component of pyruvate dehydrogenase complex. *J Pediatr* **111**, 525-533, doi:10.1016/s0022-3476(87)80112-9 (1987).
- 34 Archer, S. L., Weir, E. K. & Wilkins, M. R. Basic science of pulmonary arterial hypertension for clinicians: new concepts and experimental therapies. *Circulation* **121**, 2045-2066, doi:10.1161/CIRCULATIONAHA.108.847707 (2010).
- 35 Michelakis, E. D. *et al.* Inhibition of pyruvate dehydrogenase kinase improves pulmonary arterial hypertension in genetically susceptible patients. *Sci Transl Med* **9**, doi:10.1126/scitranslmed.aao4583 (2017).
- 36 Pastorino, J. G., Hoek, J. B. & Shulga, N. Activation of glycogen synthase kinase 3beta disrupts the binding of hexokinase II to mitochondria by phosphorylating voltage-dependent anion channel and potentiates chemotherapy-induced cytotoxicity. *Cancer Res* **65**, 10545-10554, doi:10.1158/0008-5472.CAN-05-1925 (2005).
- 37 McFate, T. *et al.* Pyruvate dehydrogenase complex activity controls metabolic and malignant phenotype in cancer cells. *J Biol Chem* **283**, 22700-22708, doi:10.1074/jbc.M801765200 (2008).
- 38 Dunbar, E. M. *et al.* Phase 1 trial of dichloroacetate (DCA) in adults with recurrent malignant brain tumors. *Invest New Drugs* **32**, 452-464, doi:10.1007/s10637-013-0047-4 (2014).

- 39 Michelakis, E. D. *et al.* Metabolic modulation of glioblastoma with dichloroacetate. *Sci Transl Med* **2**, 31ra34, doi:10.1126/scitranslmed.3000677 (2010).
- 40 Ahrens, E. H., Jr., Payne, M. A., Kunkel, H. G., Eisenmenger, W. J. & Blondheim, S. H. Primary biliary cirrhosis. *Medicine (Baltimore)* **29**, 299-364, doi:10.1097/00005792-195012000-00002 (1950).
- 41 Baum, H. & Palmer, C. The PBC-specific antigen. *Mol Aspects Med* **8**, 201-234, doi:10.1016/0098-2997(85)90007-x (1985).
- 42 Frazer, I. H., Mackay, I. R., Jordan, T. W., Whittingham, S. & Marzuki, S. Reactivity of anti-mitochondrial autoantibodies in primary biliary cirrhosis: definition of two novel mitochondrial polypeptide autoantigens. *J Immunol* **135**, 1739-1745 (1985).
- 43 Caviston, J. P. & Holzbaur, E. L. Microtubule motors at the intersection of trafficking and transport. *Trends Cell Biol* **16**, 530-537, doi:10.1016/j.tcb.2006.08.002 (2006).
- 44 Akhmanova, A. & Steinmetz, M. O. Control of microtubule organization and dynamics: two ends in the limelight. *Nat Rev Mol Cell Biol* **16**, 711-726, doi:10.1038/nrm4084 (2015).
- 45 Roberts, A. J., Kon, T., Knight, P. J., Sutoh, K. & Burgess, S. A. Functions and mechanics of dynein motor proteins. *Nat Rev Mol Cell Biol* **14**, 713-726, doi:10.1038/nrm3667 (2013).

- 46 Hirokawa, N., Noda, Y., Tanaka, Y. & Niwa, S. Kinesin superfamily motor proteins and intracellular transport. *Nat Rev Mol Cell Biol* **10**, 682-696, doi:10.1038/nrm2774 (2009).
- 47 Reck-Peterson, S. L., Redwine, W. B., Vale, R. D. & Carter, A. P. The cytoplasmic dynein transport machinery and its many cargoes. *Nat Rev Mol Cell Biol* **19**, 382-398, doi:10.1038/s41580-018-0004-3 (2018).
- 48 Lindquist, S. The heat-shock response. *Annu Rev Biochem* **55**, 1151-1191, doi:10.1146/annurev.bi.55.070186.005443 (1986).
- 49 Hache, R. J., Tse, R., Reich, T., Savory, J. G. & Lefebvre, Y. A. Nucleocytoplasmic trafficking of steroid-free glucocorticoid receptor. *J Biol Chem* **274**, 1432-1439, doi:10.1074/jbc.274.3.1432 (1999).
- 50 Kanno, Y., Miyama, Y., Ando, M. & Inouye, Y. Dependence on the microtubule network and 90-kDa heat shock protein of phenobarbital-induced nuclear translocation of the rat constitutive androstane receptor. *Mol Pharmacol* **77**, 311-316, doi:10.1124/mol.109.060434 (2010).
- 51 Reed, N. A. *et al.* Microtubule acetylation promotes kinesin-1 binding and transport. *Curr Biol* **16**, 2166-2172, doi:10.1016/j.cub.2006.09.014 (2006).
- 52 Alper, J. D., Decker, F., Agana, B. & Howard, J. The motility of axonemal dynein is regulated by the tubulin code. *Biophys J* **107**, 2872-2880, doi:10.1016/j.bpj.2014.10.061 (2014).

- 53 Friedman, J. R., Webster, B. M., Mastronarde, D. N., Verhey, K. J. & Voeltz, G. K. ER sliding dynamics and ER-mitochondrial contacts occur on acetylated microtubules. *J Cell Biol* **190**, 363-375, doi:10.1083/jcb.200911024 (2010).
- 54 Howard, J. & Hyman, A. A. Dynamics and mechanics of the microtubule plus end. *Nature* **422**, 753-758, doi:10.1038/nature01600 (2003).
- 55 Kardon, J. R. & Vale, R. D. Regulators of the cytoplasmic dynein motor. *Nat Rev Mol Cell Biol* **10**, 854-865, doi:10.1038/nrm2804 (2009).
- 56 Carbonaro, M., Escuin, D., O'Brate, A., Thadani-Mulero, M. & Giannakakou, P. Microtubules regulate hypoxia-inducible factor-1alpha protein trafficking and activity: implications for taxane therapy. *J Biol Chem* **287**, 11859-11869, doi:10.1074/jbc.M112.345587 (2012).
- 57 Giannakakou, P. *et al.* Enhanced microtubule-dependent trafficking and p53 nuclear accumulation by suppression of microtubule dynamics. *Proc Natl Acad Sci U S A* **99**, 10855-10860, doi:10.1073/pnas.132275599 (2002).
- 58 Wu, Y. *et al.* Herpesvirus acts with the cytoskeleton and promotes cancer progression. *J Cancer* **10**, 2185-2193, doi:10.7150/jca.30222 (2019).
- 59 Iwamoto, M. *et al.* Functional association of cellular microtubules with viral capsid assembly supports efficient hepatitis B virus replication. *Sci Rep* **7**, 10620, doi:10.1038/s41598-017-11015-4 (2017).

- 60 Neuspiel, M. *et al.* Cargo-selected transport from the mitochondria to peroxisomes is mediated by vesicular carriers. *Curr Biol* **18**, 102-108, doi:10.1016/j.cub.2007.12.038 (2008).
- 61 Soubannier, V. *et al.* A vesicular transport pathway shuttles cargo from mitochondria to lysosomes. *Curr Biol* **22**, 135-141, doi:10.1016/j.cub.2011.11.057 (2012).
- 62 Fahrenkrog, B. & Aebi, U. The nuclear pore complex: nucleocytoplasmic transport and beyond. *Nat Rev Mol Cell Biol* **4**, 757-766, doi:10.1038/nrm1230 (2003).
- 63 Fahrenkrog, B. & Aebi, U. The vertebrate nuclear pore complex: from structure to function. *Results Probl Cell Differ* **35**, 25-48 (2002).
- 64 Stoffler, D., Fahrenkrog, B. & Aebi, U. The nuclear pore complex: from molecular architecture to functional dynamics. *Curr Opin Cell Biol* **11**, 391-401, doi:10.1016/S0955-0674(99)80055-6 (1999).
- 65 Fahrenkrog, B. *et al.* Domain-specific antibodies reveal multiple-site topology of Nup153 within the nuclear pore complex. *J Struct Biol* **140**, 254-267 (2002).
- 66 Bayliss, R., Littlewood, T. & Stewart, M. Structural basis for the interaction between FxFG nucleoporin repeats and importin-beta in nuclear trafficking. *Cell* **102**, 99-108, doi:10.1016/s0092-8674(00)00014-3 (2000).

- 67 Guo, Y. & Zheng, Y. Lamins position the nuclear pores and centrosomes by modulating dynein. *Mol Biol Cell* **26**, 3379-3389, doi:10.1091/mbc.E15-07-0482 (2015).
- 68 Wentz, S. R. & Rout, M. P. The nuclear pore complex and nuclear transport. *Cold Spring Harb Perspect Biol* **2**, a000562, doi:10.1101/cshperspect.a000562 (2010).
- 69 Pante, N. & Kann, M. Nuclear pore complex is able to transport macromolecules with diameters of about 39 nm. *Mol Biol Cell* **13**, 425-434, doi:10.1091/mbc.01-06-0308 (2002).
- 70 Nigg, E. A. Nucleocytoplasmic transport: signals, mechanisms and regulation. *Nature* **386**, 779-787, doi:10.1038/386779a0 (1997).
- 71 Lange, A. *et al.* Classical nuclear localization signals: definition, function, and interaction with importin alpha. *J Biol Chem* **282**, 5101-5105, doi:10.1074/jbc.R600026200 (2007).
- 72 Stewart, M. Molecular mechanism of the nuclear protein import cycle. *Nat Rev Mol Cell Biol* **8**, 195-208, doi:10.1038/nrm2114 (2007).
- 73 Fagotto, F., Gluck, U. & Gumbiner, B. M. Nuclear localization signal-independent and importin/karyopherin-independent nuclear import of beta-catenin. *Curr Biol* **8**, 181-190, doi:10.1016/s0960-9822(98)70082-x (1998).
- 74 De Magistris, P. & Antonin, W. The Dynamic Nature of the Nuclear Envelope. *Curr Biol* **28**, R487-R497, doi:10.1016/j.cub.2018.01.073 (2018).

- 75 Watson, M. L. The nuclear envelope; its structure and relation to cytoplasmic membranes. *J Biophys Biochem Cytol* **1**, 257-270, doi:10.1083/jcb.1.3.257 (1955).
- 76 Wilson, K. L. & Berk, J. M. The nuclear envelope at a glance. *J Cell Sci* **123**, 1973-1978, doi:10.1242/jcs.019042 (2010).
- 77 Gruenbaum, Y., Margalit, A., Goldman, R. D., Shumaker, D. K. & Wilson, K. L. The nuclear lamina comes of age. *Nat Rev Mol Cell Biol* **6**, 21-31, doi:10.1038/nrm1550 (2005).
- 78 Goldman, A. E., Maul, G., Steinert, P. M., Yang, H. Y. & Goldman, R. D. Keratin-like proteins that coisolate with intermediate filaments of BHK-21 cells are nuclear lamins. *Proc Natl Acad Sci U S A* **83**, 3839-3843, doi:10.1073/pnas.83.11.3839 (1986).
- 79 Nakajima, N. & Abe, K. Genomic structure of the mouse A-type lamin gene locus encoding somatic and germ cell-specific lamins. *FEBS Lett* **365**, 108-114, doi:10.1016/0014-5793(95)00453-g (1995).
- 80 Machiels, B. M. *et al.* Subcellular localization of proteasomes in apoptotic lung tumor cells and persistence as compared to intermediate filaments. *Eur J Cell Biol* **70**, 250-259 (1996).
- 81 Burke, B. & Stewart, C. L. The nuclear lamins: flexibility in function. *Nat Rev Mol Cell Biol* **14**, 13-24, doi:10.1038/nrm3488 (2013).

- 82 Furukawa, K. & Hotta, Y. cDNA cloning of a germ cell specific lamin B3 from mouse spermatocytes and analysis of its function by ectopic expression in somatic cells. *EMBO J* **12**, 97-106 (1993).
- 83 Beck, L. A., Hosick, T. J. & Sinensky, M. Isoprenylation is required for the processing of the lamin A precursor. *J Cell Biol* **110**, 1489-1499, doi:10.1083/jcb.110.5.1489 (1990).
- 84 Kitten, G. T. & Nigg, E. A. The CaaX motif is required for isoprenylation, carboxyl methylation, and nuclear membrane association of lamin B2. *J Cell Biol* **113**, 13-23, doi:10.1083/jcb.113.1.13 (1991).
- 85 Sinensky, M. *et al.* The processing pathway of prelamin A. *J Cell Sci* **107 (Pt 1)**, 61-67 (1994).
- 86 Holtz, D., Tanaka, R. A., Hartwig, J. & McKeon, F. The CaaX motif of lamin A functions in conjunction with the nuclear localization signal to target assembly to the nuclear envelope. *Cell* **59**, 969-977, doi:10.1016/0092-8674(89)90753-8 (1989).
- 87 Weber, K., Plessmann, U. & Traub, P. Maturation of nuclear lamin A involves a specific carboxy-terminal trimming, which removes the polyisoprenylation site from the precursor; implications for the structure of the nuclear lamina. *FEBS Lett* **257**, 411-414, doi:10.1016/0014-5793(89)81584-4 (1989).
- 88 Fisher, D. Z., Chaudhary, N. & Blobel, G. cDNA sequencing of nuclear lamins A and C reveals primary and secondary structural homology to intermediate filament

- proteins. *Proc Natl Acad Sci U S A* **83**, 6450-6454, doi:10.1073/pnas.83.17.6450 (1986).
- 89 McKeon, F. D., Kirschner, M. W. & Caput, D. Homologies in both primary and secondary structure between nuclear envelope and intermediate filament proteins. *Nature* **319**, 463-468, doi:10.1038/319463a0 (1986).
- 90 Dhe-Paganon, S., Werner, E. D., Chi, Y. I. & Shoelson, S. E. Structure of the globular tail of nuclear lamin. *J Biol Chem* **277**, 17381-17384, doi:10.1074/jbc.C200038200 (2002).
- 91 Williams, A. F. & Barclay, A. N. The immunoglobulin superfamily--domains for cell surface recognition. *Annu Rev Immunol* **6**, 381-405, doi:10.1146/annurev.iy.06.040188.002121 (1988).
- 92 Wilson, K. L. & Foisner, R. Lamin-binding Proteins. *Cold Spring Harb Perspect Biol* **2**, a000554, doi:10.1101/cshperspect.a000554 (2010).
- 93 Harada, T. *et al.* Nuclear lamin stiffness is a barrier to 3D migration, but softness can limit survival. *J Cell Biol* **204**, 669-682, doi:10.1083/jcb.201308029 (2014).
- 94 Simon, D. N. & Wilson, K. L. Partners and post-translational modifications of nuclear lamins. *Chromosoma* **122**, 13-31, doi:10.1007/s00412-013-0399-8 (2013).
- 95 Heald, R. & McKeon, F. Mutations of phosphorylation sites in lamin A that prevent nuclear lamina disassembly in mitosis. *Cell* **61**, 579-589, doi:10.1016/0092-8674(90)90470-y (1990).

- 96 Peter, M., Nakagawa, J., Doree, M., Labbe, J. C. & Nigg, E. A. In vitro disassembly of the nuclear lamina and M phase-specific phosphorylation of lamins by cdc2 kinase. *Cell* **61**, 591-602, doi:10.1016/0092-8674(90)90471-p (1990).
- 97 Gerace, L. & Blobel, G. The nuclear envelope lamina is reversibly depolymerized during mitosis. *Cell* **19**, 277-287, doi:10.1016/0092-8674(80)90409-2 (1980).
- 98 Karoutas, A. *et al.* The NSL complex maintains nuclear architecture stability via lamin A/C acetylation. *Nat Cell Biol* **21**, 1248-1260, doi:10.1038/s41556-019-0397-z (2019).
- 99 Murray, L. A., Sheng, X. & Cristea, I. M. Orchestration of protein acetylation as a toggle for cellular defense and virus replication. *Nat Commun* **9**, 4967, doi:10.1038/s41467-018-07179-w (2018).
- 100 Xie, W. *et al.* A-type Lamins Form Distinct Filamentous Networks with Differential Nuclear Pore Complex Associations. *Curr Biol* **26**, 2651-2658, doi:10.1016/j.cub.2016.07.049 (2016).
- 101 Schirmer, E. C., Guan, T. & Gerace, L. Involvement of the lamin rod domain in heterotypic lamin interactions important for nuclear organization. *J Cell Biol* **153**, 479-489, doi:10.1083/jcb.153.3.479 (2001).
- 102 Laguri, C. *et al.* Structural characterization of the LEM motif common to three human inner nuclear membrane proteins. *Structure* **9**, 503-511, doi:10.1016/s0969-2126(01)00611-6 (2001).

- 103 Margalit, A., Brachner, A., Gotzmann, J., Foisner, R. & Gruenbaum, Y. Barrier-to-autointegration factor--a BAFfling little protein. *Trends Cell Biol* **17**, 202-208, doi:10.1016/j.tcb.2007.02.004 (2007).
- 104 Taniura, H., Glass, C. & Gerace, L. A chromatin binding site in the tail domain of nuclear lamins that interacts with core histones. *J Cell Biol* **131**, 33-44, doi:10.1083/jcb.131.1.33 (1995).
- 105 Mattout, A., Goldberg, M., Tzur, Y., Margalit, A. & Gruenbaum, Y. Specific and conserved sequences in *D. melanogaster* and *C. elegans* lamins and histone H2A mediate the attachment of lamins to chromosomes. *J Cell Sci* **120**, 77-85, doi:10.1242/jcs.03325 (2007).
- 106 Dorner, D. *et al.* Lamina-associated polypeptide 2alpha regulates cell cycle progression and differentiation via the retinoblastoma-E2F pathway. *J Cell Biol* **173**, 83-93, doi:10.1083/jcb.200511149 (2006).
- 107 Kumaran, R. I., Muralikrishna, B. & Parnaik, V. K. Lamin A/C speckles mediate spatial organization of splicing factor compartments and RNA polymerase II transcription. *J Cell Biol* **159**, 783-793, doi:10.1083/jcb.200204149 (2002).
- 108 Giacinti, C. & Giordano, A. RB and cell cycle progression. *Oncogene* **25**, 5220-5227, doi:10.1038/sj.onc.1209615 (2006).
- 109 Cesarini, E. *et al.* Lamin A/C sustains PcG protein architecture, maintaining transcriptional repression at target genes. *J Cell Biol* **211**, 533-551, doi:10.1083/jcb.201504035 (2015).

- 110 Marullo, F. *et al.* Nucleoplasmic Lamin A/C and Polycomb group of proteins: An evolutionarily conserved interplay. *Nucleus* **7**, 103-111, doi:10.1080/19491034.2016.1157675 (2016).
- 111 Hozak, P., Sasseville, A. M., Raymond, Y. & Cook, P. R. Lamin proteins form an internal nucleoskeleton as well as a peripheral lamina in human cells. *J Cell Sci* **108 (Pt 2)**, 635-644 (1995).
- 112 Bridger, J. M., Kill, I. R., O'Farrell, M. & Hutchison, C. J. Internal lamin structures within G1 nuclei of human dermal fibroblasts. *J Cell Sci* **104 (Pt 2)**, 297-306 (1993).
- 113 Shimi, T. *et al.* The A- and B-type nuclear lamin networks: microdomains involved in chromatin organization and transcription. *Genes Dev* **22**, 3409-3421, doi:10.1101/gad.1735208 (2008).
- 114 Schreiber, K. H. & Kennedy, B. K. When lamins go bad: nuclear structure and disease. *Cell* **152**, 1365-1375, doi:10.1016/j.cell.2013.02.015 (2013).
- 115 Eriksson, M. *et al.* Recurrent de novo point mutations in lamin A cause Hutchinson-Gilford progeria syndrome. *Nature* **423**, 293-298, doi:10.1038/nature01629 (2003).
- 116 Hennekam, R. C. Hutchinson-Gilford progeria syndrome: review of the phenotype. *Am J Med Genet A* **140**, 2603-2624, doi:10.1002/ajmg.a.31346 (2006).

- 117 Foster, C. R., Przyborski, S. A., Wilson, R. G. & Hutchison, C. J. Lamins as cancer biomarkers. *Biochem Soc Trans* **38**, 297-300, doi:10.1042/BST0380297 (2010).
- 118 Irianto, J., Pfeifer, C. R., Ivanovska, I. L., Swift, J. & Discher, D. E. Nuclear lamins in cancer. *Cell Mol Bioeng* **9**, 258-267, doi:10.1007/s12195-016-0437-8 (2016).
- 119 Simon, D. N., Zastrow, M. S. & Wilson, K. L. Direct actin binding to A- and B-type lamin tails and actin filament bundling by the lamin A tail. *Nucleus* **1**, 264-272, doi:10.4161/nucl.1.3.11799 (2010).
- 120 Zastrow, M. S., Flaherty, D. B., Benian, G. M. & Wilson, K. L. Nuclear titin interacts with A- and B-type lamins in vitro and in vivo. *J Cell Sci* **119**, 239-249, doi:10.1242/jcs.02728 (2006).
- 121 Libotte, T. *et al.* Lamin A/C-dependent localization of Nesprin-2, a giant scaffold at the nuclear envelope. *Mol Biol Cell* **16**, 3411-3424, doi:10.1091/mbc.e04-11-1009 (2005).
- 122 Mislow, J. M. *et al.* Nesprin-1alpha self-associates and binds directly to emerin and lamin A in vitro. *FEBS Lett* **525**, 135-140, doi:10.1016/s0014-5793(02)03105-8 (2002).
- 123 Vlcek, S., Foisner, R. & Wilson, K. L. Lco1 is a novel widely expressed lamin-binding protein in the nuclear interior. *Exp Cell Res* **298**, 499-511, doi:10.1016/j.yexcr.2004.04.028 (2004).

- 124 Haque, F. *et al.* SUN1 interacts with nuclear lamin A and cytoplasmic nesprins to provide a physical connection between the nuclear lamina and the cytoskeleton. *Mol Cell Biol* **26**, 3738-3751, doi:10.1128/MCB.26.10.3738-3751.2006 (2006).
- 125 Crisp, M. *et al.* Coupling of the nucleus and cytoplasm: role of the LINC complex. *J Cell Biol* **172**, 41-53, doi:10.1083/jcb.200509124 (2006).
- 126 Al-Haboubi, T., Shumaker, D. K., Koser, J., Wehnert, M. & Fahrenkrog, B. Distinct association of the nuclear pore protein Nup153 with A- and B-type lamins. *Nucleus* **2**, 500-509, doi:10.4161/nucl.2.5.17913 (2011).
- 127 Lussi, Y. C., Hugi, I., Laurell, E., Kutay, U. & Fahrenkrog, B. The nucleoporin Nup88 is interacting with nuclear lamin A. *Mol Biol Cell* **22**, 1080-1090, doi:10.1091/mbc.E10-05-0463 (2011).
- 128 Dechat, T. *et al.* Lamina-associated polypeptide 2alpha binds intranuclear A-type lamins. *J Cell Sci* **113 Pt 19**, 3473-3484 (2000).
- 129 Mansharamani, M. & Wilson, K. L. Direct binding of nuclear membrane protein MAN1 to emerin in vitro and two modes of binding to barrier-to-autointegration factor. *J Biol Chem* **280**, 13863-13870, doi:10.1074/jbc.M413020200 (2005).
- 130 Brachner, A., Reipert, S., Foisner, R. & Gotzmann, J. LEM2 is a novel MAN1-related inner nuclear membrane protein associated with A-type lamins. *J Cell Sci* **118**, 5797-5810, doi:10.1242/jcs.02701 (2005).

- 131 Sakaki, M. *et al.* Interaction between emerin and nuclear lamins. *J Biochem* **129**, 321-327, doi:10.1093/oxfordjournals.jbchem.a002860 (2001).
- 132 Lee, K. K. *et al.* Distinct functional domains in emerin bind lamin A and DNA-bridging protein BAF. *J Cell Sci* **114**, 4567-4573 (2001).
- 133 Shumaker, D. K. *et al.* The highly conserved nuclear lamin Ig-fold binds to PCNA: its role in DNA replication. *J Cell Biol* **181**, 269-280, doi:10.1083/jcb.200708155 (2008).
- 134 Stierle, V. *et al.* The carboxyl-terminal region common to lamins A and C contains a DNA binding domain. *Biochemistry* **42**, 4819-4828, doi:10.1021/bi020704g (2003).
- 135 Lloyd, D. J., Trembath, R. C. & Shackleton, S. A novel interaction between lamin A and SREBP1: implications for partial lipodystrophy and other laminopathies. *Hum Mol Genet* **11**, 769-777, doi:10.1093/hmg/11.7.769 (2002).
- 136 Martelli, A. M. *et al.* Molecular characterization of protein kinase C-alpha binding to lamin A. *J Cell Biochem* **86**, 320-330, doi:10.1002/jcb.10227 (2002).
- 137 Barton, R. M. & Worman, H. J. Prenylated prelamin A interacts with Narf, a novel nuclear protein. *J Biol Chem* **274**, 30008-30018, doi:10.1074/jbc.274.42.30008 (1999).

Chapter Two: Extramitochondrial PDC translocates into the nucleus via acetylated microtubules and it is involved in the process of tubulin acetylation

Abstract

The mitochondrial pyruvate dehydrogenase complex (PDC) is one of the largest complexes within the cell with diameters up to 45 nm based on the stoichiometry and organization of its individual subunits. PDC was thought to reside in the mitochondrial matrix linking glycolysis to oxidative phosphorylation but we recently showed that it can translocate into the nucleus after association with the molecular chaperone Hsp70 upon exposure to stimuli inducing cell proliferation (i.e. serum and epidermal growth factor) and mitochondrial inhibition (i.e. rotenone). Intracellular protein trafficking is mediated by protein carriers (including molecular chaperones) moving along microtubules. Tubulin acetylation stabilizes protein binding onto the microtubules and enhances the binding of protein carriers, thus facilitating protein trafficking. Here we show that extramitochondrial PDC binds to acetylated microtubules via Hsp70 before it enters the nucleus. Exposure to proliferative stimuli increase both the binding of PDC onto acetylated microtubules and its nuclear levels. Loss of tubulin acetylation results in decreased nuclear PDC levels, while its pharmacologic increase results in faster translocation of PDC into the nucleus. PDC interacts directly with acetylated tubulin through its E2 subunit independently of microtubule stability. Loss of PDC but not ATP citrate lyase (ACLY), the main cytoplasmic acetyl-CoA producer, decreases tubulin acetylation, suggesting that extramitochondrial PDC is involved in the process of tubulin acetylation and might act as a novel tubulin acetyltransferase. Our work highlights acetylated tubulin as a pathway for the nuclear translocation of PDC that can potentially be extended to other mitochondrial proteins known to translocate into the nucleus. We believe that this pathway is relevant to smaller size PDC complexes (<39

nm in diameter) that are able to cross the nuclear pore. Moreover, our findings that PDC might act as a tubulin acetyltransferase provide a new angle for future PDC studies and have implications in diseases with aberrant intracellular protein trafficking.

2.1 Introduction

Pyruvate dehydrogenase complex (PDC) is a key mitochondrial enzyme residing in the mitochondrial matrix, where it produces acetyl-CoA using glucose-derived pyruvate and feeding it into the Krebs cycle¹. It consists of three main subunits, the pyruvate dehydrogenase E1 (a heterodimer of E1 α and E1 β) that removes an acetyl-group from pyruvate, the dihydrolipoamide acetyltransferase E2 that attaches the acetyl-group to a CoA-SH molecule resulting in the formation of acetyl-CoA and the dihydrolipoamide dehydrogenase E3 that re-oxidizes the lipoamide groups of the E2 subunit resulting in the formation of NADH₂². PDC is one of the largest enzymatic complexes within the cell with molecular weights that can reach up to 10 MDa and diameters ranging from 25-45 nm based on the different conformations that its individual subunits can obtain³⁻⁵. We recently showed that active PDC translocates into the nucleus without its inhibitor pyruvate dehydrogenase kinase via interaction with the molecular chaperone Hsp70 upon exposure to proliferative stimuli, like serum and epidermal growth factor (EGF), where it carries out its canonical function (i.e. acetyl-CoA production) facilitating histone acetylation that is necessary for cell cycle progression⁶. Even though these findings were provocative they have now been verified by various independent research groups⁷⁻¹². However, the presence of PDC in the nucleus raises the question of how one of the largest enzymatic complexes within the cell leaves the mitochondria and navigates through the cytoplasm before entering the nucleus.

Intracellular protein trafficking occurs via movement of carrier proteins on the microtubules that are parts of the cytoskeleton and are consisted of heterodimers of α -

and β -tubulin¹³. Carrier proteins, like dyneins, kinesins and molecular chaperones (including Hsp70) bind to them and transfer proteins or entire organelles (e.g. mitochondria) towards the minus end (towards the nucleus) or the plus end (away from the nucleus) of microtubules^{14,15}. Microtubules can undergo several post-translational modifications (reviewed in ¹⁶), including acetylation of α -tubulin on the lysine 40 (K40) residue that resides within the microtubule lumen. This modification has been associated with increased stability of the microtubule network^{17,18} and binding of protein carriers including molecular chaperones like heat shock protein 90 (Hsp90) and Hsp70, hence facilitating intracellular protein trafficking¹⁹⁻²².

Here we provide evidence that extramitochondrial PDC colocalizes with acetylated microtubules and Hsp70 and this colocalization is enhanced upon exposure to serum and EGF. We found that PDC interacts directly with acetylated microtubules via its E2 subunit and this interaction is lost when tubulin acetylation is decreased. We also show that tubulin acetylation is positively correlated with the levels of nuclear PDC. Moreover, we show that tubulin acetylation levels oscillate throughout the cell cycle following the same pattern as nuclear PDC levels and knockdown of PDCE2, a subunit with an intrinsic acetyl-transferase activity, but not ATP citrate lyase (ACLY), the main acetyl-CoA producer in the cytoplasm, results in decreased tubulin acetylation levels, suggesting that extramitochondrial PDC might be a novel tubulin acetyl-transferase. Our work enhances the concept of interorganellar communication and highlights the importance of an intact microtubule network and tubulin acetylation in the intracellular trafficking of large complexes that are destined to enter the nucleus.

Results

2.2 Proliferative stimuli induce the colocalization of extramitochondrial PDC with Hsp70 and acetylated microtubules

Newly synthesized PDC subunits have to first enter the mitochondrial matrix and undergo a processing step by the mitochondrial processing peptidase (cleavage of the mitochondrial localization sequence) before forming the whole complex that can then translocate into the nucleus^{6,23}. Therefore, cytoplasmic PDC that is translocating into the nucleus will contain all four of its subunits. We visualized extramitochondrial PDC after we induced its nuclear translocation by exposing synchronized A549 cells to serum and EGF (500 ng/ml) for 2 hours before staining them for PDCE1 α , PDCE2, PDCE3 and mitotracker and obtained super resolution confocal images that increase the lateral resolution to ~160 nm compared to 260 nm that classical confocal microscopy offers (**Fig. 2-1**). By following this approach, we were able to detect PDC in the cytoplasm (white arrows), suggesting that this complex had left the mitochondria and it was translocating into the nucleus.

Since the majority of the intracellular protein and organelle trafficking occurs along the microtubule network and it is enhanced by α -tubulin acetylation we wanted to test whether extramitochondrial PDC that is translocating into the nucleus colocalizes with acetyl-tubulin. To visualize this colocalization we stimulated both A549 and HEK293 cells with serum and EGF and stained them for PDCE2, acetyl-tubulin and mitotracker before imaging them under a super resolution confocal microscope. To visualize extramitochondrial PDC we developed a code on an image analysis software that allowed us to measure the area occupied by **a) mitochondrial PDCE2, b)**

extramitochondrial PDCE2 and **c**) extramitochondrial PDCE2 that colocalizes with acetyl-tubulin (**Fig. 2-2A and 2-2B**) and we found that almost 57% of the extramitochondrial PDCE2 (white arrows) colocalizes with acetylated microtubules.

We previously showed that the nuclear translocation of PDC is mediated by the molecular chaperone Hsp70⁶ that has been found to preferentially associate with acetylated microtubules during the nuclear translocation of large molecules, e.g. the glucocorticoid receptor^{24,25}. Thus, it is reasonable to assume that a complex of extramitochondrial PDC and Hsp70 will be colocalizing with acetylated microtubules upon stimulation with serum and EGF, while being transferred into the nucleus. To visualize this colocalization we obtained super resolution confocal images of serum and EGF-stimulated A549 cells that were stained with antibodies against PDCE2, Hsp70 and acetyl-tubulin (**Fig. 2-3**). In this experiment we were not able to stain the cells with mitotracker or for any other of the PDC's subunits due to overlap of the emission spectrum of the fluorophores we used. To exclude mitochondrial PDC from our analysis we hypothesized that the brightest intensity PDCE2 signal will be observed only in the mitochondria, while the rest will be coming from extramitochondrial subunits since the nuclear and hence extramitochondrial PDC is only a small fraction of the mitochondrial one⁶. To visualize extramitochondrial PDC we developed an image analysis code to exclude areas with high intensity PDCE2 signal and show only areas with low intensity signal. This analysis revealed that Hsp70 colocalizes with both PDCE2 and acetyl-tubulin in the cytoplasm, suggesting that extramitochondrial PDC forms a complex with Hsp70 that moves along acetylated microtubules before entering the nucleus.

Next, we wanted to test whether exposure to stimuli that induce the nuclear translocation of PDC will result in an increase of its colocalization with acetylated tubulin. Therefore, we exposed A549 cells to serum and EGF and stained them for PDCE1 α , PDCE2, acetyl-tubulin and mitotracker before we obtained images with a super resolution confocal microscope. By using the same image analysis code as in **Fig. 2-1** we found that exposure to serum and EGF increased the colocalization of extramitochondrial PDC (i.e. both PDCE1 α and PDCE2) with acetylated microtubules by ~25% compared to baseline (**Fig. 2-4**), suggesting that the nuclear translocation of PDC occurs via acetylated microtubules. To further strengthen this result, we performed a proximity ligation assay (PLA) that allows the visualization of the subcellular localization of proteins lying within 40 nm from each other. We used synchronized (i.e. serum deprived) and stimulated (exposed to serum and EGF) A549 cells and stained them for PDCE2 and acetyl-tubulin and performed z stacks under a confocal microscope to capture the entire volume of the cell (**Fig. 2-5**). We found that exposure to serum and EGF greatly increased the association of the two proteins, further strengthening our previous findings that PDC translocates into the nucleus by moving along acetylated microtubules.

2.3 PDC interacts with acetylated tubulin directly via its E2 subunit

Since extramitochondrial PDC colocalizes with acetylated microtubules and proliferative stimuli increase their association we wanted to test whether the two proteins interact directly. Therefore, we performed a co-immunoprecipitation experiment, where we pulled down PDCE2 from stimulated A549 cells and found that

both PDCE1 α and acetyl-tubulin precipitated along with it (**Fig. 2-6A**). The presence of PDCE1 α in the precipitates suggests that we pulled down the whole complex and PDC interacts directly with acetylated tubulin through its E2 subunit. To further strengthen this result, we performed the reverse experiment, where we pulled down acetylated tubulin and also found PDCE2 in the precipitates. More importantly, neither the mitochondrial succinate dehydrogenase B (SDHB) nor PDCE1 α were detected among the precipitated proteins, further suggesting that acetylated tubulin interacts directly with the E2 subunit of PDC (**Fig 2-6B**). To test whether this interaction is enhanced upon exposure to stimuli that induce the nuclear translocation of PDC, we exposed synchronized A549 cells to serum and EGF and pulled down PDCE2. We found that cell cycle arrested cells (i.e. synchronized to the G0 phase after serum deprivation) showed no interaction of PDCE2 with acetyl-tubulin but exposure to serum and EGF greatly increased the interaction of the two proteins (**Fig. 2-6C**), suggesting that PDCE2 binds to acetylated microtubules only when the whole complex has left the mitochondria and it is being translocated into the nucleus. Moreover, exposure to serum and EGF had no effect on the total PDCE2 levels as seen in the input groups, suggesting that proliferative stimuli do not increase the total PDCE2 levels and therefore it is not newly synthesized PDCE2 that is interacting with acetyl-tubulin but the one incorporated into the whole complex as it moves towards the nucleus.

Since extramitochondrial PDC interacts directly with acetylated microtubules through its E2 subunit we wanted to test whether loss of tubulin acetylation will decrease the interaction of the two proteins. Tubulin acetylation is regulated via the opposing actions of α -tubulin N-acetyltransferase 1 (α TAT1) and histone deacetylase

6 (HDAC6)^{26,27}. Therefore, to decrease the levels of tubulin acetylation, we knocked down α TAT1 by using siRNA (**Fig. 2-7A and 2-7B**) and pulled down α -tubulin from A549 cells that were exposed to serum and EGF. Since the molecular weight of tubulin is at 50 kDa we were afraid that a harsher elution method for detaching the bound antibodies from the magnetic beads (such as boiling the samples for 5 minutes at 55 °C in SDS buffer) might result in the release of IgG, the heavy chain of which is at 50 kDa and can potentially mask the tubulin band. Therefore, we decided to continue with a milder elution method by acidifying the sample with glycine (pH 2.6) for 10 minutes that results in the release of the bound proteins from the beads by breaking the bonds between them. After elution we neutralized the pH by adding Tris buffer (pH 8.0). However, this technique results in a different pH between the input and the IP groups that can lead to differences on the separation speeds of the samples on the gel, since the speed of the protein separation on a polyacrylamide gel is affected by the charge (hence the pH) of the sample²⁸. This explains the molecular weight differences that we observed between the IP and the input groups. In this experiment we found that loss of tubulin acetylation resulted in decreased tethering of PDCE2 on the microtubules (**Fig. 2-7C**), which is in agreement with the idea that tubulin acetylation strengthens protein – protein interactions between the microtubules and their interacting partners (e.g. motor proteins and molecular chaperones)¹⁹⁻²². Moreover, we found that loss of tubulin acetylation did not alter the levels of detyrosinated tubulin, which is also a marker of stable microtubules along with acetyl-tubulin, suggesting that the interaction of PDC with microtubules is affected only by their acetylation levels and not their stability.

2.4 Extramitochondrial PDC regulates tubulin acetylation during its nuclear translocation

The E2 subunit of PDC is an acetyltransferase and it is responsible for the addition of an acetyl-group from pyruvate to a CoA-SH molecule. Since it interacts directly with acetylated microtubules it is reasonable to assume that extramitochondrial PDC might be regulating tubulin acetylation. First, we wanted to test how exposure to proliferative stimuli that induce the nuclear translocation of PDC affect tubulin acetylation. Therefore, we performed a time course experiment where we stimulated synchronized A549 cells with serum and EGF for 2, 4, 8 and 12 hours before measuring acetyl-tubulin levels by immunoblots. We found that tubulin acetylation levels peaked after 2 hours of treatment (**Fig. 2-8**), which resemble the same pattern that nuclear PDC levels follow under the same stimuli⁶. To assess whether PDC is involved in tubulin acetylation we used A549 cells and knocked down PDCE1 α and PDCE2 by shRNA and siRNA respectively (**Fig. 2-9A and 2-9B**). The transfections resulted in a great decrease of total PDCE1 α and PDCE2 levels, which in turn decreased the levels of tubulin acetylation by ~ 30% for PDCE2 and ~50% for PDCE1 α , suggesting that PDC is involved in the process of tubulin acetylation. However, the cytosolic pool of acetyl-CoA is mostly generated by ATP citrate lyase (ACLY) and to a lesser extent by acetyl-CoA synthetase 2 (AcCS2)²⁹ that use citrate and acetate respectively. Citrate is mostly derived from the TCA cycle¹ and the reductive glutamine pathway, which is known to be upregulated in cancer cells³⁰ (**Fig. 2-9C**). Thus, it is reasonable to assume that loss of PDC's activity by knocking down any of its individual subunits will result in decreased levels of citrate deriving from the TCA cycle, which can further decrease the cytosolic pool of acetyl-CoA and eventually tubulin acetylation. Nevertheless, it has

been shown that knockdown of ACLY does not decrease the levels of tubulin acetylation in cell cycle arrested (i.e. serum deprived) fibroblasts that were stimulated with serum³¹. To verify these findings, we used synchronized A549 cells that were re-exposed to serum and EGF for 2 hours after we knocked down ACLY or PDCE2 by siRNA. Exposure to proliferative stimuli increased the levels of tubulin acetylation on both the scrambled and ACLY siRNA group equally, verifying the previous findings that ACLY does not provide acetyl-CoA towards tubulin acetylation. On the contrary, loss of PDCE2 resulted in lower tubulin acetylation levels similar to our previous findings (**Fig. 2-9D**), suggesting that extramitochondrial PDC can be potentially a novel tubulin acetyltransferase that is responsible for the residual tubulin acetylation when α TAT1 is knocked out³².

2.5 Loss of tubulin acetylation decreases nuclear PDC levels

If PDC interacts with acetylated microtubules and translocates into the nucleus along them, then it is reasonable to assume that loss of tubulin acetylation will also result in decreased levels of nuclear PDC. To test this hypothesis, we used siRNA to knock down α TAT1 in A549 cells and then synchronized them to the G0 phase by serum deprivation before stimulating them with serum and EGF for two hours. We then stained them for PDCE2 and the outer mitochondrial membrane marker TOM20 before we measured nuclear PDCE2 levels under a confocal microscope. The addition of serum and EGF increased nuclear PDCE2 levels in the scrambled group but had no effect in the si α TAT1 group, where the levels were comparable to baseline (**Fig. 2-10A**). To expand our findings on a different metabolic enzyme that is known to

navigate through the cytoplasm before entering the nucleus under proliferative stimuli we decided to study nuclear PKM2 levels after exposure to hypoxia (1% O₂). By using siRNA we knocked down α TAT1 on A549 cells and exposed them to hypoxia for 24 hours before staining them for PDCE2 and PKM2 and examined them under a confocal microscope. Loss of tubulin acetylation resulted in decreased nuclear PDCE2 levels on both normoxic and hypoxic conditions but had no effect on nuclear PKM2; the levels of which increased under hypoxia (**Fig. 2-10B**), suggesting that not all metabolic enzymes entering the nucleus navigate the cytoplasm along acetylated microtubules.

We previously showed that nuclear PDC regulates histone acetylation by generating acetyl-CoA in the nucleus⁶. This would suggest that loss of tubulin acetylation will also result in decreased levels of acetylated histones due to decreased nuclear translocation of PDC. To test this idea, we stimulated A549 cells with serum and EGF for 2 hours after knocking down α TAT1 by siRNA. We then extracted histones by using a commercially available kit and measured acetyl-histone 3 levels by immunoblots and found that exposure to serum resulted in almost 30% increase of histone 3 acetylation in the scrambled siRNA group, while loss of tubulin acetylation had no effect on acetyl-histone 3 levels when compared to baseline (**Fig. 2-10C**), further strengthening our previous findings that loss of tubulin decreases the nuclear translocation of PDC.

2.6 Increased tubulin acetylation results in a faster translocation of PDC into the nucleus

Next, we wanted to test whether increased tubulin acetylation will also increase the levels of nuclear PDC by inhibiting HDAC6, the main tubulin deacetylase^{33,34}. HDAC6

is a unique deacetylase that contains two deacetylase domains and is mainly localized in the cytoplasm³⁵. It is involved in many functions other than tubulin acetylation, including degradation of misfolded proteins, maturation of the glucocorticoid receptor and cell migration^{36,37}. Moreover, HDAC6 has also been found in the nucleus, where it regulates gene transcription via histone deacetylation³⁸. These suggest that knock down of HDAC6 by siRNA might result in various off-target effects and therefore mask the effect of tubulin acetylation on the nuclear translocation of PDC. For that reason, we decided to use tubacin (**Fig. 2-11A**); a small-molecule inhibitor that shows high specificity for HDAC6 at low doses³⁵. First, we were interested on studying the dynamics of tubacin on tubulin acetylation. We used A549 cells that were treated with the drug for 15, 30 and 60 minutes at a low and a high dose; 2.5 μ M and 10 μ M respectively. By using immunoblots we found that tubacin greatly increased tubulin acetylation even after 15 minutes of treatment with 2.5 μ M (**Fig. 2-11B**). Since we were concerned that high doses of tubacin might also show off-target effects by inhibiting other HDACs we decided to continue with the lower dose in all of our subsequent experiments. To test whether increased tubulin acetylation results in higher nuclear PDC levels we used synchronized A549 cells that we stimulated with serum and EGF for 2 hours and added tubacin at the same time. We then stained the cells for PDCE2 and mitotracker, while the effects of tubacin were visualized after staining of the cells with antibodies against tubulin and acetyl-tubulin (**Fig. 2-12A and 2-12B**). Increased tubulin acetylation did not alter the levels of nuclear PDCE2 when compared to the vehicle group. However, since tubulin acetylation is known to increase and stabilize protein – protein interactions¹⁹⁻²² we speculated that increased tubulin acetylation

might result in a sturdier association of the Hsp70-PDC complex with the microtubules and thus prevent its dissociation from the microtubules (due to its large size), resulting in the faster and more efficient translocation of the complex into the nucleus. To test the efficiency of the nuclear translocation of PDC under conditions that increase tubulin acetylation, we stimulated A549 cells with serum and EGF and treated them with 2.5 μ M of tubacin for 1 and 2 hours respectively before staining them with antibodies against PDCE2, acetyl-tubulin and mitotracker and measured nuclear PDCE2 levels under a confocal microscope. Increased tubulin acetylation resulted in higher nuclear PDCE2 levels after 1 hour compared to the vehicle group, while both groups had the same nuclear PDCE2 levels after 2 hours of treatment (**Fig. 2-12C**). To verify these findings with another technique we isolated nuclei from synchronized A549 cells that were exposed to serum and EGF for 1 hour in the presence or absence of tubacin (2.5 μ M) before we measured nuclear PDCE1 α levels by immunoblots (**Fig. 2-12D**). Tubacin treatment resulted in higher nuclear PDCE1 α levels compared to the stimulated vehicle group, further strengthening our previous finding that increased tubulin acetylation results in a faster and more efficient translocation of PDC into the nucleus.

2.7 Discussion

Here we show that extramitochondrial PDC navigates through the cytoplasm as a whole complex via acetylated microtubules before it enters the nucleus in response to proliferative stimuli that induce its nuclear translocation (i.e. serum and EGF)⁶. By using super resolution confocal microscopy, we visualized for the first time

extramitochondrial PDC that colocalized with both Hsp70 and acetylated microtubules and studied this association under exposure to serum and EGF on both cancer and non-cancer cells. Moreover, exposure to serum and EGF increased tubulin acetylation similarly to how it increases nuclear PDC levels. Loss of tubulin acetylation by α TAT1 knockdown decreased nuclear PDC levels, while pharmacologic induction of tubulin acetylation by tubacin, a specific small-drug inhibitor of HDAC6, resulted in the faster and more efficient translocation of PDC into the nucleus. Extramitochondrial PDC interacts directly with acetylated microtubules via its E2 subunit and we provide evidence for the first time that the interaction of PDC with acetylated microtubules regulates tubulin acetylation.

Tubulin acetylation has been shown to enhance intracellular protein trafficking by facilitating the binding of cargo carriers like dynein and heat shock proteins¹⁹⁻²² on the microtubule network. For example, Hsp70 has been shown to mediate the nuclear translocation of various large complexes along microtubules, like the glucocorticoid^{24,37} (97 kDa) and androgen receptors^{39,40} (110 kDa). Hence, a complex of PDC and Hsp70 that moves along acetylated microtubules is not surprising as a means of PDC's navigation through the cytoplasm before entering the nucleus. We were able to show that extramitochondrial PDC colocalizes with both Hsp70 and acetylated microtubules and exposure to serum and EGF increased this colocalization. Loss of tubulin acetylation greatly decreased the levels of nuclear PDC along with histone 3 acetylation. Moreover, increased tubulin acetylation via inhibition of HDAC6 did not increase the levels of nuclear PDC but resulted in the faster translocation of the

complex into the nucleus, suggesting that tubulin acetylation is important for fine-tuning and stabilizing the Hsp70-PDC complex while it moves along microtubules.

Although Hsp70 binds to and moves along microtubules to carry its cargo within the cytoplasm, we found that extramitochondrial PDC also interacts with acetylated microtubules directly via its E2 subunit (by co-immunoprecipitation and a PLA assay), potentially fine-tuning the nuclear translocation of PDC by offering a secondary binding site of the Hsp70-PDC complex on the microtubule network. Even though the formation of a secondary binding site of a motor protein with the microtubules is not a new concept (e.g. dynein-dynactin)⁴¹ it has never been described between the cargo and microtubules. Therefore, given the large size of PDC, we speculate that its interaction with both Hsp70 (via the E1 α subunit) and acetylated microtubules (via the E2 subunit) might offer a sturdier association of the Hsp70-PDC complex with the microtubule network and therefore prevent its dissociation while it is being translocated into the nucleus.

The only tubulin acetyltransferase known to date is α TAT1³². Knockout of α TAT1 in mice results in almost complete loss of tubulin acetylation³² but the presence of residual tubulin acetylation in some tissues indicates the presence of another yet undiscovered tubulin acetyltransferase. Our work suggests that PDC might act as a novel tubulin acetyltransferase through its E2 subunit by adding an acetyl-group to K40 of α -tubulin due to its intrinsic acetyltransferase activity, since its substrate (i.e. pyruvate) is highly available in the cytoplasm. Even though further research is needed the verification that PDCE2 can use its acetyltransferase activity in reactions other than acetyl-CoA production will provide a new angle to approach PDC in the future and might offer a

potential target for various diseases where tubulin acetylation and thus protein trafficking is altered. One example is primary biliary cirrhosis (PBC), where PDCE2 is one of the antimitochondrial antibodies presented on the cell surface triggering an immune response that eventually results in hepatic failure^{42,43}. Along this line of thought, it is tempting to speculate that hepatic cells of PBC patients might show intracellular trafficking abnormalities due to the altered PDCE2 acetyltransferase function and/or tubulin – PDCE2 interactions that can potentially result in the mistargeted translocation of PDCE2 onto the cell membrane.

Deacetylation of microtubules is regulated by the action of HDAC6, which is the main tubulin acetyltransferase, and sirtuin 2 (SIRT2). The function of SIRT2 is highly dependent on the availability of NAD^+ , while the presence NADH_2 inhibits it⁴⁴. Since the oxidation of pyruvate to acetyl-CoA by PDC results in the formation of NADH_2 from its E3 subunit, it is reasonable to assume that extramitochondrial PDC translocating into the nucleus can further increase tubulin acetylation by inhibiting SIRT2 via local production of NADH_2 and thus self-enhancing the efficiency of its intracellular navigation towards the nucleus.

Tubulin acetylation is increased during times that cell proliferation is increased like the early stages of development and it is decreased later on⁴⁵. During these times, nuclear PDC levels are also elevated potentially for sustaining the high demand for acetyl-CoA in the nucleus^{6,10} that is used towards histone acetylation⁴⁶. Therefore, pharmacologic inhibition of tubulin acetylation and hence the nuclear translocation of PDC might offer a new tool for controlling the nuclear pool of acetyl-CoA and cell proliferation that has implications in various diseases, like cancer or aging. Increased

histone acetylation is also necessary for undifferentiated cells to maintain their pluripotency⁴⁷, thus it is reasonable to speculate that both tubulin acetylation and nuclear PDC levels will be increased in these cells. Therefore, altering the interaction between PDC and microtubules by pharmacologically modifying the tubulin acetylation status might offer a novel way to control pluripotency.

Protein entry into the nucleus occurs via the nuclear pores that allow crossing of proteins up to 39 nm in diameter⁴⁸. Moreover, proteins with diameters larger than 5 nm⁴⁹ need to be carried into the nucleoplasm via specialized cargo carriers⁵⁰. PDC's size and diameter are dynamic and they are dependent upon the stoichiometry of its individual subunits, resulting in diameters ranging from 25 to 45 nm^{3,5}. This suggests that smaller size complexes (i.e. less than 39 nm of diameter) meet the size exclusion criterion of the nuclear pore and are able to go through it with the aid of a carrier protein like Hsp70 that is known to facilitate crossing of its cargo through the nuclear pores⁵¹.

Overall, our work suggests that PDC's translocation into the nucleus is dependent on an intact microtubule network and the levels of tubulin acetylation (**Fig. 2-13**). Our findings shed more light on the mechanism of nuclear translocation of PDC and open a broad field of research that can have implications in various aspects of modern biology and disease, where cell proliferation is altered. Nevertheless, more research is needed before elucidating all the key proteins of this mechanism that might be relevant to other proteins translocating into the nucleus and meet the size exclusion criterion of the nuclear pore, like the smaller size PDC complexes (<39 nm in diameter).

2.8 Materials and methods

Cell culture

Human non-small cell lung cancer cells (A549) and embryonic kidney (HEK293) cells were purchased from ATCC (Manassas, VA). A549 cells were grown in F12K medium (Gibco – Thermo Fisher Scientific, Waltham, Massachusetts, US) while HEK293 cells were maintained in EMEM medium (ATCC). All media were supplemented with 10% FBS (unless otherwise stated) and 1% antimycotic.

Transfection with siRNA

siRNA transfections were carried out by Lipofectamine RNAiMax (Thermo Fisher Scientific, Waltham, MA, USA) following manufacturer's specifications. Briefly, cells were seeded onto a 35 mm dish at a 50-60% confluency and let to adhere overnight. The cells were transfected the following day with 25 pmol of siRNA diluted into OptiMem medium (Gibco – Thermo Fisher Scientific, Waltham, Massachusetts, US) and mixed with Lipofectamine RNAiMax. The mixture was incubated for 10 minutes at room temperature and then added to the cells without changing the medium for 72 hours in order to achieve maximum knockdown of the gene of interest.

Immunofluorescence

Cells were grown onto coverslips and treated accordingly for each experiment. Fixation occurred in 2% paraformaldehyde (PFA) for 10 minutes at 37 degrees. The cells were permeabilized with 0.25% Triton for 10 minutes at room temperature, followed by a blocking step with Image-iT FX signal Enhancer (Thermo Fisher

Scientific, Waltham, Massachusetts, US) for 30 minutes at room temperature. Further blocking occurred with a one-hour incubation of the cells with 10% serum from the host of the secondary antibody. Cells were incubated with the primary antibodies overnight at 4 degrees. The following day the cells were incubated with the secondary antibodies (raised in donkey) for 1 hour at room temperature followed by subsequent washes with 1X PBS. If an experiment required the use of two mouse antibodies (e.g. experiments depicted on **Fig. 2-1**, **Fig. 2-3** and **Fig. 2-4**) we used isotype specific secondary antibodies (IgG1, IgG2a or IgG2b) raised in goat. In the end of this step the cells were counterstained with 1 μ M DAPI (Molecular Probes, Oregon, USA) for 10 minutes at room temperature and mounted on slides with ProLong Glass antifade mountant (Thermo Fisher Scientific, Waltham, Massachusetts, US). For information on antibody dilutions see **Appendix I**.

Confocal microscopy

All images were obtained on a ZEISS LSM 710 microscopy (Carl ZEISS AG, Oberkochen, Germany), equipped with a GaAsp detector and the AiryScan module, allowing us to obtain super-resolution images with lateral resolution of \sim 140 nm. Images were acquired with a 40x Oil objective at optimal pixel size and interval (for z-stacks) based on the zoom factor and the fluorophores used in each experiment. After acquisition, the Airyscan images were processed with the ZEN software (Carl ZEISS AG, Oberkochen, Germany) resulting in the final super resolution images.

Proximity ligation assay (PLA)

Duolink In Situ detection Orange kit against mouse and rabbit antibodies was purchased from Sigma Aldrich and performed based on the manufacturer's recommendations. Briefly, we followed the immunofluorescence protocol described above until the overnight primary antibody incubation step. The following day the cells were washed with the buffer A that included within the kit and incubated with the secondary antibodies coupled to the DNA probes for one hour at 37 degrees. After this step we induced the ligation of the DNA probes that are in close proximity by adding the DNA ligase for 30 minutes at 37 degrees, followed by a signal amplification step after incubation with the kit's DNA polymerase for 200 minutes at 37 degrees. After the necessary washing steps, the cells were mounted on #1.5 coverslips with the DAPI-containing mounting medium that came with the kit and sealed with nail polish.

Staining of the cells with mitotraker

Mitotracker dyes were purchased from Molecular probes (Oregon, USA) and used according to manufacturer's instructions. Briefly, the mitotracker dyes were dissolved into DMSO, aliquoted and stored at -20 degrees. Cells were stained with 150 nM of mitotracker added into the medium for 30 minutes at 37 degrees. If the cells had to be fixed, we followed the immunofluorescence protocol.

Image analysis and 3D video reconstruction

All images were analyzed with FIJI⁵², either manually or via macros written in the ImageJ macro language. In general, we thresholded all the channels of interest by using

the Otsu thresholding algorithm after a smoothing step by using a Gaussian blur filter with a radius of 2 pixels. All the macros used in this chapter can be found in **Appendix II**.

Immunoblots

Standard SDS-PAGE experiments performed as described previously⁵³. Cells were pelleted and lysed on ice cold RIPA buffer for 30 minutes while vortexing every 10 minutes. The samples were then centrifuged at 10,000 rpm for 20 minutes in a TA-15 rotor of an Allegra 25R centrifuge (Beckman Coulter, Brea, CA, USA). After the centrifugation step we discarded the pellet and used the supernatant for further experiments. Protein concentration was identified by using a BCA kit (Thermo Fisher Scientific, Waltham, Massachusetts, US) and measured on a SpectraMax i3 (Molecular Devices, San Jose, CA, USA). The samples were then diluted to a final concentration of 1 mg/ml in RIPA buffer and 1X SDS buffer (Bio Rad, Hercules, CA, USA). The samples were then boiled to 98 degrees for 5 minutes. If the initial sample contained nuclei, we lysed it in RIPA for 10 minutes and sonicated it with three quick pulses using a 60 sonic dismembrator (Thermo Fisher Scientific, Waltham, Massachusetts, US). The sonication power was set to 20%. After that step we continued with the centrifugation as described before.

All samples were loaded on 12% polyacrylamide gels. The gels were transferred to 0.22 nm pore nitrocellulose membranes (Bio Rad, Hercules, CA, USA) using a Trans-blot turbo transfer apparatus following the manufacturer's instructions (Bio Rad, Hercules, CA, USA). After transferring we incubated the membranes with Ponceau S

(Thermo Fisher Scientific, Waltham, Massachusetts, US) to verify efficient loading and transferring of the proteins onto the membrane. Membranes were then washed with TBS-T and blocked with 5% milk in TBS-T for 1 hour at room temperature. The membranes were then incubated with the primary antibody in TBS-T containing 2% milk overnight at 4 degrees with gentle rotation. The following day the membranes were washed with TBS-T and incubated with the appropriate secondary antibodies coupled to horseradish peroxidase (Cell Signaling Technology, Danvers, MA, USA). Protein bands were detected after incubation of the membranes with ECL buffer (Thermo Fisher Scientific, Waltham, Massachusetts, US) and visualized on a Chemidoc machine (Bio Rad, Hercules, CA, USA). If stripping was necessary, we used a commercially available stripping buffer (Thermo Fisher Scientific, Waltham, Massachusetts, US) and repeated the procedure described above starting from the initial blocking step with 5% milk in TBS-T. For information on antibody dilutions see **Appendix I**.

Co-immunoprecipitation

Co-immunoprecipitation experiments were performed as previously described. Briefly, cells were grown on 150 mm dishes until 90-95% confluency. The cells were lysed in the plate after addition of a commercially available lysis buffer suitable for co-immunoprecipitation experiments (Thermo Fisher Scientific, Waltham, Massachusetts, US) and measured protein via a BCA kit purchased from Thermo Fisher Scientific following the manufacturer's instructions. We pulled down the protein of interest from 500 µg of protein by adding a primary antibody in the tube, while rotating it at 4 degrees

overnight. The following day we added 30 μ L magnetic beads slurry (Thermo Fisher Scientific, Waltham, Massachusetts, US) coupled with either protein A or G (based on the antibody host and IgG subtype) in each tube and incubated for 1 hour at 4 degrees under gentle rotation. Protein elution from the beads for all experiments but the one depicted on **Fig. 2-7C** was done after addition of 2X loading buffer (Bio Rad, Hercules, CA, USA) in each tube and boiling for 10 minutes at 55 degrees. The eluted fraction was diluted into 1X by addition of equal volume of lysis buffer and then loaded on a polyacrylamide gel for further analysis by western blot. For the experiment depicted on **Fig. 2-7C** we eluted the proteins from the beads by adding 100 μ L of Glycine 0.2 M (pH 2.6) for 10 minutes followed by removal of the magnetic beads. The acidified sample was neutralized by the addition of 100 μ L of Tris (pH 8.0) and 2X loading buffer (Bio Rad, Hercules, CA, USA).

Histone extraction

Histones extracted by using a commercially available kit bought from EpigenTek (Brooklyn, NY) following the manufacturer's instructions. Briefly, cells were pelleted by centrifugation and lysed with the lysis buffer that came with the kit followed by a centrifugation step. The supernatant that contained histones was transferred to a new tube and mixed with a balance buffer for pH normalization that came with the kit.

Isolation of functional nuclei

A nuclear isolation kit: Nuclei PURE prep was purchased from Sigma Aldrich. Functional nuclei were isolated based on the manufacturer's instructions. Briefly, cells

grew in a 150 mm dish until 90-95% confluency. Cells were scrapped from the plate and lysed on the kit's lysis buffer for 30 minutes while mixing them every 10 minutes. After the lysis step the nuclei were loaded on a 2 M sucrose cushion and centrifuged at 30,000 g for 45 minutes at 4 degrees. The isolated nuclei were maintained in the kit's nuclear storage buffer until used for downstream experiments.

Treatment of cells with EGF

Before treatment with EGF cells were synchronized to the G0 phase of the cell cycle by serum deprivation for 24 hours. Then we treated the cells with 500 ng/ml EGF (Sigma Aldrich) into complete medium (10% FBS) for 2 hours before ending the experiment unless otherwise stated.

Statistical analyses

All statistical analyses performed on STATA (StataCorp LLC, Texas, USA). We used student's t test (for comparison between two groups) or one-way ANOVA (for multiple groups). For one-way ANOVA, significance was obtained by applying a Bonferroni post-hoc analysis. Significance for all statistical testing was considered to be $P < 0.05$.

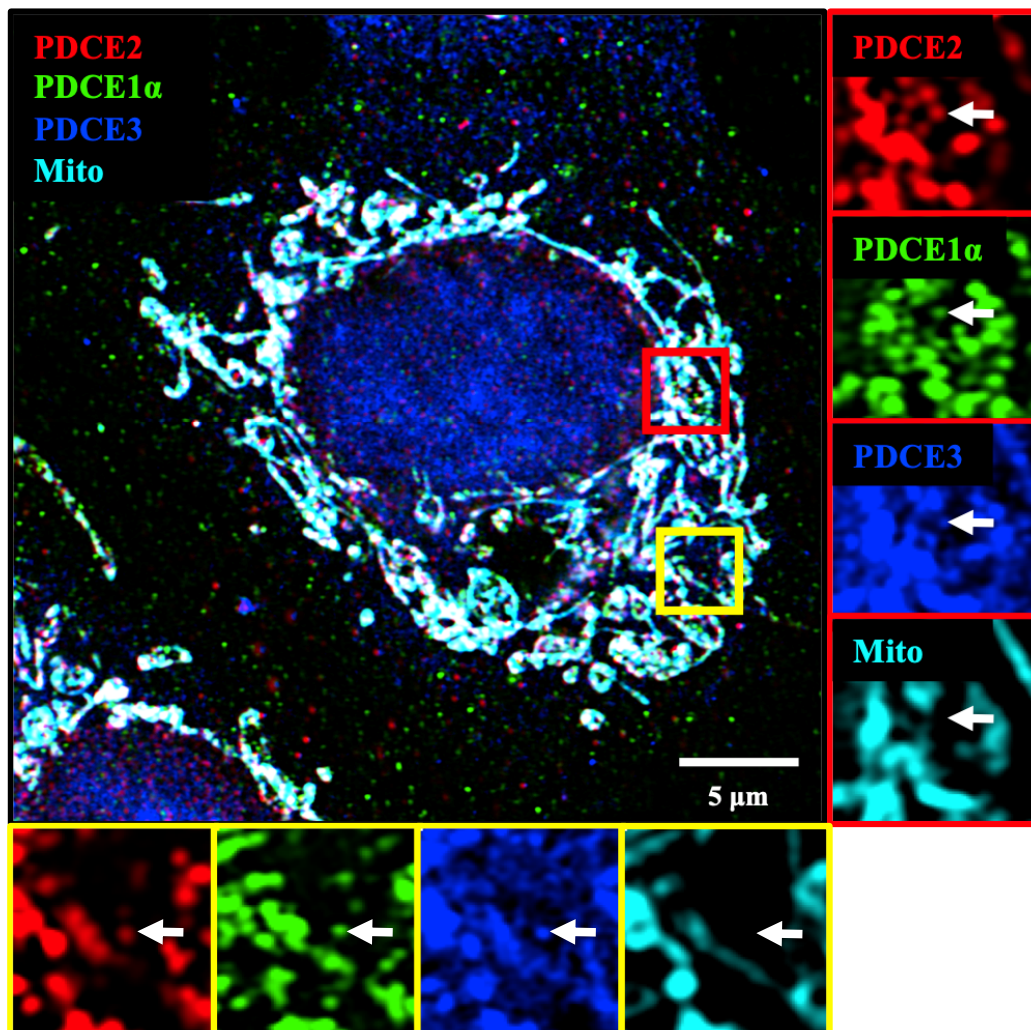
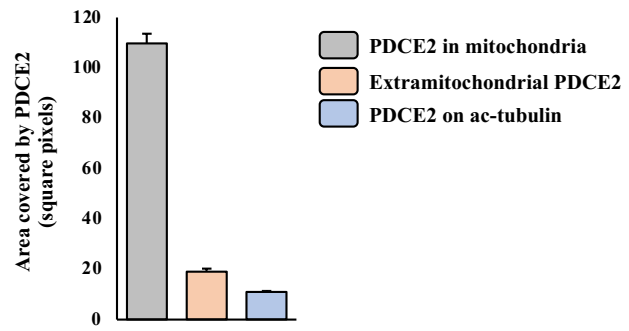
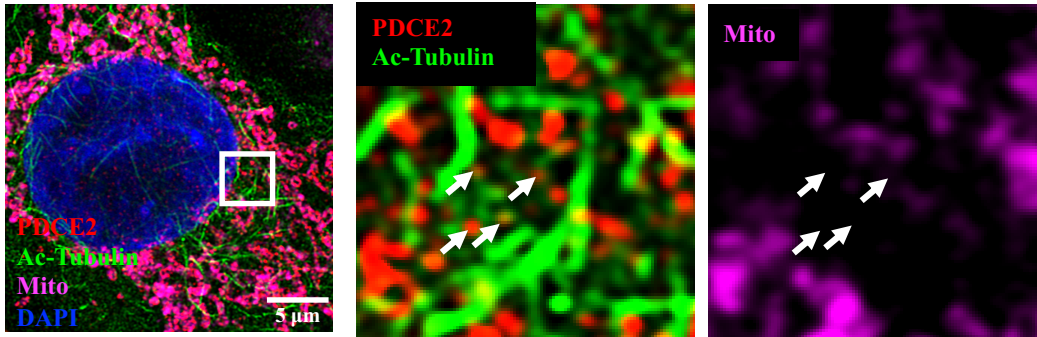


Fig. 2-1 PDC can be found outside the mitochondria as a whole complex while translocating into the nucleus. A super resolution confocal microscope image of an A549 cell stimulated with serum and EGF (500 ng/ml) showing extramitochondrial PDC while translocating into the nucleus (white arrows). The cells were stained with antibodies against PDCE2 (red), PDCE1 α (green) and PDCE3 (blue). Mitochondria were stained with mitotracker red (cyan). Scale bar is set at 5 μ m.

A

A549 cells



B

HEK cells

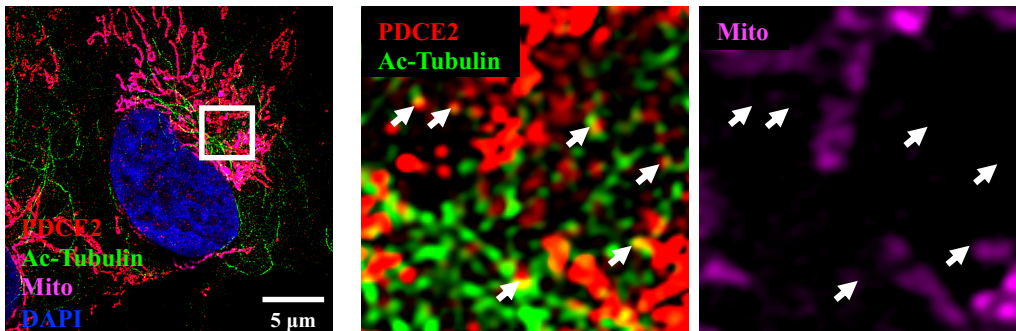


Fig. 2-2 Extramitochondrial PDC is localized on acetylated microtubules while translocating into the nucleus. Super resolution confocal images of A549 (A) and HEK (B) cells stimulated with serum and EGF (500 ng/ml) for 2 hours. The cells were stained with antibodies against PDCE2 (green) and acetyl-tubulin (red). The nucleus was counterstained with DAPI (blue). White arrows point to extramitochondrial PDCE2 that colocalizes with acetylated microtubules. n = 60 cells of 3 experiments. Error bars represent SEM. Scale bar is at 5 μ m.

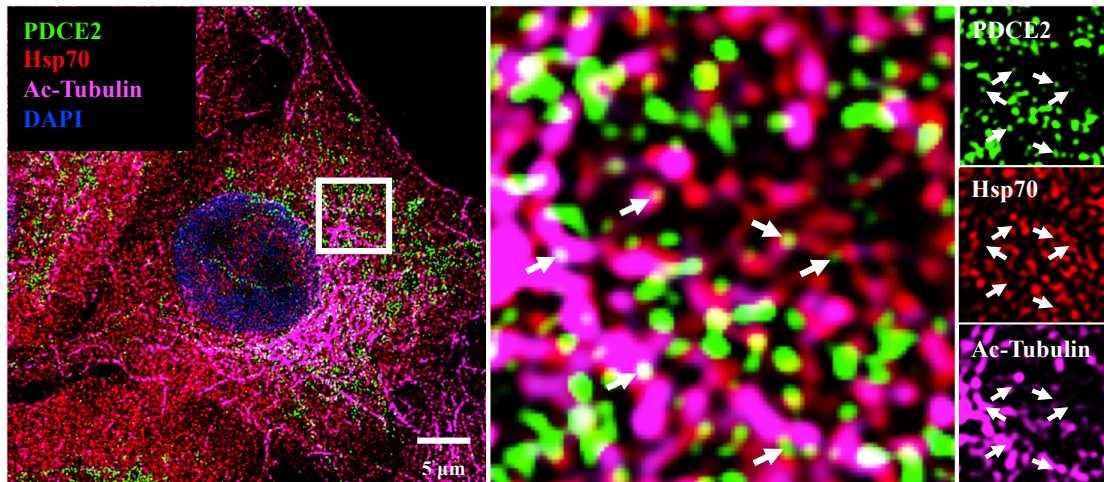


Fig. 2-3 Extramitochondrial PDC colocalizes with both acetylated microtubules and Hsp70. PDCE2 (green), indicated by white arrows, colocalizes with Hsp70 (red) on acetylated microtubules (magenta) of A549 cells stimulated with serum and EGF (500 ng/ml). Cells were imaged under a super resolution microscope. The nucleus was counterstained with DAPI (blue). Scale bar is at 5 μm.

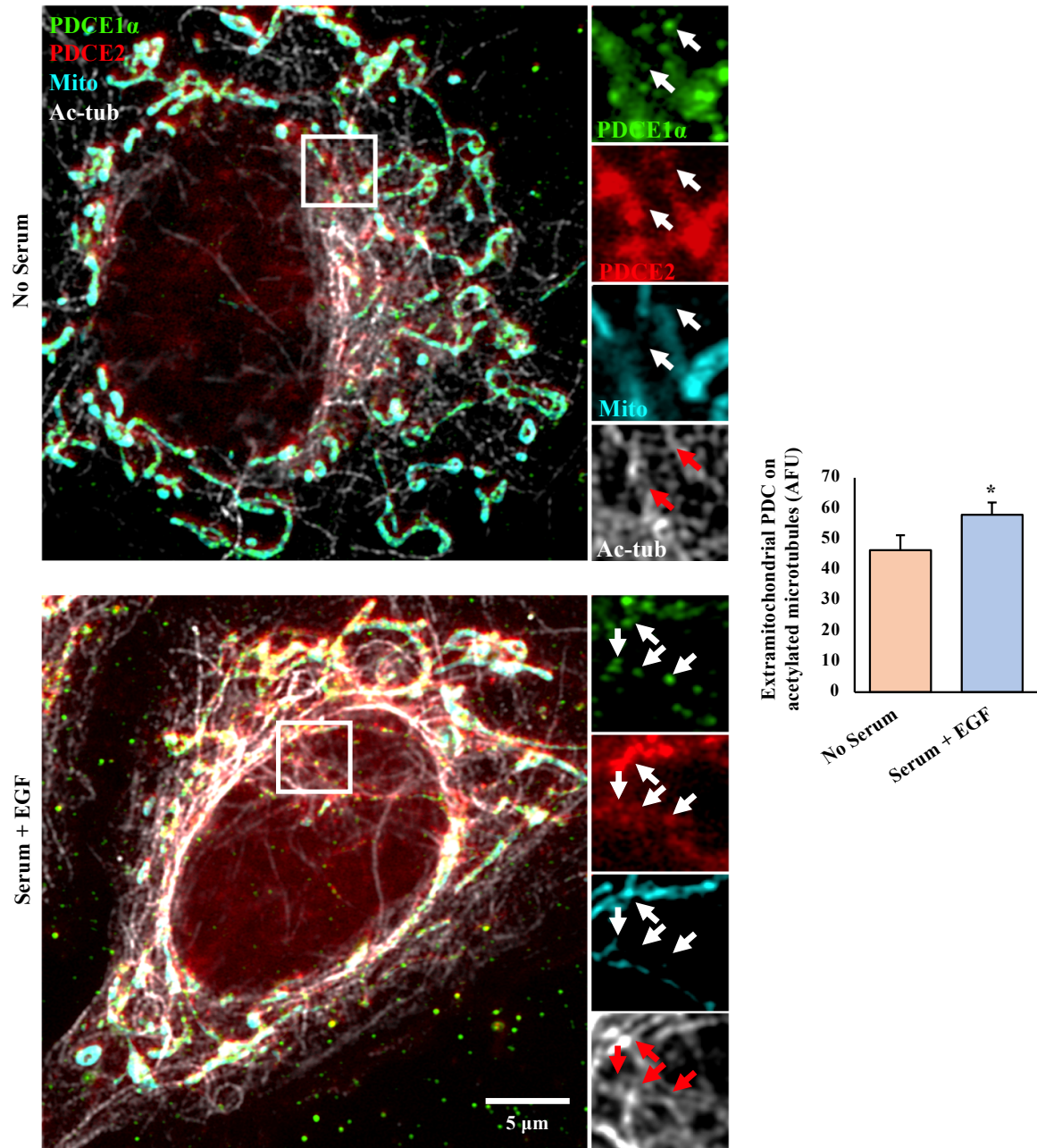


Fig. 2-4 Proliferative stimuli increase the colocalization of extramitochondrial PDC with acetylated microtubules. Super resolution confocal images of an A549 cell stained for PDCE1 α (green), PDCE2 (red), acetyl-tubulin (grey) and mitotracker (cyan). Exposure to serum and EGF (500 ng/ml) increased the association of extramitochondrial PDC (E1 α and E2) with acetyl-tubulin (white and red arrows), suggesting that PDC translocates into the nucleus via acetylated microtubules. n = 80 cells per group in 3 experiments. P value is 0.042 obtained by student's t test. Scale bar is at 5 μ m.

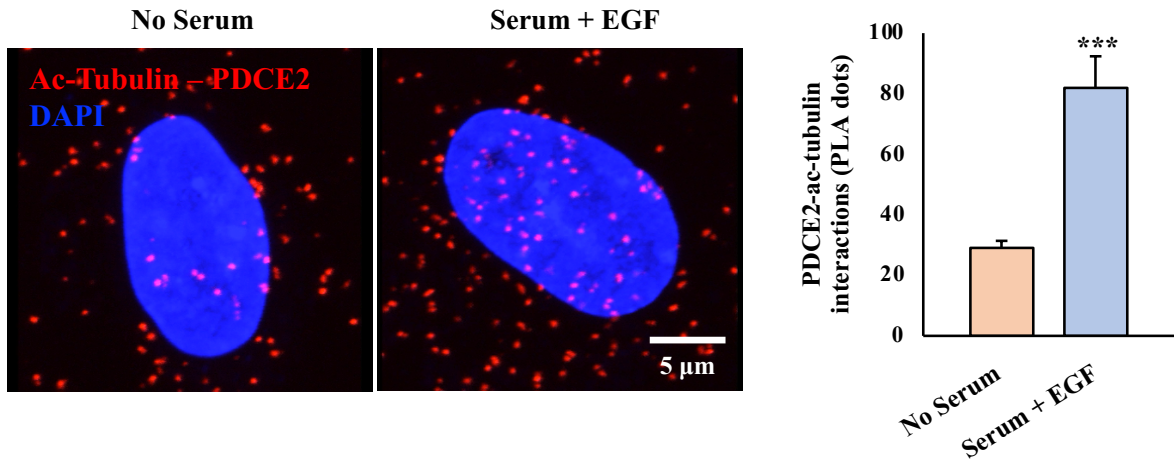


Fig. 2-5 Proliferative stimuli increase the association of extramitochondrial PDC with acetylated microtubules. PLA assay between PDCE2 and acetylated tubulin (red dots) on A549 cells that were exposed to serum and EGF (500 ng/ml) for 1 hour. Exposure to serum and EGF increases the association of the two proteins. The nuclei were counterstained with DAPI (blue). n = 100 cells per group in 3 experiments. P value <0.0001 assessed by student's t test.

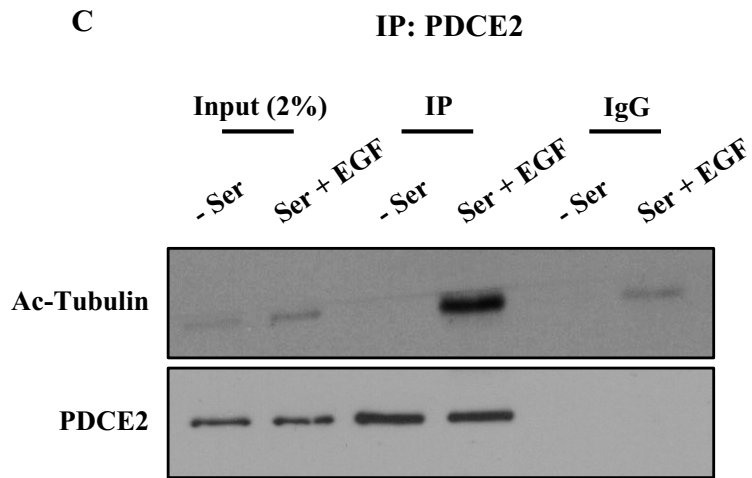
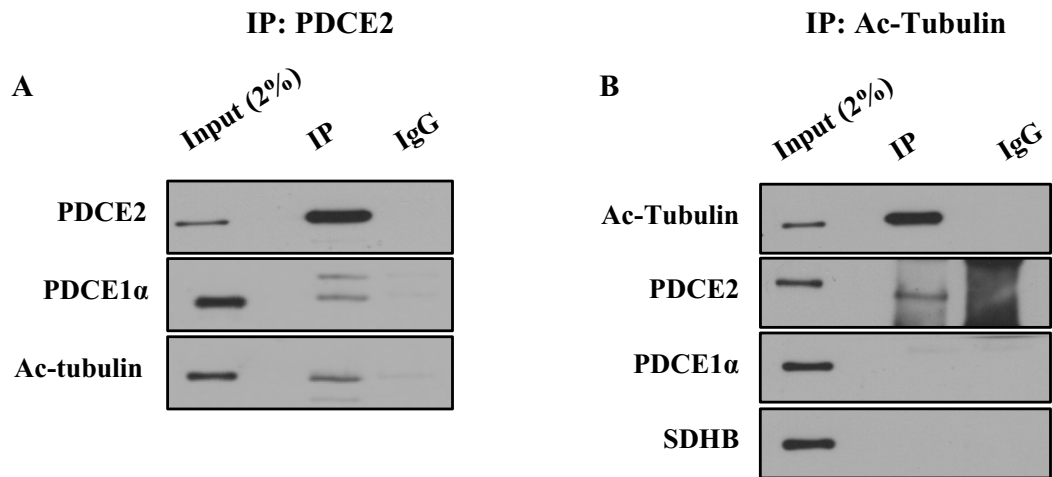


Fig. 2-6 PDC interacts directly with acetylated tubulin via its E2 subunit. co-immunoprecipitation of PDCE2 (**A**) and acetyl-tubulin (**B**) from A549 cells that were previously synchronized and re-exposed to serum and EGF (500 ng/ml) for 1 hour showing that the two proteins interact directly. PDCE1 α was present when we immunoprecipitated PDCE2 but not acetyl-tubulin, suggesting that PDC binds to acetylated microtubules via its E2 subunit, potentially offering a secondary binding site of the Hsp70-PDC complex on the microtubules while navigating the cytoplasm. SDHB was used as a negative control when we immunoprecipitated acetyl-tubulin. The input for both experiments was 2% of the total amount of protein from which we performed the co-immunoprecipitation. **C**) A co-immunoprecipitation experiment (PDCE2) showing that exposure of A549 cells to serum and EGF (500 ng/ml) increases the binding of PDC onto acetylated microtubules via its E2 subunit.

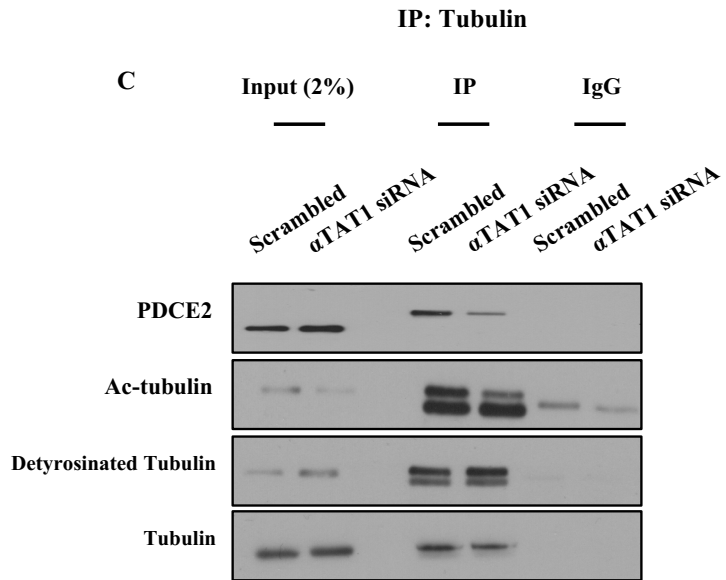
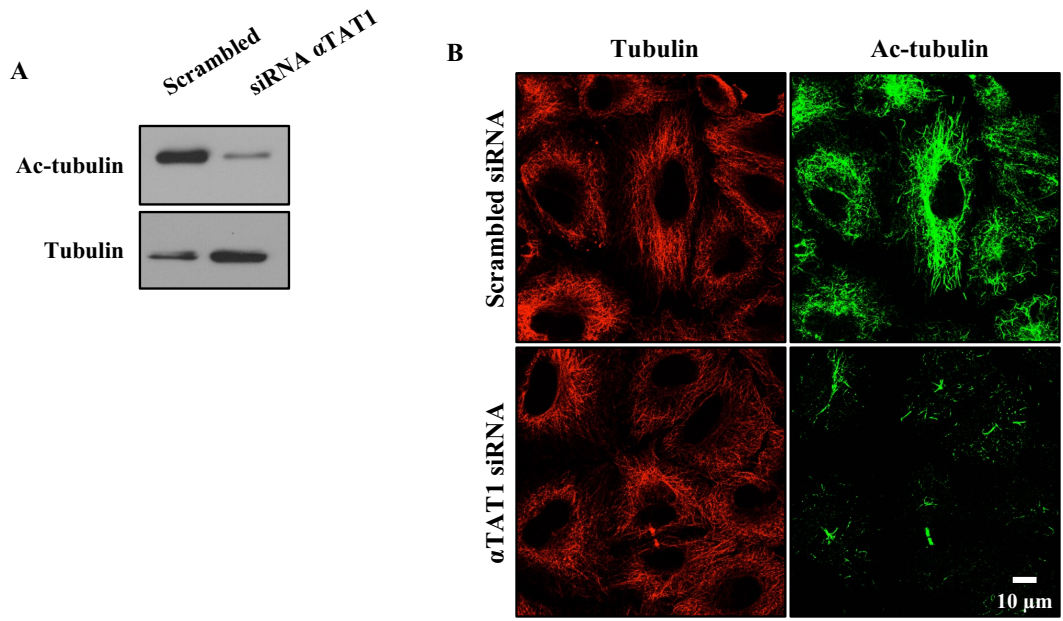


Fig. 2-7 Binding of PDC onto microtubules is regulated by tubulin acetylation and not the stability of the microtubule network. (A-B) siRNA knockdown of the main tubulin acetyltransferase α TAT1 greatly decreases tubulin acetylation on A549 cells as seen on an immunoblot and an immunofluorescence experiment. **C)** A co-immunoprecipitation experiment (tubulin) showing that loss of tubulin acetylation by α TAT1 knockdown via siRNA decreases the binding of PDC onto microtubules after exposure to serum and EGF (500 ng/ml). The presence of detyrosinated-tubulin, another marker of microtubule stability along acetyl-tubulin, suggests that PDC's binding onto microtubules is regulated by tubulin acetylation and not microtubule stability.

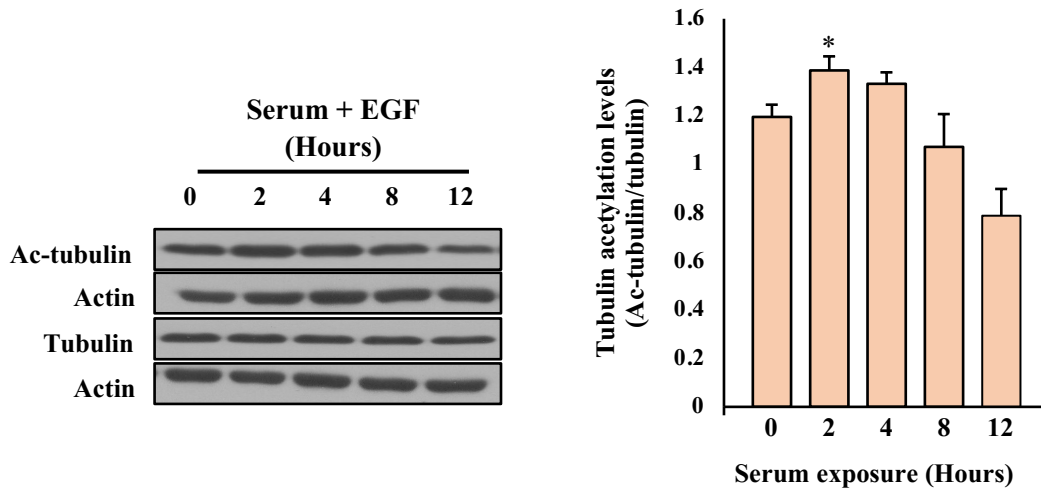


Fig. 2-8 Tubulin acetylation peaks after two hours of exposure to serum and EGF.

Immunoblot of synchronized A549 cells that were re-exposed to serum and EGF (500 ng/ml) for 2, 4, 8 and 12 hours. Serum + EGF increased tubulin acetylation that peaked after two hours from the initiation of the experiment. Acetyl-tubulin levels remained unchanged at four hours since the addition of serum and started to decrease thereafter. P value = 0.012 between the 0 and 2 hours group as assessed by ANOVA with Bonferroni post-hoc analysis. n = three experiments. Error bars represent SEM.

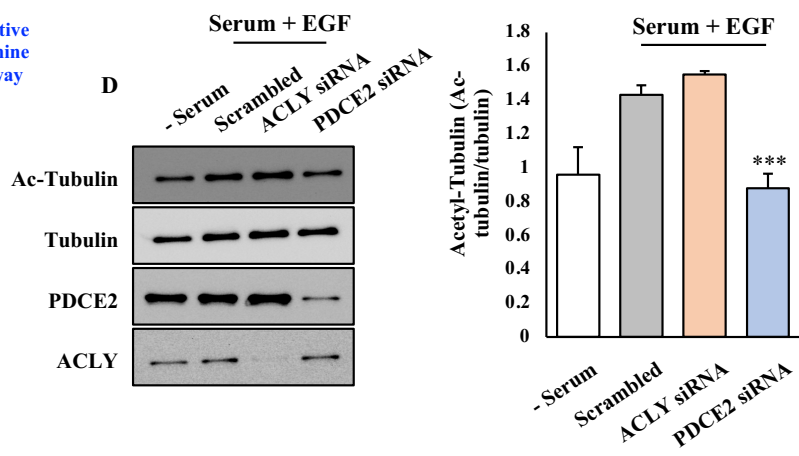
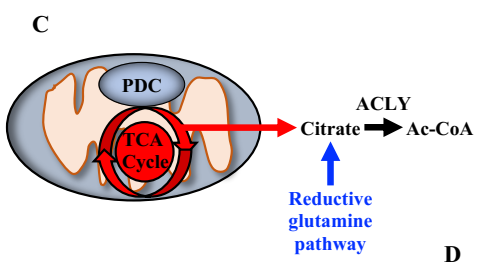
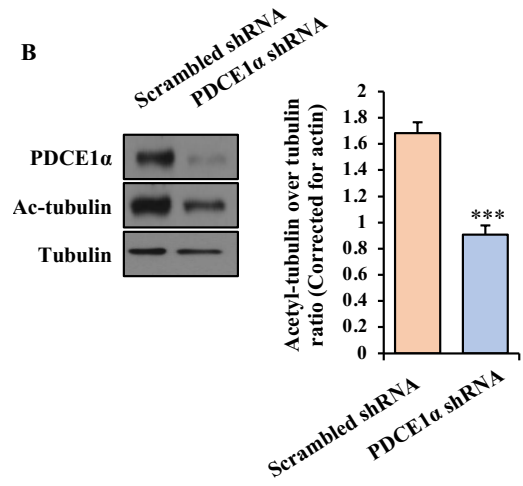
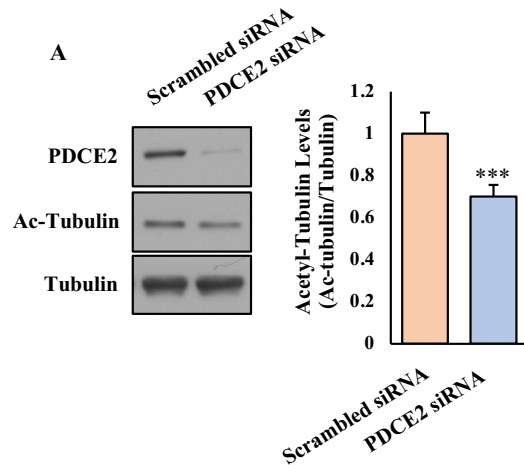


Fig. 2-9 Loss of PDC decreases tubulin acetylation. (A-B) Knock down of PDCE2 and PDCE1 α in A549 cells by siRNA and shRNA respectively resulted in a decrease of tubulin acetylation as seen on immunoblots. n = 4 experiments. Error bars represent SEM. P values > 0.001 in both experiments as assessed by student's t test. **C)** Cytoplasmic citrate is generated either through the TCA cycle in the mitochondria or the reductive glutamine pathway in the cytoplasm, which is used by ACLY to generate acetyl-CoA, contributing to the cytoplasmic pool of the metabolite. **D)** Immunoblot showing that loss of PDCE2 but not ACLY, one of the main acetyl-CoA producers in the cytoplasm, results in decreased tubulin acetylation levels. n = 3 experiments. Error bars represent SEM. P value > 0.001 as assessed by one-way ANOVA with Bonferroni post-hoc analysis.

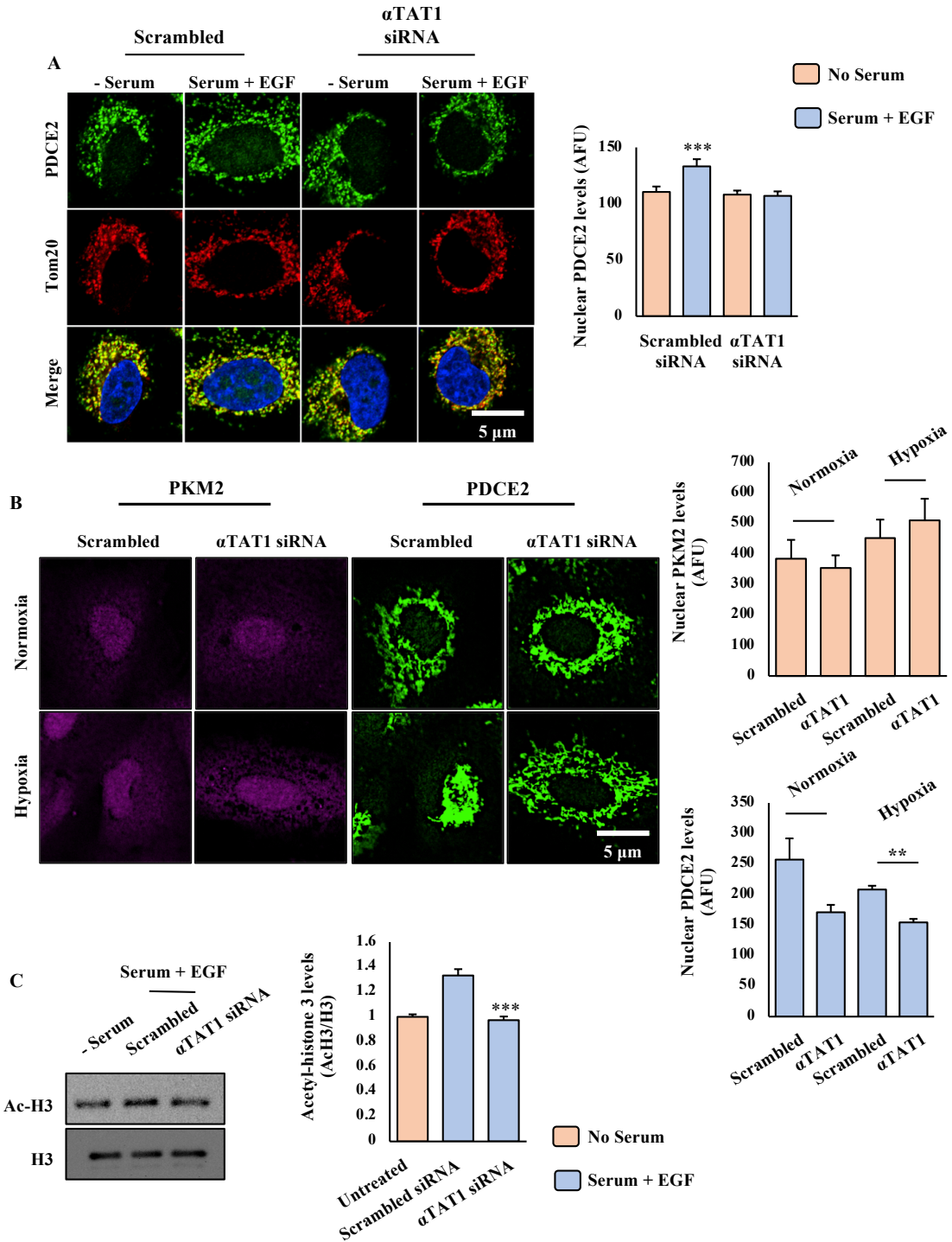


Fig. 2-10 Loss of tubulin acetylation decreases nuclear PDC and acetyl-histone 3 levels. **A)** Loss of α TAT1 by siRNA decreased nuclear PDCE2 (green) levels in A549 cells that were stimulated with serum and EGF (500 ng/ml) for two hours. Mitochondria were stained with an antibody against the mitochondrial outer membrane marker Tom20 (red). Nuclei were stained with DAPI (blue). P value < 0.001 between the scrambled and α TAT1 siRNA groups when exposed to serum and EGF as assessed by one-way ANOVA with Bonferroni post-hoc analysis. n = 90 cells per group in 3 experiments. **B)** Immunofluorescence experiment showing A549 cells that were exposed to 1% hypoxia for 24 hours after treatment with scrambled and α TAT1 siRNA. The cells were stained with antibodies against PKM2 (magenta) and PDCE2 (green). Loss of tubulin acetylation decreased the levels of nuclear PDCE2 compared to the normoxic group but had no effect on PKM2. Scale bar at 5 μ m. P value for the nuclear PDCE2 levels between the scrambled and α TAT1 siRNA groups in hypoxia was 0.0021 as assessed by one-way ANOVA. Error bars represent SEM. n = 80 cells per group in 3 experiments. **C)** Loss of α TAT1 by siRNA resulted in decreased acetyl-histone 3 levels after exposure of synchronized A549 cells to serum and EGF. n = 3 experiments. P value < 0.001 between the scrambled and α TAT1 siRNA groups when exposed to serum and EGF as assessed by student's t test. Error bars represent SEM on both analyses.

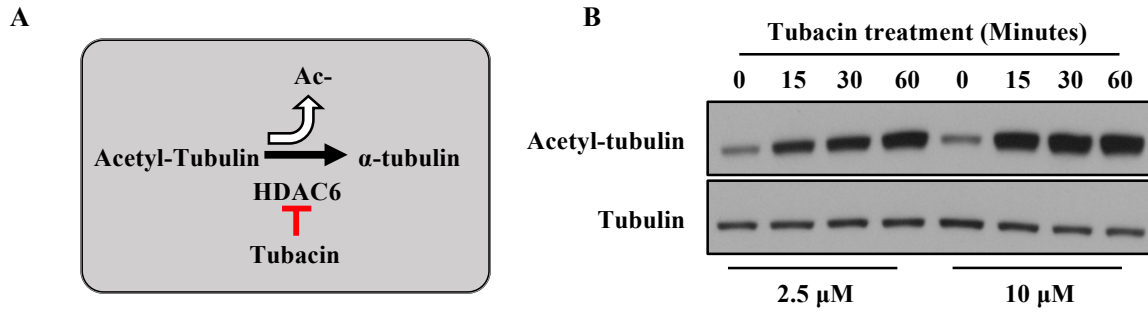


Fig. 2-11 Tubacin increases tubulin acetylation. **A)** Mechanism of action of tubacin. **B)** Immunoblot of A549 cells treated with two different doses of tubacin (2.5 μ M and 10 μ M) for 15, 30 and 60 minutes. Treatment with tubacin greatly increases tubulin acetylation even after 15 minutes of treatment with the lower dose (2.5 μ M).

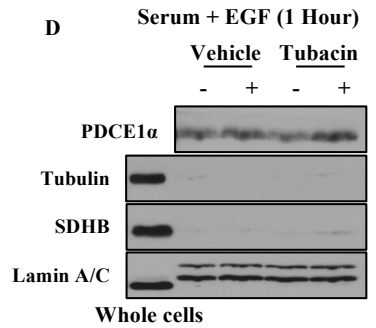
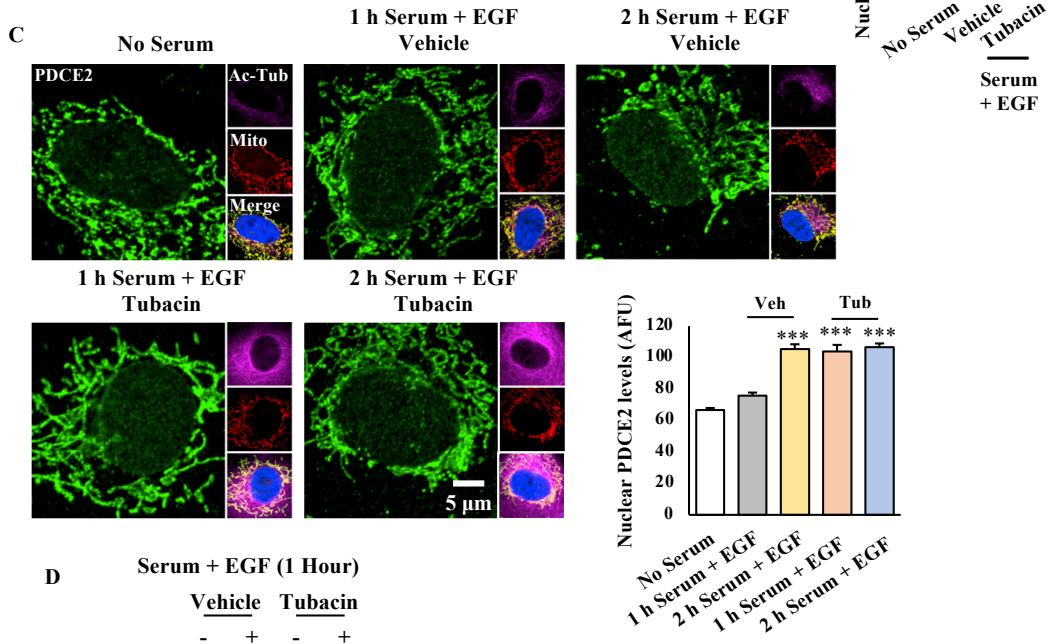
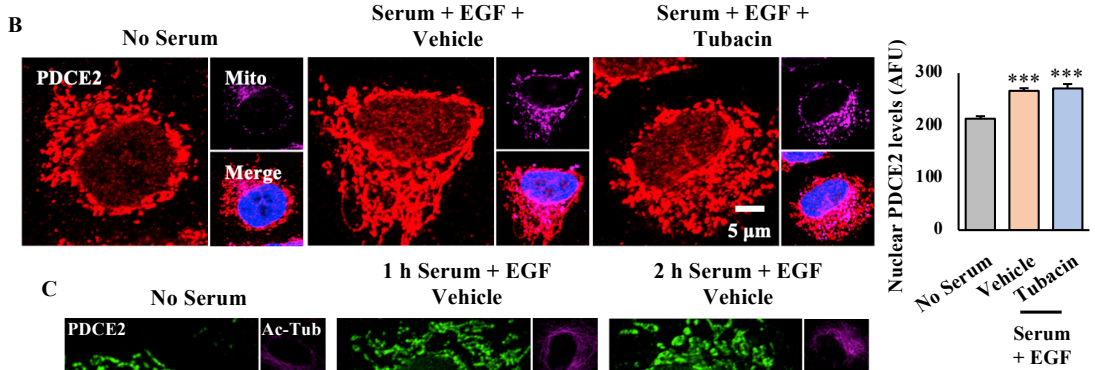
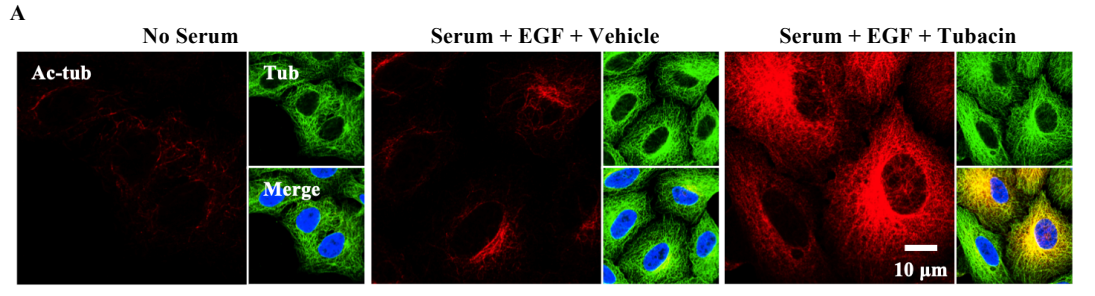
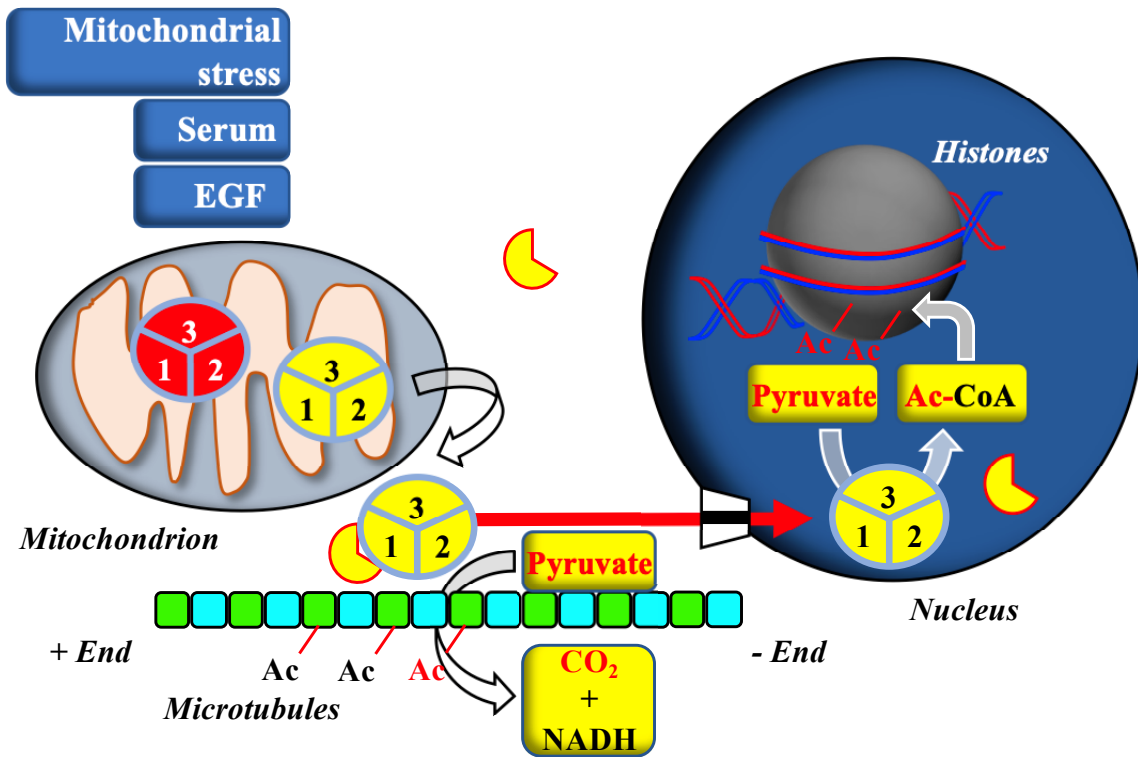


Fig. 2-12 Increased tubulin acetylation results in a faster and more efficient nuclear translocation of PDC. **A)** A549 cells treated with 2.5 μ M of tubacin for 2 hours and stained for tubulin (green) and acetyl-tubulin (red). Nuclei were stained with DAPI (blue). Scale bar is at 5 μ m. **B)** A549 cells stimulated with serum and EGF (500 ng/ml) and treated with 2.5 μ M of tubacin for 2 hours were stained for PDCE2 (red) and mitotracker (magenta). Increased tubulin acetylation did not result in higher nuclear PDC levels. Nuclei were stained with DAPI (blue). n = 100 cells per group in 3. P values were less than 0.0001 as assessed by one-way ANOVA with Bonferroni post-hoc analysis. Scale bar is at 5 μ m. **C)** A549 cells treated with 2.5 μ M of tubacin and serum + EGF (500 ng/ml) for 1 and 2 hours and stained for PDCE2 (green) acetyl-tubulin (magenta) and mitotracker (red). Increased tubulin acetylation resulted in increased levels of nuclear PDCE2 after 1 hour of treatment, suggesting that increased tubulin acetylation results in a faster and more efficient nuclear translocation of PDC. Nuclei were stained with DAPI (blue). n = 90 cells per group in 3 experiments. P values were less than 0.0001 as assessed by one-way ANOVA with Bonferroni post-hoc analysis. Scale bar is at 5 μ m. **D)** Immunoblot of isolated nuclei from A549 cells stimulated with serum and EGF (500 ng/ml) for 1 hour in the presence or absence of tubacin (2.5 μ M). Treatment with tubacin resulted in higher nuclear PDCE1 α levels compared to the vehicle group upon stimulation with serum and EGF. Nuclear purity was assessed by the absence of tubulin and the mitochondrial succinate dehydrogenase B (SDHB) and the presence of lamin A/C.



Legend

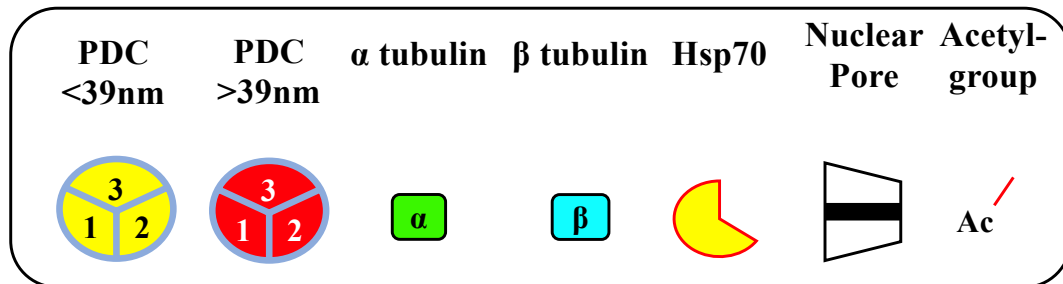


Fig. 2-13 Proposed model for the nuclear translocation of PDC along acetylated microtubules.

References

- 1 Berg, J. M., Tymoczko, J. L., Stryer, L., & Stryer, L. *Biochemistry*. 7th edn, (New York: W.H. Freeman, 2002).
- 2 Patel, M. S., Nemeria, N. S., Furey, W. & Jordan, F. The pyruvate dehydrogenase complexes: structure-based function and regulation. *J Biol Chem* **289**, 16615-16623, doi:10.1074/jbc.R114.563148 (2014).
- 3 Zhou, Z. H. *et al.* Direct evidence for the size and conformational variability of the pyruvate dehydrogenase complex revealed by three-dimensional electron microscopy. The "breathing" core and its functional relationship to protein dynamics. *J Biol Chem* **276**, 21704-21713, doi:10.1074/jbc.M101765200 (2001).
- 4 Vijaykrishnan, S. *et al.* Solution structure and characterisation of the human pyruvate dehydrogenase complex core assembly. *J Mol Biol* **399**, 71-93, doi:10.1016/j.jmb.2010.03.043 (2010).
- 5 Sumegi, B., Liposits, Z., Inman, L., Paull, W. K. & Srere, P. A. Electron microscopic study on the size of pyruvate dehydrogenase complex in situ. *Eur J Biochem* **169**, 223-230, doi:10.1111/j.1432-1033.1987.tb13601.x (1987).
- 6 Sutendra, G. *et al.* A nuclear pyruvate dehydrogenase complex is important for the generation of acetyl-CoA and histone acetylation. *Cell* **158**, 84-97, doi:10.1016/j.cell.2014.04.046 (2014).

- 7 Chen, J. *et al.* Compartmentalized activities of the pyruvate dehydrogenase complex sustain lipogenesis in prostate cancer. *Nat Genet* **50**, 219-228, doi:10.1038/s41588-017-0026-3 (2018).
- 8 Ferriero, R. *et al.* Pyruvate dehydrogenase complex and lactate dehydrogenase are targets for therapy of acute liver failure. *J Hepatol* **69**, 325-335, doi:10.1016/j.jhep.2018.03.016 (2018).
- 9 Matsuda, S. *et al.* Nuclear pyruvate kinase M2 complex serves as a transcriptional coactivator of arylhydrocarbon receptor. *Nucleic Acids Res* **44**, 636-647, doi:10.1093/nar/gkv967 (2016).
- 10 Nagaraj, R. *et al.* Nuclear Localization of Mitochondrial TCA Cycle Enzymes as a Critical Step in Mammalian Zygotic Genome Activation. *Cell* **168**, 210-223 e211, doi:10.1016/j.cell.2016.12.026 (2017).
- 11 Richard, A. J., Hang, H. & Stephens, J. M. Pyruvate dehydrogenase complex (PDC) subunits moonlight as interaction partners of phosphorylated STAT5 in adipocytes and adipose tissue. *J Biol Chem* **292**, 19733-19742, doi:10.1074/jbc.M117.811794 (2017).
- 12 Zhou, W. *et al.* Nuclear accumulation of pyruvate dehydrogenase alpha 1 promotes histone acetylation and is essential for zygotic genome activation in porcine embryos. *Biochim Biophys Acta Mol Cell Res* **1867**, 118648, doi:10.1016/j.bbamcr.2020.118648 (2020).

- 13 Brouhard, G. J. & Rice, L. M. Microtubule dynamics: an interplay of biochemistry and mechanics. *Nat Rev Mol Cell Biol* **19**, 451-463, doi:10.1038/s41580-018-0009-y (2018).
- 14 Hirokawa, N., Noda, Y., Tanaka, Y. & Niwa, S. Kinesin superfamily motor proteins and intracellular transport. *Nat Rev Mol Cell Biol* **10**, 682-696, doi:10.1038/nrm2774 (2009).
- 15 Kardon, J. R. & Vale, R. D. Regulators of the cytoplasmic dynein motor. *Nat Rev Mol Cell Biol* **10**, 854-865, doi:10.1038/nrm2804 (2009).
- 16 Wloga, D. & Gaertig, J. Post-translational modifications of microtubules. *J Cell Sci* **123**, 3447-3455, doi:10.1242/jcs.063727 (2010).
- 17 Maruta, H., Greer, K. & Rosenbaum, J. L. The acetylation of alpha-tubulin and its relationship to the assembly and disassembly of microtubules. *J Cell Biol* **103**, 571-579, doi:10.1083/jcb.103.2.571 (1986).
- 18 Piperno, G., LeDizet, M. & Chang, X. J. Microtubules containing acetylated alpha-tubulin in mammalian cells in culture. *J Cell Biol* **104**, 289-302, doi:10.1083/jcb.104.2.289 (1987).
- 19 Balabanian, L., Berger, C. L. & Hendricks, A. G. Acetylated Microtubules Are Preferentially Bundled Leading to Enhanced Kinesin-1 Motility. *Biophys J* **113**, 1551-1560, doi:10.1016/j.bpj.2017.08.009 (2017).

- 20 Reed, N. A. *et al.* Microtubule acetylation promotes kinesin-1 binding and transport. *Curr Biol* **16**, 2166-2172, doi:10.1016/j.cub.2006.09.014 (2006).
- 21 Giustiniani, J. *et al.* Tubulin acetylation favors Hsp90 recruitment to microtubules and stimulates the signaling function of the Hsp90 clients Akt/PKB and p53. *Cell Signal* **21**, 529-539, doi:10.1016/j.cellsig.2008.12.004 (2009).
- 22 Husain, M. & Harrod, K. S. Enhanced acetylation of alpha-tubulin in influenza A virus infected epithelial cells. *FEBS Lett* **585**, 128-132, doi:10.1016/j.febslet.2010.11.023 (2011).
- 23 Chacinska, A., Koehler, C. M., Milenkovic, D., Lithgow, T. & Pfanner, N. Importing mitochondrial proteins: machineries and mechanisms. *Cell* **138**, 628-644, doi:10.1016/j.cell.2009.08.005 (2009).
- 24 Kirschke, E., Goswami, D., Southworth, D., Griffin, P. R. & Agard, D. A. Glucocorticoid receptor function regulated by coordinated action of the Hsp90 and Hsp70 chaperone cycles. *Cell* **157**, 1685-1697, doi:10.1016/j.cell.2014.04.038 (2014).
- 25 Trebble, P. J. *et al.* A ligand-specific kinetic switch regulates glucocorticoid receptor trafficking and function. *J Cell Sci* **126**, 3159-3169, doi:10.1242/jcs.124784 (2013).
- 26 Akella, J. S. *et al.* MEC-17 is an alpha-tubulin acetyltransferase. *Nature* **467**, 218-222, doi:10.1038/nature09324 (2010).

- 27 Li, L. & Yang, X. J. Tubulin acetylation: responsible enzymes, biological functions and human diseases. *Cell Mol Life Sci* **72**, 4237-4255, doi:10.1007/s00018-015-2000-5 (2015).
- 28 Smith, B. J. SDS Polyacrylamide Gel Electrophoresis of Proteins. *Methods Mol Biol* **1**, 41-55, doi:10.1385/0-89603-062-8:41 (1984).
- 29 Kinnaird, A., Zhao, S., Wellen, K. E. & Michelakis, E. D. Metabolic control of epigenetics in cancer. *Nat Rev Cancer* **16**, 694-707, doi:10.1038/nrc.2016.82 (2016).
- 30 Anastasiou, D. & Cantley, L. C. Breathless cancer cells get fat on glutamine. *Cell Res* **22**, 443-446, doi:10.1038/cr.2012.5 (2012).
- 31 Wellen, K. E. *et al.* ATP-citrate lyase links cellular metabolism to histone acetylation. *Science* **324**, 1076-1080, doi:10.1126/science.1164097 (2009).
- 32 Kalebic, N. *et al.* alphaTAT1 is the major alpha-tubulin acetyltransferase in mice. *Nat Commun* **4**, 1962, doi:10.1038/ncomms2962 (2013).
- 33 Hubbert, C. *et al.* HDAC6 is a microtubule-associated deacetylase. *Nature* **417**, 455-458, doi:10.1038/417455a (2002).
- 34 Matsuyama, A. *et al.* In vivo destabilization of dynamic microtubules by HDAC6-mediated deacetylation. *EMBO J* **21**, 6820-6831, doi:10.1093/emboj/cdf682 (2002).

- 35 Haggarty, S. J., Koeller, K. M., Wong, J. C., Grozinger, C. M. & Schreiber, S. L. Domain-selective small-molecule inhibitor of histone deacetylase 6 (HDAC6)-mediated tubulin deacetylation. *Proc Natl Acad Sci U S A* **100**, 4389-4394, doi:10.1073/pnas.0430973100 (2003).
- 36 Zhang, X. *et al.* HDAC6 modulates cell motility by altering the acetylation level of cortactin. *Mol Cell* **27**, 197-213, doi:10.1016/j.molcel.2007.05.033 (2007).
- 37 Kovacs, J. J. *et al.* HDAC6 regulates Hsp90 acetylation and chaperone-dependent activation of glucocorticoid receptor. *Mol Cell* **18**, 601-607, doi:10.1016/j.molcel.2005.04.021 (2005).
- 38 Yoshida, N. *et al.* Prediction of prognosis of estrogen receptor-positive breast cancer with combination of selected estrogen-regulated genes. *Cancer Sci* **95**, 496-502, doi:10.1111/j.1349-7006.2004.tb03239.x (2004).
- 39 Dong, J. *et al.* Hsp70 Binds to the Androgen Receptor N-terminal Domain and Modulates the Receptor Function in Prostate Cancer Cells. *Mol Cancer Ther* **18**, 39-50, doi:10.1158/1535-7163.MCT-18-0432 (2019).
- 40 Thadani-Mulero, M., Nanus, D. M. & Giannakakou, P. Androgen receptor on the move: boarding the microtubule expressway to the nucleus. *Cancer Res* **72**, 4611-4615, doi:10.1158/0008-5472.CAN-12-0783 (2012).
- 41 Kincaid, M. M. & King, S. J. Motors and their tethers: the role of secondary binding sites in processive motility. *Cell Cycle* **5**, 2733-2737, doi:10.4161/cc.5.23.3521 (2006).

- 42 Ahrens, E. H., Jr., Payne, M. A., Kunkel, H. G., Eisenmenger, W. J. & Blondheim, S. H. Primary biliary cirrhosis. *Medicine (Baltimore)* **29**, 299-364, doi:10.1097/00005792-195012000-00002 (1950).
- 43 Baum, H. & Palmer, C. The PBC-specific antigen. *Mol Aspects Med* **8**, 201-234, doi:10.1016/0098-2997(85)90007-x (1985).
- 44 Houtkooper, R. H., Pirinen, E. & Auwerx, J. Sirtuins as regulators of metabolism and healthspan. *Nat Rev Mol Cell Biol* **13**, 225-238, doi:10.1038/nrm3293 (2012).
- 45 Chu, D. T. & Klymkowsky, M. W. The appearance of acetylated alpha-tubulin during early development and cellular differentiation in *Xenopus*. *Dev Biol* **136**, 104-117, doi:10.1016/0012-1606(89)90134-6 (1989).
- 46 Almouzni, G., Khochbin, S., Dimitrov, S. & Wolffe, A. P. Histone acetylation influences both gene expression and development of *Xenopus laevis*. *Dev Biol* **165**, 654-669, doi:10.1006/dbio.1994.1283 (1994).
- 47 Moussaieff, A. *et al.* Glycolysis-mediated changes in acetyl-CoA and histone acetylation control the early differentiation of embryonic stem cells. *Cell Metab* **21**, 392-402, doi:10.1016/j.cmet.2015.02.002 (2015).
- 48 Pante, N. & Kann, M. Nuclear pore complex is able to transport macromolecules with diameters of about 39 nm. *Mol Biol Cell* **13**, 425-434, doi:10.1091/mbc.01-06-0308 (2002).

- 49 Knockenhauer, K. E. & Schwartz, T. U. The Nuclear Pore Complex as a Flexible and Dynamic Gate. *Cell* **164**, 1162-1171, doi:10.1016/j.cell.2016.01.034 (2016).
- 50 Stewart, M. Molecular mechanism of the nuclear protein import cycle. *Nat Rev Mol Cell Biol* **8**, 195-208, doi:10.1038/nrm2114 (2007).
- 51 Echeverria, P. C. *et al.* Nuclear import of the glucocorticoid receptor-hsp90 complex through the nuclear pore complex is mediated by its interaction with Nup62 and importin beta. *Mol Cell Biol* **29**, 4788-4797, doi:10.1128/MCB.00649-09 (2009).
- 52 Schindelin, J. *et al.* Fiji: an open-source platform for biological-image analysis. *Nat Methods* **9**, 676-682, doi:10.1038/nmeth.2019 (2012).
- 53 Bonnet, S. *et al.* A mitochondria-K⁺ channel axis is suppressed in cancer and its normalization promotes apoptosis and inhibits cancer growth. *Cancer Cell* **11**, 37-51, doi:10.1016/j.ccr.2006.10.020 (2007).

***Chapter three: A non-canonical pathway for the entrance of
the large mitochondrial enzyme Pyruvate Dehydrogenase
Complex (PDC) into the nucleus***

Abstract

Nuclear protein import occurs via the nuclear pores (NPs) that allow the entrance of proteins containing a nuclear localization sequence (NLS) and are up to 39 nm in diameter. The mitochondrial pyruvate dehydrogenase complex (PDC) translocates into the nucleus upon exposure to proliferative stimuli (e.g. serum and epidermal growth factor) facilitating histone acetylation by producing acetyl-CoA. PDC is among the largest enzymatic complexes with diameters up to 45 nm and it does not contain a known NLS. Its large diameter and the lack of an NLS suggest that it does not enter the nucleus by the canonical pathway. Here we describe a novel pathway for PDC's nuclear import that does not involve the NPs. Mitochondria cluster around the nucleus in response to various proliferative stimuli (serum + EGF and hypoxia) and tether to the nuclear envelope (NE) via MFN2 rich contact points (in a manner similar to their tethering onto the endoplasmic reticulum) before releasing PDC into the nucleoplasm. By using super resolution and electron microscopy we visualized PDC on the NE in areas away from the NPs. Blockage of NP trafficking via microinjection of wheat germ agglutinin decreased the levels of STAT3, a protein known to cross the NPs, but had no effect on the nuclear PDC levels. Nuclear PDC interacts with lamin A that is part of the inner nuclear membrane through its E2 subunit. This interaction is maintained during cell division, where lamin A is depolymerized and dispersed throughout the cytoplasm before forming the NE in the daughter cells, providing a way for the PDC to be released into the nucleoplasm. Our work provides a novel angle on visualizing the mitochondrial to nucleus communication and suggests the presence of a novel

mechanism for the nuclear entry of large PDC complexes that might have implications on other proteins.

3.1 Introduction

The mitochondrial pyruvate Dehydrogenase Complex (PDC) is the gatekeeping enzyme for glucose oxidation and one of the largest known enzymes in nature, with a complex and dynamic stoichiometry of 4 subunits (PDCE1-4), that can reach sizes of 10 MDa^{1,2} and diameters of 45 nm^{1,3,4}. Following translation and driven by a mitochondria-localization sequence (MLS) (and since they have no known nuclear localization sequences, NLS) the 4 subunits directly reach and enter the mitochondria, where they are folded and assembled into the PDC mega complex in the inner membrane and the MLS is excised⁵. PDC catalyzes the oxidation of pyruvate (the end product of glycolysis) to acetyl-CoA, which then enters the Krebs' cycle to complete glucose oxidation. We recently showed that PDC can translocate into the nucleus, upon exposure to proliferative stimuli like serum and epidermal growth factor (EGF) or hypoxia, as a constitutively active whole complex (Pyruvate Dehydrogenase Kinase, which inhibits the PDC function in the mitochondria, does not follow PDC into the nucleus)⁶. We also showed that nuclear (nPDC) oxidizes pyruvate into acetyl-CoA in the nucleoplasm, providing a source of acetyl-groups for the histone acetylation required for cell cycle progression⁶. This is important because the high energy state of acetyl-CoA makes it energetically unstable, requiring that it is produced close to where it is needed. Our findings were provocative because PDC's extremely large size and lack of a known NLS make it difficult to enter through the canonical pathway, i.e. through the nuclear pores (NP), which (although their diameter is somewhat dynamic in size) allow the entrance of molecules less than 39 nm⁷. Yet, our findings were soon confirmed by several independent groups that also showed functional PDC in the nucleus in both cancer and normal cells⁸⁻¹³.

Here we show that intact PDC can enter the nucleus via a non-canonical pathway that does not involve the NPs. We found that under proliferative stimuli, mitochondria cluster around the nucleus and tether onto the outer membrane of the nuclear envelope (NE), an extension of the endoplasmic reticulum, via mitofusin 2 (MFN2); in a process analogous to the MFN2-mediated tethering of mitochondria to the endoplasmic reticulum (ER) to allow inter-organelle molecule exchange^{14,15}. The tethered mitochondria then release PDC through the NE and onto the lamin layer, which forms the inner nuclear membrane. We found that PDC can bind to lamin A before entering the nucleoplasm. With live imaging we directly visualized PDC going through the lamin layer and entering the nucleoplasm at sites where no NP was present, particularly within nuclear invaginations. More PDC entered the nucleus at the time of cell division, when the lamin layer disassembles due to lamin depolymerization¹⁶. When it reassembles later to form the daughter nuclei, lamin-bound PDC can enter the nucleoplasm. Our work describes for the first time a mechanism for direct entrance of very large molecules into the nucleus, independent of nuclear pores, that may also be relevant to the mechanisms that bacteria or viruses use to enter the nucleus. For example, retroviruses like the Murine Leukemia Virus (diameter 80-130 nm) can enter the nucleus during mitosis (when the NE and lamin layer are disrupted) and the smaller Parvoviruses (diameter 18-26 nm) enter the nucleus not through NPs, but directly by causing localized disruptions of the NE and lamin layer¹⁷. Rickettsia, considered potential ancestors of mitochondria¹⁸, are found to nest and grow into the nucleus of mammalian cells, via an unknown mechanism of entry¹⁹.

Results

3.2 Mitochondria cluster around the nucleus and tether on the nuclear envelope, following proliferation stimuli

Since mitochondria can travel in the cytoplasm with the help of motor proteins on microtubules, we hypothesized that clustering around the nucleus may facilitate the translocation of PDC from mitochondria into the nucleoplasm. We used synchronized A549 cells and exposed them to serum and Epidermal Growth Factor (EGF) for 1, 2 and 4 hours before fixing and staining them with antibodies against PDCE2 and lamin A, while mitochondria were stained with mitotracker-red. To measure the distance of the mitochondria from the nuclear periphery we obtained z stacked super-resolution confocal images and used a software code that allowed us to measure the intensity of the mitotracker signal within 350 nm (i.e. the size of ~ 2 pixels in our super-resolution confocal microscope which has a resolution of ~160 nm) from the outer edge of the lamin layer (which includes the ~50 nm thickness of the NE). We found clustering of mitochondria around the nucleus, that peaked 1 hour after the treatment, while nuclear PDCE2 (nPDCe2) levels peaked after 2 hours, in keeping with our hypothesis that perinuclear mitochondrial clustering precedes PDC's nuclear entry (**Fig. 3-1A**). To test this with another cell type, another PDC subunit (i.e. PDCE1), a different proliferative stimulus and a different method, we used human foreskin fibroblasts (HFF-1) exposed to 1% hypoxia for 24 hours and found again clustering of mitochondria around the nucleus (decreased shortest distance of mitochondria from the nuclear envelope) using transmission electron microscopy (EM) (**Fig. 3-1B**). In these cells, hypoxia also resulted in 44% increase of the nPDC levels, measured by confocal microscopy and immunoblots in isolated nuclei (**Fig. 3-2A**). Using EM we also observed that some of

the clustered perinuclear mitochondria formed electron dense structures with the nuclear envelope that resembled the contact points between mitochondria and the ER (**Fig. 3-1C**).

We then used live imaging to visualize the mitochondria as they cluster around the nucleus. We transfected cells with a Dendra2-PDCE2, a photosensitive construct which changes colour when activated by a focused laser beam. We focused the laser beam in an area of the cell away from the nucleus, which changed the colour of the PDCE2 in the mitochondria at that area to red from green. When 2 hours later, and after serum+EGF treatment we imaged the cell, we found that these mitochondria had traveled and clustered around the nucleus. We observed a pattern in which the perinuclear mitochondria (with the red PDCE2) were actually rolling on the NE, and either rolled away or tethered on the NE (**Fig. 3-2B**).

3.3 Mitofusin 2 (MFN2) tethers mitochondria onto the nuclear envelope (NE)

MFN2 was originally thought to be present only in mitochondria, before it was also found to be present in the ER as well²⁰. Since the outer nuclear membrane is an extension of the ER, we looked for MFN2 in the nucleus. We first used immunoblots and a kit that allows the isolation of NE proteins and showed that MFN2 is present at the NE (**Fig. 3-3A**). In the same immunoblot, we compared the expression of MFN2 to the cytosolic cellular fraction, that includes mitochondria and ER, and found that NE MFN2 has exactly the same molecular weight with the MFN2 in mitochondria and ER, suggesting that it is the same protein, rather than a different isoform. We also found MFN2 to be present in the NE using electron microscopy (**Fig. 3-3B**) and super-

resolution confocal microscopy (z stacked images), which showed that MFN2 was present throughout the whole depth of the nuclear envelope and embedded into the lamin layer, protruding through lamin towards the cytoplasmic site (**Fig. 3-3C and Fig. 3-4A**). We observed MFN2 to be present at contact points between mitochondria and the lamin layer by super-resolution (**Fig. 3-3D and Fig. 3-4B**) and electron microscopy (**Fig. 3-3E**), suggesting that MFN2 can act as a potential tether between the two organelles. We also found that in response to proliferative stimuli, the levels of MFN2 increase further within the NE, in a manner that correlates temporally with the clustering of the mitochondria around the nuclear envelope (i.e. 1 hour post exposure to serum+EGF) (**Fig. 3-4C**). We managed to measure NE MFN2 by excluding any MFN2 signal that associated with the mitotracker signal in the cytoplasmic side and with the DAPI signal in the nucleoplasmic side, visualizing MFN2 as a ring, on top of the lamin layer, which was partial in the untreated cells and full in the serum+EGF-treated cells. (**Fig. 3-4C**).

We then wanted to study the effects of siRNA-mediated knockdown of MFN2 on mitochondrial tethering to the NE and the PDC entrance into the nucleus. However, MFN2 is involved in various mitochondrial functions other than mitochondrial fusion and ER tethering, like autophagy, mitochondrial bioenergetics and apoptosis²¹. This suggests that knocking down MFN2 will confound its specific effects on mitochondrial tethering to the NE and the subsequent nuclear translocation of PDC, since it will alter mitochondrial function. In fact, we did find that nPDC decreased significantly after treatment with MFN2 siRNA, but at the same time confocal imaging showed that the mitochondria were not only decreased in number but they appeared dysmorphic (**Fig.**

3-5A). Therefore, we designed an *in vitro* experiment, similar to the one followed to prove the same concept in the mitochondria-ER tethering¹⁴. We studied whether isolated mitochondria will still tether to isolated intact and functional nuclei *in vitro* (we have previously shown that with this method the isolated nuclei are functional⁶), when the nuclei lack MFN2. We first isolated mitochondria from A549 cells at baseline and mixed them with intact functional nuclei from cells that had been previously transfected with either a scrambled or MFN2 siRNA. (**Fig. 3-5B**). To ensure that any mitochondria we detect tethered on nuclei after we mixed them together are not due to nuclei contaminated with attached mitochondria during the nuclear isolation, we stained the cells from which we isolated mitochondria with mitotracker red, while those that we isolated nuclei from were stained with mitotracker deep-red. We then placed the nuclei on coverslips and mixed them with mitochondria, ensuring that both groups (i.e. the scramble and the siRNA treated nuclei) received the same amount of mitochondria (80 μ g of protein) for 1 hour, before confocal imaging. Both mitochondria and nuclei were placed in a commercially available cytoplasmic buffer, in which we had added 0.5 μ M of GTP to ensure the proper function of MFN2 (a GTPase). After fixation of the samples we counted the nuclei (stained with DAPI) that were bound with mitotracker red-stained mitochondria and not mitotracker deep red-stained mitochondria. We found that loss of nuclear MFN2 resulted in almost 60% loss of mitochondrial tethering on the NE (**Fig. 3-5B**), suggesting that MFN2 participates in the tethering of the two organelles, even out of the cell.

3.4 PDC is released from nucleus-tethered mitochondria and deposited on the lamin layer, before entering the nucleus

We observed that perinuclear mitochondria release free PDC (i.e. PDC signal not associated with mitotracker) which is deposited onto the lamin layer, forming a ring pattern (**Fig. 3-6**). This suggested that PDC may interact with lamin, a protein that is known to associate with a large number of proteins²². Confocal microscopy, with z stack imaging and 3D reconstruction, revealed the presence of extra-mitochondrial PDCE2 that was embedded throughout the whole depth of the lamin A (LMNA) layer (**Fig. 3-7A**). To prove this beyond the spatial detection limits of Airy scan super-resolution confocal microscopy (i.e. ~160 nm), we used the Proximity Ligation Assay (PLA), where an association of two proteins in proximity of less than 40 nm can be visualized²³. In the PLA assay, two proteins of interest are stained with two antibodies covalently linked to specific DNA primers, followed by hybridization and PCR amplification with fluorescent probes that marks the proximity of the proteins. To assess the proximity of PDCE2 and LMNA in the nucleus we performed z stacks of the whole nucleus that was stained with DAPI and counted only the PDCE2-LMNA interactions (i.e. the PLA signal) that occurred within the nucleoplasm and the nuclear periphery (**Fig. 3-7B**). As a positive control for the PLA assay we used the known close interaction between LMNA and LMNB1. Exposure of the cells to serum/EGF resulted in a significantly higher number of interactions between PDCE2 and LMNA (**Fig. 3-7B**), which suggests a dynamic process. We also used EM in cells exposed to serum/EGF as well as immunoblots of isolated nuclei or isolated NE proteins (using a NE protein isolation kit) and verified the localization of PDCE2 on the NE (**Fig. 3-7C**). The presence of PDCE2 in the NE specifically was shown by the purity of the NE

protein isolation, lacking cytoplasm (no MEK), or mitochondria (no succinate dehydrogenase) or nucleoplasm (no nucleolin) in the immunoblot. EM also showed free PDCE2 (extra-mitochondrial) located in the NE as well as the periphery of the nucleoplasm (**Fig. 3-7C**) Finally, we found that PDCE2, but not PDCE1, co-immunoprecipitated with lamin A/C (**Fig. 3-7D**). We were not able to do the reverse, i.e. find PDC when we immunoprecipitated lamin A/C, even with the use of the crosslinker DSS, but we believe that this interaction may be weak, allowing perhaps a temporary association with PDC. Nevertheless, because protein-protein interactions can be facilitated by acetylation and there are several lysine residues on the segment of lamin that interacts with proteins²⁴, we found it interesting that the subunit of PDC which is responsible for the formation of acetyl-CoA and has acetyl-transferase activity (transferring the acetyl-group on the CoA-SH molecule in its enzymatic reaction) is the one that associates with lamin.

We then used live super-resolution confocal imaging to study the trafficking of PDC from the perinuclear mitochondria through the NE. To visualize PDC and the nuclear periphery we generated plasmids expressing PDCE1 α coupled to GFP and LMNA coupled to mCherry. We used synchronized A549 cells on which we labeled the mitochondria with mitotracker and transfected them with the above plasmids before exposing them to serum and EGF for 2 hours. We started acquiring super-resolution images every 6 seconds and found that PDCE1 α layered on the lamin and free of NE-tethered mitochondria (not associated with the mitotracker signal) entered directly in small amounts into the nucleus, braking through the lamin layer (see images at 24 and 30 sec) (**Fig. 3-8A**). To further verify this observation in a different cell type we used

HFF-1 cells that were transfected with the PDCE1 α -GFP and LMNA-mCherry plasmids and stained mitochondria with mitotracker red. We then exposed the cells to 1% hypoxia for 24 hours and obtained live super-resolution images every 14 seconds, showing the same pattern of extra-mitochondrial PDCE1 α entering the nucleus through the lamin layer (**Fig. 3-9**).

For these live imaging experiments, we had to label PDC which means that we could label only one of its subunits. To show that all PDC subunits can cross the lamin layer as a complex, we simultaneously stained for several subunits and used super resolution confocal microscopy. We found that the whole PDC complex traveled through the lamin layer, particularly in nuclear invaginations. These invaginations have long been described and originally thought to allow easy reach of cytoplasmic proteins to the nucleolus, since they reach deep into the nucleoplasm. A 3D confocal image of a large invagination is shown in **Fig. 3-10A**. However, by increasing the nuclear surface, we speculated that these invaginations may also facilitate the tethering and exchange of molecules with organelles like mitochondria. In fact, using EM, we were able to detect intact mitochondria deep within these invaginations forming contact points with the NE (**Fig. 3-10B**). By using stacked imaging, we were able to measure these invaginations in each nucleus and found that not only nuclear invaginations increased after exposure to serum/EGF (which we have shown to bring mitochondria closer to the nucleus) but they are increased in number in cancer vs non-cancer cells, further enabling our proposed mechanism to the proliferative cancer cells (**Fig. 3-10A**). **Fig. 3-10C** shows a 3D reconstructed area of the nucleus that includes an invagination, stained for lamin A/C and PDCE2. PDCE2 is embedded throughout the whole depth

and width of the lamin layer towards the nucleoplasmic site. **Fig. 3-10D** shows cells stained with 3 PDC subunits simultaneously, along with lamin A/C. Below it, we zoomed into a large invagination and show that all PDC subunits colocalize and are embedded in the lamin layer of the invagination as they cross into the nucleus. Live imaging with PDCE1 α -GFP and mitotracker-red zoomed within an invagination, showed that a mitochondrion (in red, shown by the yellow arrow) was attached on the lumen of the invagination and mitochondria-free PDCE1 α (in green, shown by the white arrow) enters, through the invagination wall, into the nucleoplasm marked by Hoechst, which in this case appears to be surrounding the nucleoplasmic side of the invagination (**Fig. 3-8B**).

We then used lamin A siRNA (versus scrambled RNA) and showed that decreasing the levels of nuclear lamin A, decreased the nPDC levels caused by serum/EGF exposure, measured both by confocal imaging and by immunoblots in isolated pure nuclei (which, as we have also previously shown, had no mitochondrial contamination⁶) (**Fig. 3-11A**). This loss of lamin A did not affect the levels of nuclear SIRT6 that is known to reside into the nucleus²⁵. To determine the effects of structural abnormalities in lamin A on nPDC levels, we studied fibroblasts from a progeria patient and a relative of this patient without progeria (a laminopathy) (**Fig. 3-11B**). We found that the progeria fibroblasts which express dysfunctional lamin had much higher levels of nPDC suggesting that the abnormal lamin was perhaps permissive of more nuclear PDC entry.

To study whether physiologically lower lamin A/C levels relate to nPDC levels, we studied a non-terminally differentiated cell type (i.e. HEK cells) that is known to have

less lamin A/C than other cells, like A549 or 786-O cancer cells²⁶. HEK cells indeed expressed much less lamin A compared to the other cell types (**Fig. 3-11C**). When we transfected HEK cells with a plasmid expressing lamin A coupled to mCherry and measured its effects on nuclear PDCE2 levels with confocal microscopy (**Fig. 3-11C**). We found that the increase in lamin levels, increased nPDCE2 levels, also suggesting that lamin A and not any of the B-type lamins regulate the nuclear translocation of PDC. The confocal images revealed that the cells that had the highest levels of nPDC were indeed the cells that had successfully expressed the lamin-mCherry construct (white arrow), compared to the cells that did not express the lamin-mCherry construct (yellow arrow).

3.5 PDC enters the nucleus independently of nuclear pores (NPs)

3D reconstruction of confocal images of cells stained with antibodies against a key component of the NP (NUP98), PDCE2 and lamin showed that PDCE2 can be seen in the nucleoplasmic site protruding through lamin independent of NUP98. A red arrow shows PDCE2 close to a NUP98 signal but the 2 white arrows show PDCE2 in no close association with NUP98 (**Fig. 3-12A**). This was confirmed by the fact that the PLA assay showed that 2 hours after exposure to serum and EGF, there was no significant association between the NUP98 and the PDCE2 signal, although there was good expression of NUP98 and perinuclear PDCE2 independently and the assay worked as shown by the positive control image (**Fig. 3-12B**). Lastly, EM revealed that PDCE2 was found in both the NE and the peripheral nucleoplasm (white arrows), at sites remote from a clear example of an NP (green arrow) (**Fig. 3-12C**).

To further support our finding that PDC can enter the nucleus independent of NPs, we used wheat germ agglutinin (WGA), a plant-based lectin that has been shown to bind to the glycoproteins of the NPs preventing all trafficking across them^{27,28}. Because WGA cannot cross the extracellular membrane, we had to microinject it into synchronized A549 cells. We microinjected WGA coupled to Alexa 555 and Hoechst that binds to nuclear DNA, so we can easily identify the microinjected cells after fixation. We then exposed the cells to serum and EGF for two hours before fixation and stained them with mitotracker-red and antibodies against PDCE2 and STAT3. STAT3 is a cytoplasmic protein that upon activation of the EGF receptor is phosphorylated²⁹⁻³¹ and translocates into the nucleus via the action of karyopherins that carry it through the NPs^{32,33}. To verify that we are measuring the nuclear PDCE2 levels of the entire nucleus, we performed z stacks on a confocal microscope and projected the images as a sum of intensities, which resulted in high values of arbitrary fluorescent units (AFU) compared to previous immunofluorescence experiments. Microinjection of the cells with WGA resulted in decreased entrance of STAT3 into the nucleus, but it had no effect on the levels of nuclear PDCE2 (**Fig. 3-12D**), confirming that PDC can enter the nucleus independent of NPs.

We then aimed to study the fate of PDC at the time of cell division, when the lamin is phosphorylated, depolymerized and disassembled as the nucleus needs to divide; only to reassemble again and form the nuclear envelopes in both daughter nuclei. We found that the PDC that was associated with lamin prior to cell division (**Fig. 3-7B**), retained its association with the disassembled lamin polymers scattered through the cytoplasm during division, using the PLA technique (**Fig. 3-13A**). We also imaged

cells during the late stages of division when lamin is still disassembled and we found a large amount of PDCE2 touching histone complexes (H3), which were heavily acetylated, in the forming daughter nuclei (**Fig. 3-13B**). This suggested that nPDC may have directly acetylated the histones and since PDCE2 has acetyl-transferase activity, as part of the canonical PDC function, it may produce acetyl-CoA from nuclear pyruvate (as we previously showed ⁶) but also directly transfer the acetyl-group on histone 3. Taken together these data allow us to speculate that it is lamin that keeps the bulk of PDC into the newly formed daughter nuclei after its entry during mitosis, since lamin has to encircle the histone/DNA complexes to form the new nuclear envelope. Nucleoplasmic lamin also forms a network, perhaps forming PDC-enriched hubs that could facilitate histone or other protein acetylation in the nucleus.

3.6 Discussion

Here we describe a novel mechanism for the nuclear entry of a large enzymatic complex into the nucleus, that resembles the way that some viruses have been shown to enter the nucleus through the NE and lamin layers (either bigger or smaller than the maximum diameter allowed for NP entrance). We show for the first time that MFN2 is not only present in the nucleus (both at the NE and the nucleoplasm) but can facilitate tethering of mitochondria to the NE. Tethered mitochondria on the NE release PDC that can bind lamin and either enter the lamin layer directly (like parvoviruses) or enter during mitosis, when the NE and lamin layers are temporarily disassembled (like the Murine Leukemia Virus). We studied both cancer and non-cancer cells and we described the PDC entry following treatment with serum+EGF, that we had recently shown to result in increase in intranuclear functional PDC levels. Using live imaging

with super-resolution confocal microscopy we were able to visualize PDC subunits entering the nucleus directly through lamin and independently of NPs, even though these fluorescent-bound PDC subunits had diameters much smaller than the intact PDC that would allow them to enter through the NPs. At the same time, we showed that all PDC subunits can enter the nuclear membrane together as part of PDC.

Although MFN2 has not been previously described in the nucleus, its presence at least in the NE is not surprising since the NE is an extension of the ER where MFN2 has previously been described. Similarly, the fact that MFN2 tethers mitochondria with the nucleus is also not surprising since it has been shown to tether mitochondria with the ER. This suggests that there is perhaps a generalized inter-organelle tethering pathway involving MFN2 throughout the cell. We were able to show that MFN2 enriched the contact points of mitochondria and nuclei, embedded between the 2 organelles.

Although decreasing MFN2 levels with siRNA resulted in decreased nPDC levels, this could be because of a primary generalized mitochondrial dysfunction, since MFN2 participates in many important mitochondrial functions. Thus we used a technique by which we mixed nuclei that lacked MFN2 (since we isolated them from cells treated with MFN2 siRNA) versus nuclei that had MFN2 (since we isolated them from cells treated with scrambled RNA) with intact mitochondria and showed that lack of nuclear MFN2 resulted in a large decrease in mitochondria tethering to nuclei in vitro.

Proliferative stimuli (serum+EGF, hypoxia) had several effects relevant to our proposed mechanism. First, they caused a clustering of mitochondria around the nucleus. This is likely mediated by changes in mitochondrial trafficking on microtubules, previously well established. With live imaging, we were able to show

that mitochondria approached the nucleus and first rolled across the NE before they hooked to a tethering spot. Second, they caused an increase in NE MFN2 levels, facilitating the tethering. And third, they increased nPDC levels. At the same time, such stimuli also increased the nuclear membrane surface area by promoting the formation of large nuclear invaginations (which are also increased in cancer versus non-cancer cells). We found that nuclear invaginations included mitochondria and were primary sites for PDC entrance. These data suggest that this mitochondria-nuclear communication is a dynamic process, activated perhaps at times that the nuclear needs for acetyl-CoA (as an acetyl-group donor for histone acetylation) are increasing, during cell cycle progression. This need characterizes either cancer cell proliferation or the proliferation of cells during embryonic development, where nPDC levels have also been shown to increase⁹.

Our finding that MFN2 contributes to the tethering of mitochondria to the nucleus does not exclude the participation of other candidate tethering proteins³⁴. For example, in the mitochondria tethering to the ER, several tethering protein couples have been described, in addition to the ER MFN2 tethering with mitochondrial MFN2 or MFN1. These include the mitochondrial fission 1 homologue (Fis1) and the ER protein BAP31³⁵, or the mitochondrial protein tyrosine phosphatase-interacting protein 51 (PTPIP51) and the ER vesicle-associated membrane protein-associated protein B (VAPB)³⁶. Thus, it is possible that other proteins can participate in the mitochondria to nucleus tethering in a cell type or condition-dependent manner, but the above pairs have not been studied in the nucleus yet. To the best of our knowledge this is the first description of an organelle tethering to the nucleus in mammalian cells. In the yeast,

tethering of the vacuole to the nucleus has been described (Nucleus to Vacuole Junctions, NVJ). Similar to our mechanism, the ER-localized protein Nvj1 associates with the vacuolar protein Vac8, but it is not known yet whether this mechanism is conserved in higher eukaryotes³⁷.

We speculate that PDC exhibits a weak association with lamin. We found that extramitochondrial PDC (after released from tethered mitochondria) layers directly on top of lamin A/C. We immunoprecipitated PDCE2 and found lamin but we could not find PDCE2 when we immunoprecipitated lamin, even after crosslinking with DSS. This may relate to the fact that the association with lamin needs to be transient and thus relatively weak or dynamic. Because there are lysine residues at the sites that lamin associates with proteins, we also speculate that PDC can directly produce acetyl-CoA upon contact with lamin (since pyruvate is present both outside and inside the nucleus) and directly transfer the acetyl-group to lamin facilitating their association, since PDC also has acetyl-transferase ability through the PDCE2 subunit. Because we found that PDC and lamin remain linked even after lamin depolymerizes at mitosis (using the PLA assay), we propose that this allows PDC to be pulled into the nucleus as lamin reassembles to form the daughter cell nuclear membrane. As lamin also forms a network in the nucleoplasm, it may allow PDC to be a part of nucleoplasmic hubs used for histone or other protein acetylation. On the other hand, the direct passage of PDC through the lamin layer needs to be studied more with future research. Parvoviruses can enter the nucleus directly through lamin and while a mechanism has not been elucidated, the involvement of caspases locally to disrupt the lamin layer has been proposed. It has also been proposed that this occurs in order to allow the co-entrance

of other molecules and proteins that parvoviruses need to succeed in their intranuclear functions. This direct mode of entrance may allow some PDC entry into the nucleus independent of cell mitosis.

The stoichiometry of PDC (i.e. how many copies of each subunit participate to the PDC megacomplex) can vary or even be dynamic in different conditions, but its mechanism remains unknown. This means that some smaller PDC complexes may have diameters smaller than 39 nm and may indeed be able to enter the nucleus through NPs. The nonspecific NP entry inhibitor WGA however, did not have any effects on nPDC levels, while it inhibited the entrance of another protein residing into the nucleus, i.e. STAT3. But the PDC stoichiometry in other cell types or conditions may be different, allowing entrance through NPs.

Our work shows for the first time how a large enzymatic complex can enter the nucleus via a non-canonical NP-independent pathway and expands the field of inter-organelle communication further³⁴. To the best of our knowledge, this is also the first description of tethering of mitochondria to the nucleus. Mitochondria-to-nucleus communication which has been gaining a lot of interest particularly in metabolic pathways in cancer³⁸, may now be approached from a new angle, since additional mitochondrial proteins can be directly entering the nucleus at rest or under mitosis, avoiding intracellular trafficking and without the need for NLSs.

3.7 Materials and methods

Cell culture

Human non-small cell lung cancer cells (A549), renal cell carcinoma (786-O), embryonic kidney (HEK293) cells and human foreskin fibroblasts (HFF-1) were purchased from ATCC (Manassas, VA). Small airway epithelial cells were purchased from ScienCell (CA, USA). Patient-derived progeria fibroblasts (ID: AG03513) and a matching control from a healthy individual (ID: AG06293) were obtained from the NIGMS Human Genetic Cell Repository at the Coriell Institute for Medical Research. A549 cells were grown in F12K medium, while 786-O cells in RPMI (Gibco – Thermo Fisher Scientific, Waltham, Massachusetts, US). Patient-derived progeria fibroblasts and HEK293 cells were maintained in EMEM medium (ATCC). Small airway epithelial cells were grown in SAEpiCM media (ScienCell, CA, USA). HFF-1 cells grown on DMEM (Gibco – Thermo Fisher Scientific, Waltham, Massachusetts, US). All media were supplemented with 10% FBS (unless otherwise stated) and 1% antimycotic.

Confocal microscopy

All images were obtained on a ZEISS LSM 710 microscopy (Carl ZEISS AG, Oberkochen, Germany), equipped with a GaAsp detector and the AiryScan module, allowing us to obtain super-resolution images with lateral resolution of ~140 nm. Images were acquired with a 40x Oil objective at optimal pixel size and interval (for z-stacks) based on the zoom factor and the fluorophores used in each experiment. After

acquisition, the Airyscan images were processed with the ZEN software (Carl ZEISS AG, Oberkochen, Germany) resulting in the final super resolution images.

Immunoblotting

Standard SDS-PAGE experiments performed as described previously³⁹. Cells were pelleted and lysed on ice cold RIPA buffer for 30 minutes while vortexing every 10 minutes. The samples were then centrifuged at 10,000 rpm for 20 minutes in a TA-15 rotor of an Allegra 25R centrifuge (Beckman Coulter, Brea, CA, USA). After the centrifugation step we discarded the pellet and used the supernatant for further experiments. Protein concentration was identified by using a BCA kit (Thermo Fisher Scientific, Waltham, Massachusetts, US) and measured on a SpectraMax i3 (Molecular Devices, San Jose, CA, USA). The samples were then diluted to a final concentration of 1 mg/ml in RIPA buffer and 1X SDS buffer (Bio Rad, Hercules, CA, USA). The samples were then boiled to 98 degrees for 5 minutes. If the initial sample contained nuclei, we lysed it in RIPA for 10 minutes and sonicated it with three quick pulses using a 60 sonic dismembrator (Thermo Fisher Scientific, Waltham, Massachusetts, US). The sonication power was set to 20%. After that step we continued with the centrifugation as described before.

All samples were loaded on 12% polyacrylamide gels. The gels were transferred to 0.22 nm pore nitrocellulose membranes (Bio Rad, Hercules, CA, USA) using a Trans-blot turbo transfer apparatus following the manufacturer's instructions (Bio Rad, Hercules, CA, USA). After transferring we incubated the membranes with Ponceau S (Thermo Fisher Scientific, Waltham, Massachusetts, US) to verify efficient loading

and transferring of the proteins on the membrane. Membranes were then washed with TBS-T and blocked with 5% milk in TBS-T for 1 hour at room temperature. The membranes were then incubated with the primary antibody in TBS-T containing 2% milk overnight at 4 degrees with gentle rotation. The following day the membranes were washed with TBS-T and incubated with the appropriate secondary antibodies coupled to horseradish peroxidase (Cell Signaling Technology, Danvers, MA, USA). Protein bands were detected after incubation of the membranes with ECL buffer (Thermo Fisher Scientific, Waltham, Massachusetts, US) and visualized on a Chemidoc machine (Bio Rad, Hercules, CA, USA). If stripping was necessary, we used a commercially available stripping buffer (Thermo Fisher Scientific, Waltham, Massachusetts, US) and repeated the procedure described above starting from the initial blocking step with 5% milk in TBS-T.

Plasmid constructs

EGFP-PDCE1 α was generated by OriGene Technologies (Rockville, MD). Briefly, a *Homo sapiens* cDNA ORF clone of pyruvate dehydrogenase alpha 1 (PDHA1) was cloned into the pEGFP-N1 vector (Clontech, Mountain View, CA). mCherry-LaminA-C 18 was a gift from Michael Davidson (Addgene plasmid #55068).

Plasmid and siRNA transfection

All plasmid transfections were carried out in 35 mm dishes by adding 7.5 μ g of DNA into the cells with CaCl₂. Briefly, we prepared two tubes from which the first one contained 7.5 μ g of the plasmid, along with water and CaCl₂, while the second one 2X

HBS buffer. We then added the content of the first tube to the second in a dropwise manner and with constant aeration. The mixture was incubated for 30 minutes at room temperature and then added to the cells in a dropwise manner and incubated overnight, followed by a medium change the following day. siRNA transfections were carried out by Lipofectamine RNAiMax (Thermo Fisher Scientific, Waltham, MA, USA) following manufacturer's specifications. Briefly, cells were seeded onto a 35 mm dish at a 50-60% confluency and let to adhere overnight. The cells were transfected the following day with 25 pmol of siRNA diluted into OptiMem medium (Gibco – Thermo Fisher Scientific, Waltham, Massachusetts, US) and mixed with Lipofectamine RNAiMax. The mixture was incubated for 10 minutes at room temperature and then added to the cells without changing the medium for 72 hours in order to achieve maximum knockdown of the gene of interest.

Immunofluorescence

Cells were grown onto coverslips and treated accordingly for each experiment. Fixation occurred in 2% paraformaldehyde (PFA) for 10 minutes at 37 degrees. The cells were permeabilized with 0.25% Triton for 10 minutes at room temperature, followed by a blocking step with Image-iT FX signal Enhancer (Thermo Fisher Scientific, Waltham, Massachusetts, US) for 30 minutes at room temperature. Further blocking occurred with a one-hour incubation of the cells with 10% serum from the host of the secondary antibody. Cells were incubated with the primary antibodies overnight at 4 degrees. The following day the cells were incubated with the secondary antibody for 1 hour at room temperature followed by subsequent washes with 1X PBS.

In the end of this step the cells were counterstained with 1 μ M DAPI (Molecular Probes, Oregon, USA) for 10 minutes at room temperature and mounted on coverslips with ProLong Glass Antifade mountant (Thermo Fisher Scientific, Waltham, Massachusetts, US). For information on antibody dilutions see Appendix I.

Proximity ligation assay

Duolink In Situ detection Orange kit against mouse and rabbit antibodies was purchased from Sigma Aldrich and performed based on the manufacturer's recommendations. Briefly, we followed the immunofluorescence protocol described above until the overnight primary antibody incubation step. The following day the cells were washed with the buffer A that included within the kit and incubated with the secondary antibodies coupled to the DNA probes for one hour at 37 degrees. After this step we induced the ligation of the DNA probes that are in close proximity by adding the DNA ligase for 30 minutes at 37 degrees, followed by a signal amplification step after incubation with the kit's DNA polymerase for 200 minutes at 37 degrees. After the necessary washing steps, the cells were mounted on #1.5 coverslips with the DAPI-containing mounting medium that came with the kit and sealed with nail polish.

Mitotracker staining

Mitotracker dyes were purchased from Molecular probes (Oregon, USA) and used according to manufacturer's instructions. Briefly, the Mitotracker dyes were dissolved into DMSO, aliquoted and stored at -20 degrees. Cells were stained by adding 150 nM of mitotracker in the medium for 30 minutes at 37 degrees. If cells had to be fixed, we

incubated them with 2% PFA in PBS for 10 minutes at 37 degrees. If the cells had to be fixed, we followed the immunofluorescence protocol.

Transmission electron microscopy (TEM)

For conventional TEM, the cells were grown on 35 mm dishes (MatTek Corporation, Ashland, Massachusetts) until the desired confluency. The cells were fixed in a solution of 5% EM-grade Glutaraldehyde (Electron Microscopy Sciences, Hatfield, Pennsylvania) for 30 minutes, followed by three five-minute washings with 0.1M cacodylate duffer (Electron Microscopy Sciences, Hatfield, Pennsylvania). The cells were then incubated with 1% $K_4Fe(CN)_5$ and 1% OsO_4 in 0.1 M cacodylate buffer for 15 minutes on ice, followed by three 3-minute washing steps in 0.1 M cacodylate buffer. The cells were further washed with 0.1M Na^{2+} in acetate buffer, pH 5.2 (Electron Microscopy Sciences, Hatfield, Pennsylvania) for three minutes. Before dehydration, the cells were washed for 2 minutes in Milli-Q water. We dehydrated the cells by subsequent incubation steps of 10%, 30%, 50%, 70%, 80%, 90% and 100% ice cold ethanol. After dehydration the cells were embedded in Spurr's Resin by following subsequent incubation steps of a mixture of 100% ethanol and Spurr's with ratios 2:1 (30 minutes at room temperature), 1:1 (1 hour at room temperature), 1:2 (2 hours at room temperature) and finally absolute Spurr's resin (overnight at room temperature). The following day we polymerized the resin by incubating it overnight in an oven that was preheated at 70 degrees. After polymerization the cell monolayer was thin sectioned using a Leica ultramicrotome (Leica, Wetzlar, Germany) and placed on a Cu Formvar / Carbon Grid (Electron Microscopy Sciences, Hatfield,

Pennsylvania). The grids were then counterstained with 1% uranyl acetate in Milli-Q water followed by subsequent washing steps with Milli-Q water. The grids were coated on a Leica EM ACE6000 Carbon evaporator (Leica, Wetzlar, Germany). The carbon coating height was set to 7 nm.

For immunogold TEM, cells were grown on 7.9 nm Thermanox coverslips (Thermo Fisher Scientific, Waltham, Massachusetts, US) and fixed in a solution with 2% EM-grade paraformaldehyde for 30 minutes. The coverslips were then washed and dehydrated by subsequent incubation steps of 10%, 30%, 50%, 70%, 80% and 90% ice cold ethanol. We further embedded the cells in LR white medium (Electron Microscopy Sciences, Hatfield, Pennsylvania) by subsequent incubation steps with 90% ethanol to LR white in ratios 2:1 (30 minutes at 4 degrees), 1:1 (1 hour at 4 degrees), 1:2 (2 hours at 4 degrees) and finally absolute LR white (overnight at 4 degrees under a UV light). After polymerization of LR white the cells were sliced and placed on Ni grids and stored until further processing. The grids that underwent antibody staining were quenched in quenching buffer (50% glycine in Milli-Q water) for 15 minutes at room temperature. The cells were then washed with washing buffer (2% BSA, 2% fish skin gelatin and 0.02 M PBS) and blocked into blocking buffer (10% BSA, 10% fish skin gelatin in 0.02 M PBS) for 30 minutes at room temperature. The cells were then incubated overnight at four degrees with the primary antibody at a concentration ten times higher than the one used for immunofluorescence in the incubation buffer (2% BSA, 2% fish skin gelatin and 0.01 M PBS). The following day the cells were washed with the washing buffer and incubated with the secondary antibody for 2 hours at room temperature in the incubation buffer. After that we washed

the cells with 0.01 M PBS (Thermo Fisher Scientific, Waltham, Massachusetts, US) and counterstained them with 1% uranyl acetate diluted into Milli-Q water followed by a washing step with Milli-Q water before continuing with imaging. TEM images obtained on a Hitachi H-7650 TEM (Hitachi). The beam voltage for all images was set to 60 kV.

Image analysis and 3D video reconstruction

All images were analyzed with FIJI⁴⁰, either manually or via macros written in the ImageJ macro language. In general, we thresholded all the channels of interest by using the Otsu thresholding algorithm after a smoothing step by using a Gaussian blur filter with a radius of 2 pixels. All the macros used in this chapter can be found in **Appendix II**. Video reconstruction took place on FIJI after processing the z stacks and rendering them using either the surface or the volume algorithm of the 3Dviewer plugin of FIJI⁴¹.

Co-immunoprecipitation

Co-immunoprecipitation experiments were performed as previously described. Briefly, cells were grown on 150 mm dishes until 90-95% confluency. The cells were lysed in the plate after addition of a commercially available lysis buffer suitable for co-immunoprecipitation experiments (Thermo Fisher Scientific, Waltham, Massachusetts, US) and measured protein via a BCA kit purchased from Thermo Fisher Scientific following the manufacturer's instructions. We pulled down the protein of interest from 500 µg of protein by adding a primary antibody directly into the tube, while rotating it at 4 degrees overnight. The following day we added 30 µL magnetic beads slurry

(Thermo Fisher Scientific, Waltham, Massachusetts, US) coupled with either protein A or G (based on the antibody host and IgG subtype) in each tube and incubated for 1 hour at 4 degrees under gentle rotation. Protein elution from the beads was done after addition of 2X loading buffer (BioRad) in each tube and boiling for 10 minutes at 55 degrees. The eluted fraction was diluted onto 1X by addition of equal volume of lysis buffer and then loaded on a polyacrylamide gel for further analysis by western blot.

Isolation of functional nuclei

A nuclear isolation kit: Nuclei PURE prep was purchased from Sigma Aldrich. Functional nuclei were isolated based on the manufacturer's instructions. Briefly, cells grew in a 150 mm dish until 90-95% confluency. Cells were scrapped from the plate and lysed on the kit's lysis buffer for 30 minutes while mixing them every 10 minutes. After the lysis step the nuclei were loaded on a 2 M sucrose cushion and centrifuged at 30,000 g for 45 minutes at 4 degrees. The isolated nuclei were maintained in the kit's nuclear storage buffer until used for downstream experiments.

WGA Microinjection

Cells were grown on 50 mm dishes suitable for microinjection (MatTek Corporation, Ashland, Massachusetts) until they reached a confluency of 50%. Cells were synchronized in serum free medium for 24 hours. The following day and three hours before the completion of 24 hours of serum synchronization we microinjected the cells with 450 µg/ml WGA along with Hoechst (Molecular probes, Oregon, USA) in 1X PBS using a FemtoJet microinjector (Eppendorf, Hamburg, Germany). After the

completion of serum synchronization, we added complete medium along with 150 ng/ml EGF (Sigma Aldrich) for two hours before fixing the cells and continuing with the staining protocol described above.

***In vitro* assay for mitochondrial tethering onto the nuclear envelope**

Functional mitochondria isolation performed as described previously⁴². Briefly, cells grew on a 150 mm plate until 90-95% confluency. Cells were scraped and diluted into IB_c buffer (1 M sucrose, 0.1 M Tris-MOPS and 0.1 mM EGTA/Tris) pH 7.4 before manual homogenization with 50 strokes in a glass-Teflon potter. Mitochondria were separated from partially lysed cells via two 10-minute centrifugation steps at 1000 g on a precooled (4 °C) tabletop centrifuge. Finally, mitochondria were collected as a pellet after two twenty-minute centrifugation steps at 8,000 g. Protein concentration of mitochondria was assessed by BCA. Cells from which we isolated nuclei were plated on a 150 mm plate until 90-95% confluency. Nuclear isolation was done as described before. Both nuclei and mitochondria were dissolved in a commercially available cytoplasmic buffer purchased from Biovision (San Francisco, CA, USA) contained 0.5 μM of GTP (Abcam, Cambridge, UK). We added nuclei equal to 80 μg of protein on a 30 mm MatTek dish (MatTek Corporation, Ashland, Massachusetts) and mixed them with an equal amount of mitochondria, while incubating at 37 degrees for 1 hour before fixing them with 2% PFA diluted in 1X PBS. The dishes were then mounted with coverslips and left to dry overnight before imaging them. To make sure that we will image the entire nucleus to assess whether any mitochondria were bound to them, we obtained z stacks with a confocal microscope.

Treatment of cells with EGF

Before treatment with EGF cells were synchronized to the G0 phase of the cell cycle by serum deprivation for 24 hours. Then we treated the cells with 150 ng/ml EGF (Sigma Aldrich) into complete medium (10% FBS) for 2 hours before ending the experiment unless otherwise stated.

Statistical analysis

All statistical analyses performed on STATA (StataCorp LLC, Texas, USA). We used student's t test (for comparison between two groups) or one-way ANOVA (for multiple groups). For one-way ANOVA, significance was obtained by applying a Bonferroni post-hoc analysis. Significance for all statistical testing was considered to be $P < 0.05$.

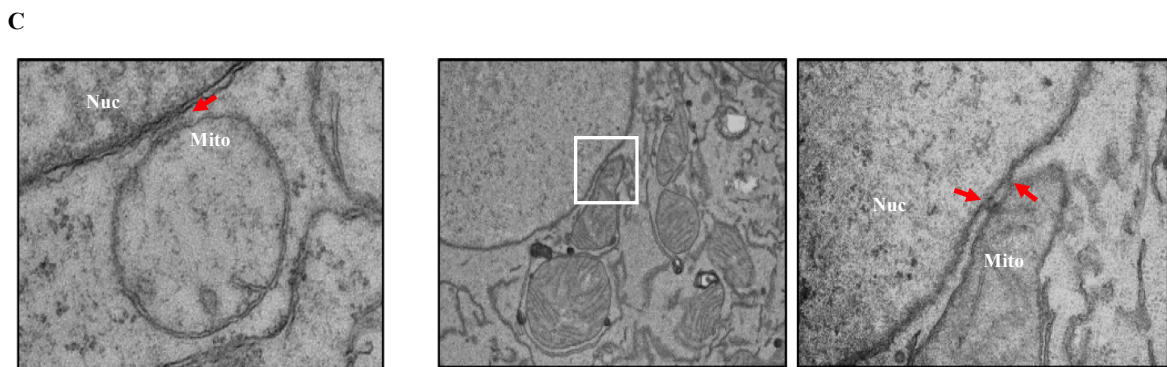
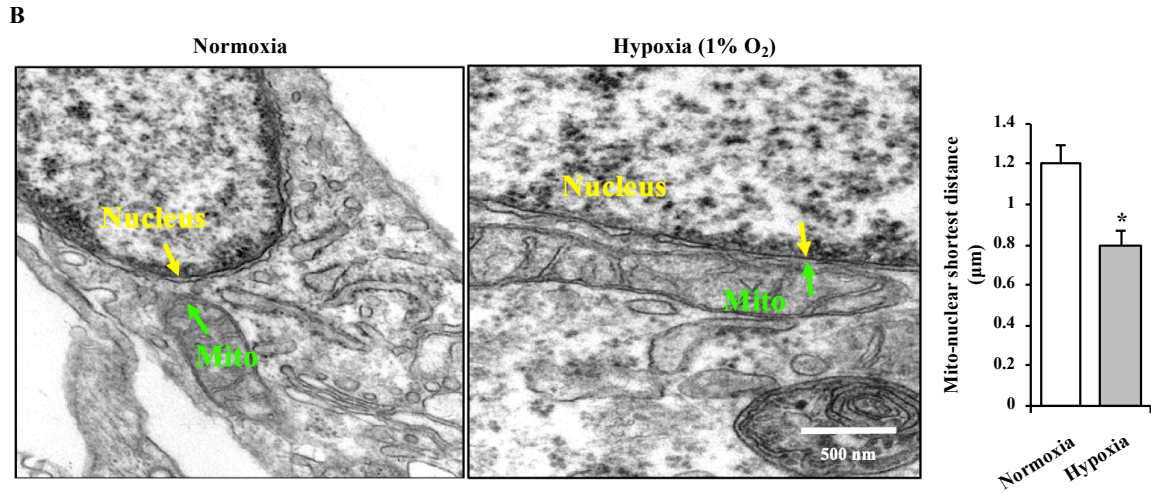
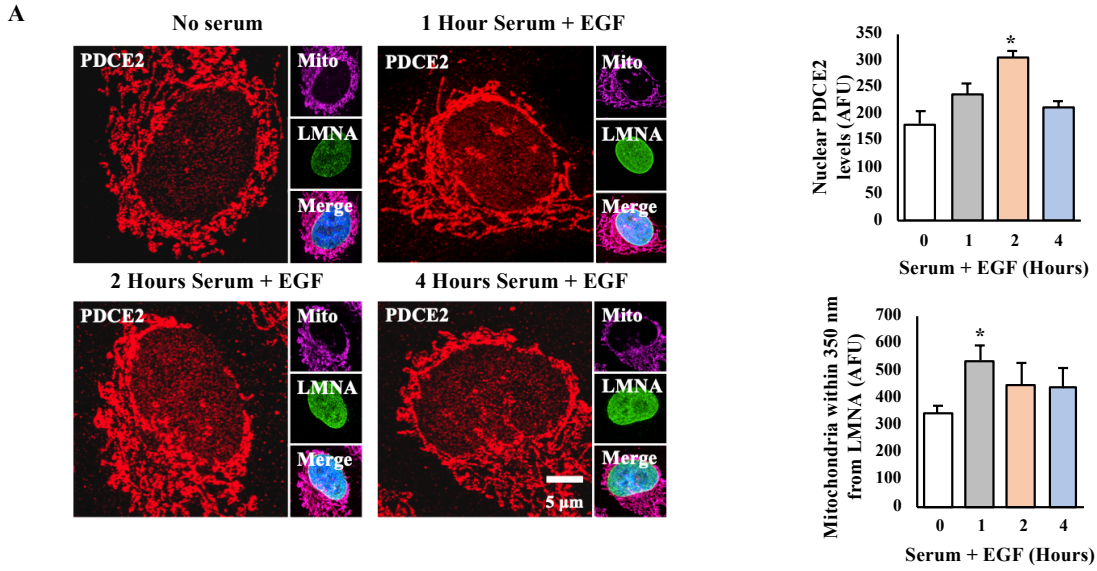
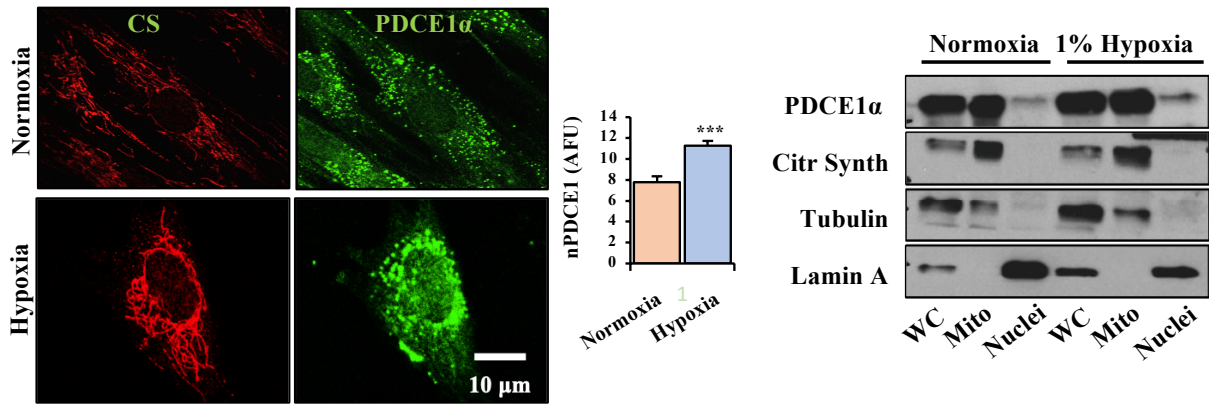


Fig. 3-1 Mitochondria cluster around the nucleus in response to proliferative stimuli and form electron dense areas with the NE. (A) A549 cells exposed to serum and EGF (500 ng/ml) for 1, 2 and 4 hours were stained for PDCE2 (red), LMNA (green), mitotracker (magenta) and DAPI (blue). Mitochondria clustered around the nucleus at 1 hour, while nuclear PDCE2 levels peaked at 2 hours after treatment. Mitochondrial distance was measured by drawing concentric circles from the edge of the nucleus by using an image analysis software. P value for nuclear PDCE2 levels was 0.038. P value for mitochondrial distance was 0.041. n = 150 cells per group in 3 experiments. Error bars represent SEM. Scale bar is at 5 μ m. **(B)** Hypoxia (1% O₂) increases mitochondrial clustering around the nucleus as seen under a TEM. A yellow arrow points at the edge of the nucleus, while a green arrow at the edge of a mitochondrion. n = 60 cells/group. P value = 0.037. Error bars represent SEM. Scale bar is at 500 nm. **(C)** A TEM image showing perinuclear mitochondria forming electron dense areas with the NE.

A



B

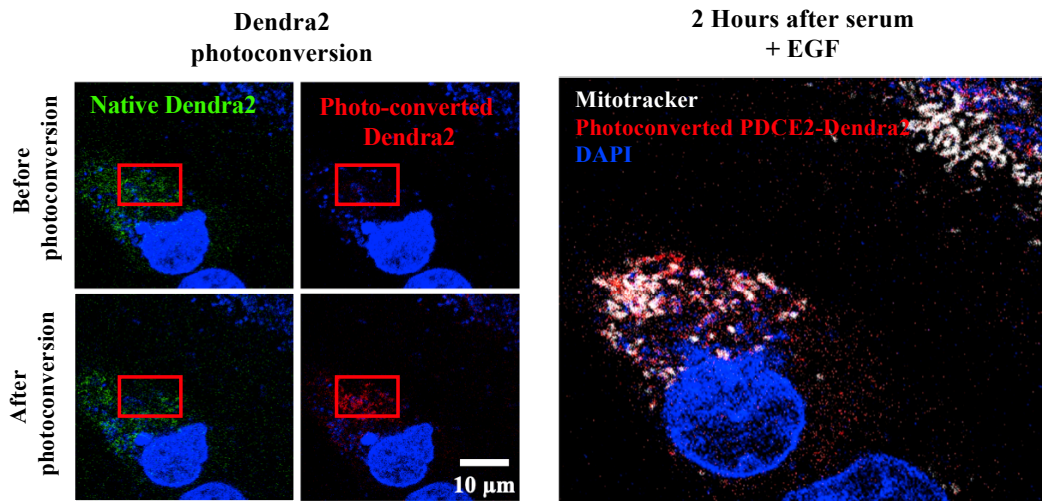


Fig. 3-2 Proliferative stimuli increase nuclear PDC levels and perinuclear mitochondrial clustering. (A) Confocal images and immunoblot (loaded with whole cell, mitochondrial and nuclear extracts) of HFF-1 cells exposed to hypoxia (1% O₂) for 24 hours. Cells were stained for citrate synthase (red) and PDCE1 α (green) showing increased nuclear PDC levels after exposure to hypoxia. n = 150 cells per group in 3 experiments. P value was less than 0.001 as assessed by student's t test. Error bars represent SEM. Scale bar is at 10 μ m. (B) Live imaging of A549 cells transfected with a construct expressing PDCE2 coupled to Dendra2. Native Dendra2 fluoresces green but it switches to red after irradiation with a 405 laser. We photoconverted Dendra2 in an area distant to the nucleus in synchronized A549 cells (red boxes on the left images) before the addition of serum and EGF (500 ng/ml). After 2 hours from the addition of serum, mitochondria (grey) with photoconverted Dendra2 (red) had moved closer to the nucleus and showed a rolling pattern on the nuclear envelope, suggesting that proliferative stimuli promote the perinuclear clustering of mitochondria. Nuclei were stained with Hoechst (blue). Scale bar is at 10 μ m. The video can be seen at <https://bit.ly/3nPK0kf>

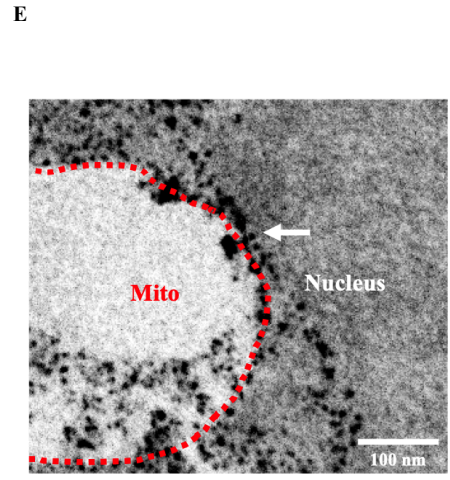
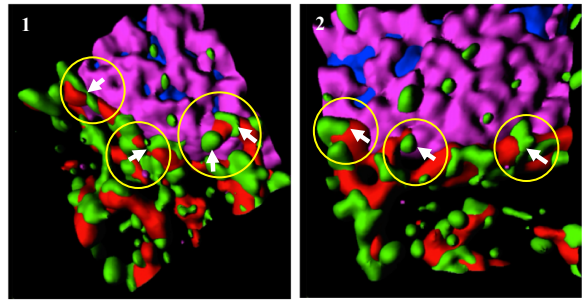
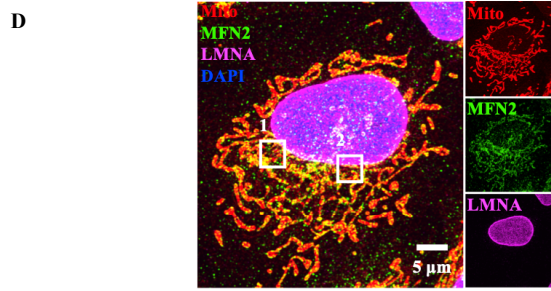
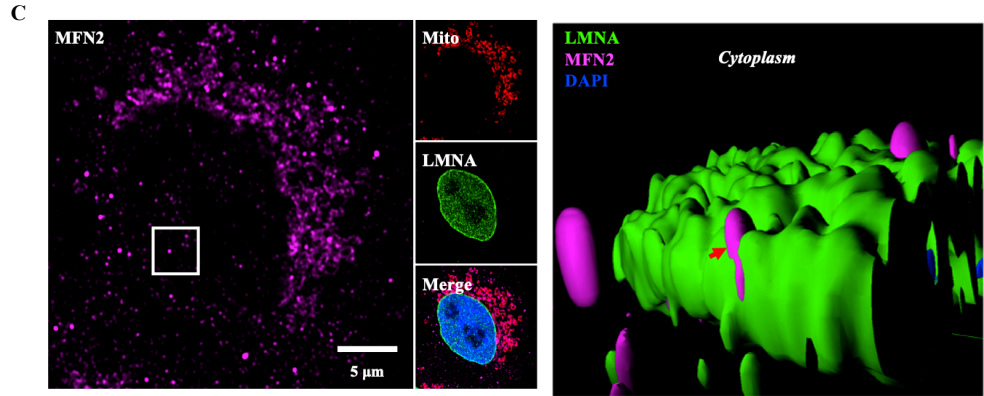
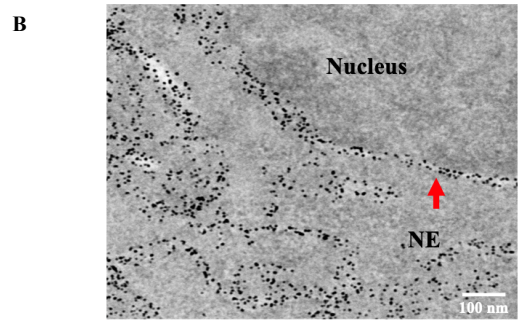
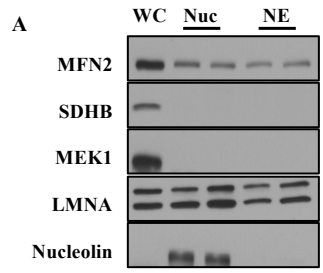
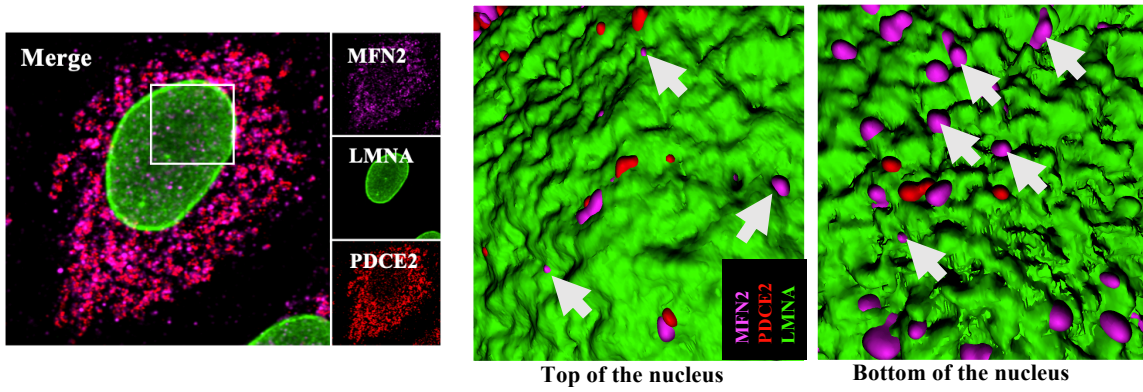
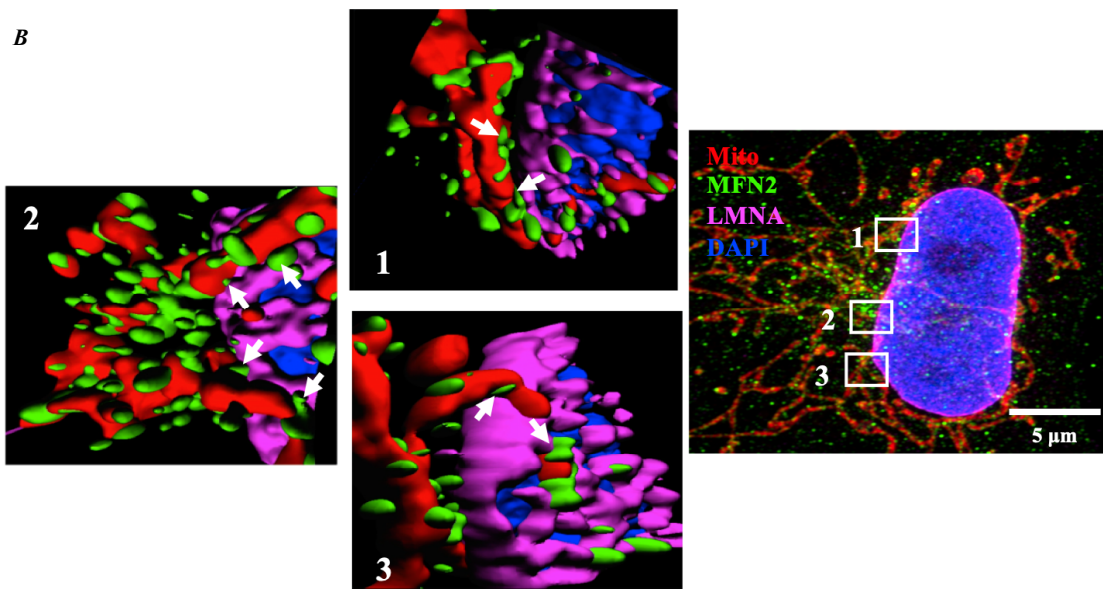


Fig. 3-3 MFN2 is between perinuclear mitochondria and the NE. (A) Immunoblot loaded with nuclear and NE protein extracts from A549 cells showing MFN2 on the NE in two different experiments. Nuclear and NE purity was assessed by the absence of the mitochondrial marker SDHB, the cytoplasmic marker MEK1 and the presence of LMNA. NE purity was assessed by the absence of the nucleolar marker nucleolin. (B) ImmunoTEM staining of an A549 cell showing MFN2 (black dots) on the NE (red arrow). Scale bar is at 100 nm. (C) A super resolution confocal image of A549 cells stained for MFN2 (magenta), LMNA (green), mitotracker (red) and DAPI (blue). On the right, we show a still from a video of a 3D reconstructed model of the area indicated by the white square, where MFN2 is embedded within the LMNA layer (red arrow). Scale bar is at 5 μ m. The video can be seen at <https://bit.ly/33UWXBi> (D) MFN2 (green) is between the NE and perinuclear mitochondria (red) touching the NE (white arrows) suggesting that MFN2 facilitates the tethering of the two. Cells were also stained with LMNA (magenta) to allow visualization of the NE. Scale bar is at 5 μ m. (E) ImmunoTEM image of an A549 cell showing MFN2 (black dots) between a mitochondrion (dotted red line) and the NE (white arrow). Scale bar is at 100 nm.

A



B



C

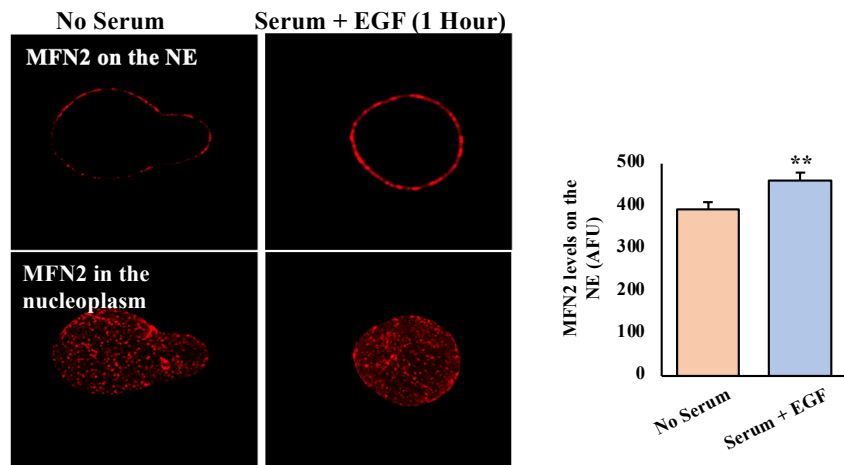


Fig. 3-4 MFN2 is present on the NE. (A) Confocal super resolution image of an A549 cell stained with MFN2 (magenta), LMNA (green) and PDCE2 (red). The white square indicates an area where we performed a z stack and created a 3D reconstruction model. On the left, the top and bottom of the nucleus as seen on the 3D reconstructed model showing the presence of MFN2 (white arrows) on the NE. (B) Super resolution confocal image of an A549 cell stained with antibodies against MFN2 (green), LMNA (magenta), mitotracker (red) and DAPI (blue) showing MFN2 on the NE. On the left, we show 3D reconstructed models of the areas indicated by the white squares (on the right), where MFN2 is embedded on the LMNA layer and is located between perinuclear mitochondria and the NE (white arrows). Scale bar is at 5 μm . (C) Exposure of A549 cells to serum and EGF (500 ng/ml) for 1 hour increases MFN2 (red) on the NE. The NE was selected based on staining of the cells with LMNA (not shown). MFN2 was also present in the nucleoplasm. n = 120 cells per group in 3 experiments. P value was 0.0021 as assessed by student's t test.

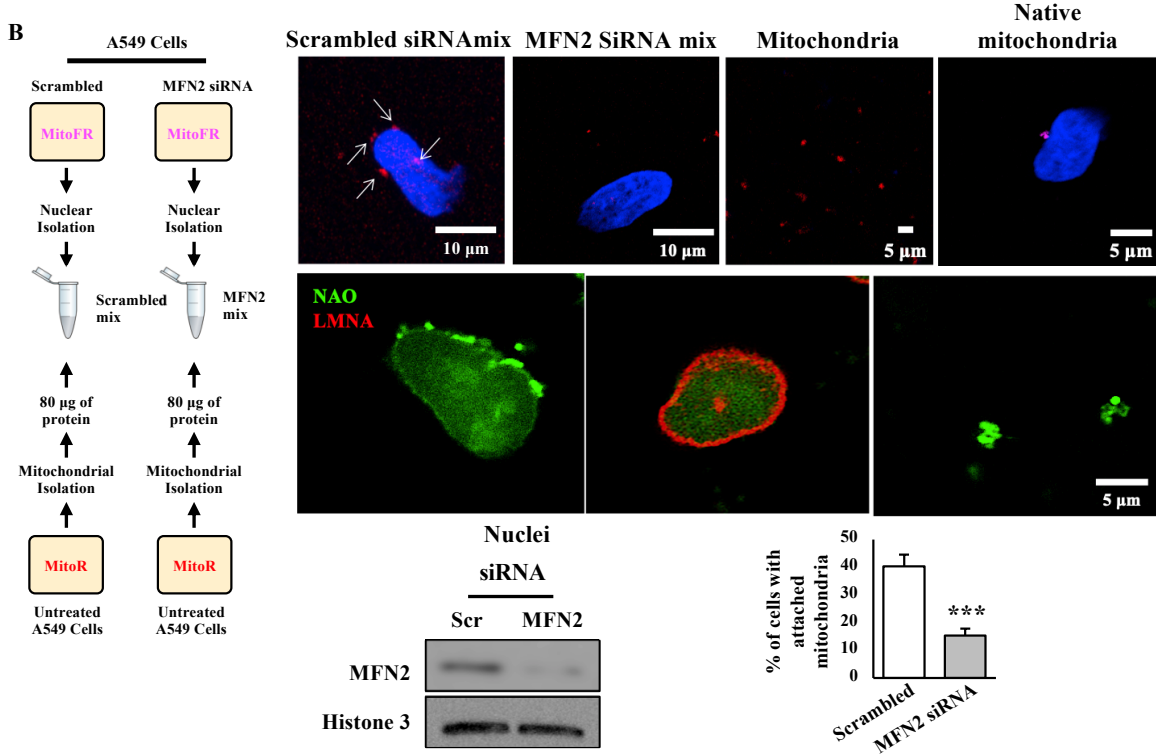
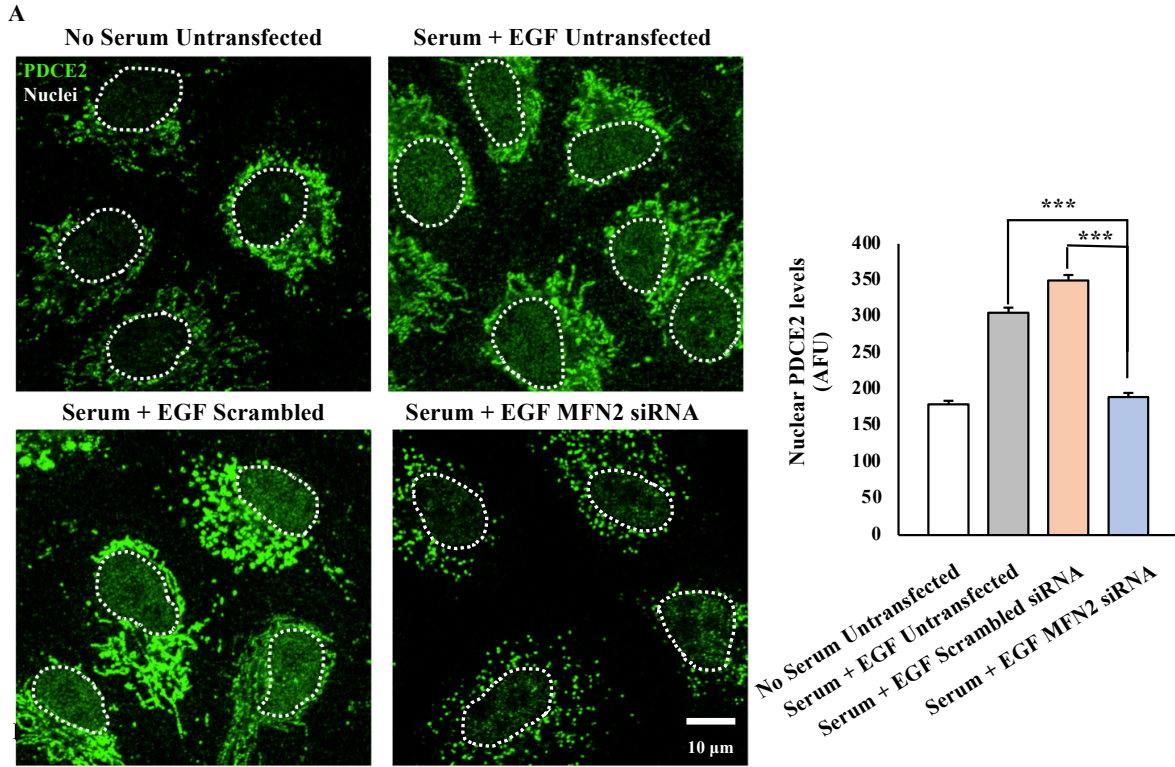


Fig. 3-5 Mitochondria tether to the NE via MFN2-rich contact points. (A) Immunostaining experiment showing MFN2 knockdown by siRNA on A549 cells decreases nuclear PDCE2 (green) levels after exposure to serum and EGF (500 ng/ml). The nucleus is indicated by a dotted white line. n = 180 cells per group in 3 experiments. P values are less than 0.001 as assessed by one-way ANOVA with Bonferroni post-hoc analysis. Error bars represent SEM. Scale bar is at 10 μ m. **(B)** Schematic representation of the experimental design and *in vitro* experiments assessing mitochondrial tethering to the NE on A549 cells. Loss of nuclear MFN2 by siRNA results in decreased tethering of untransfected mitochondria (red) to isolated nuclei (blue), indicated by white arrows. Nuclear purity was assessed by the presence of native mitochondria that were stained with mitotracker deep-red (magenta). Loss of MFN2 after the siRNA treatment was verified by an immunoblot. In another experiment mitochondria were stained with NAO and added to isolated nuclei. The nuclear envelope was visualized by LMNA staining (red). P value was less than 0.001. n = 120 nuclei per group in 3 experiments. Error bars represent SEM. Significance was assessed by student's t test.

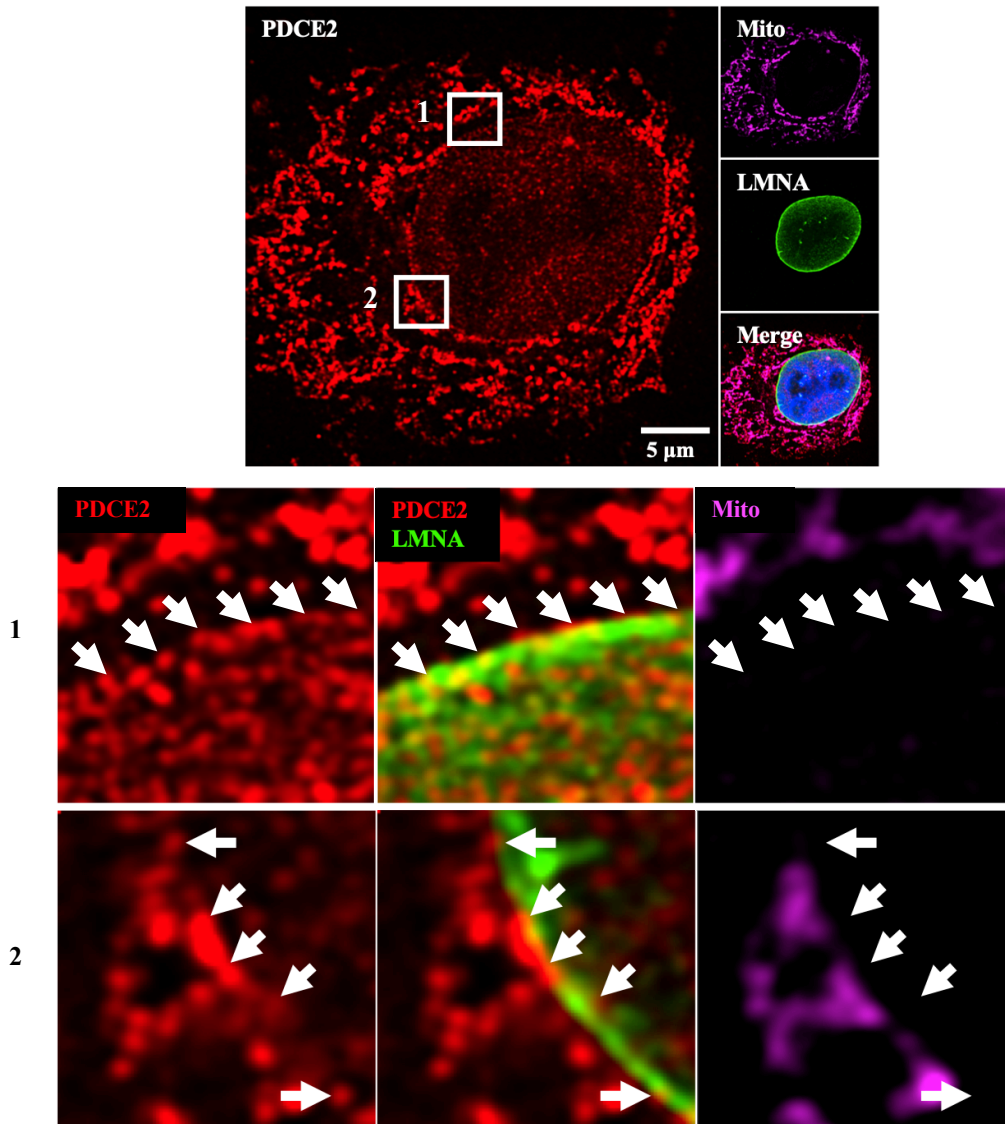
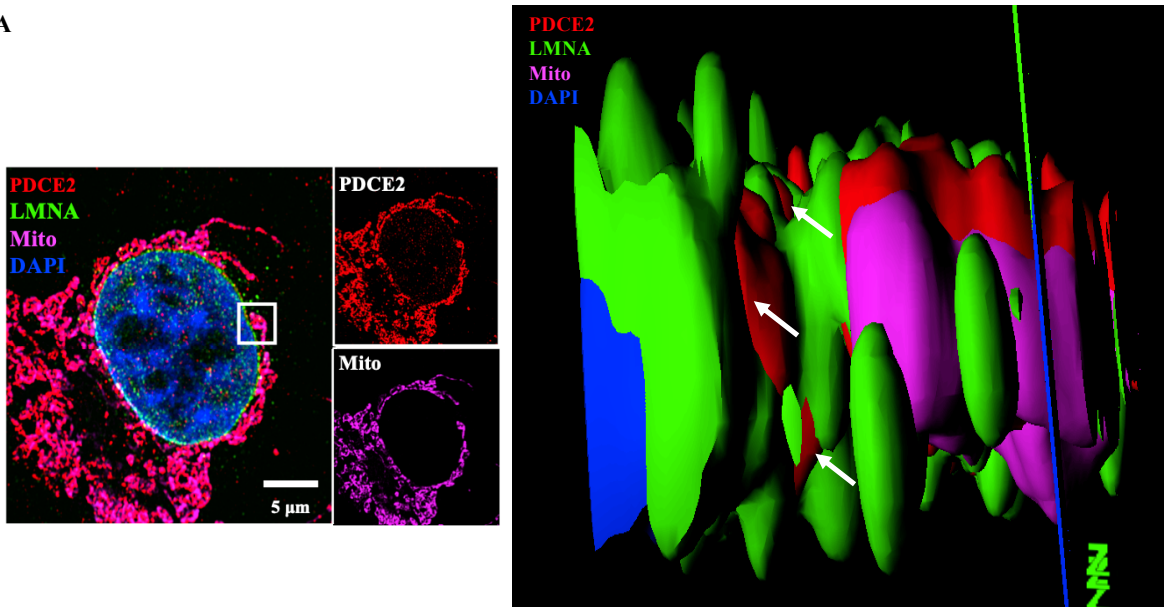
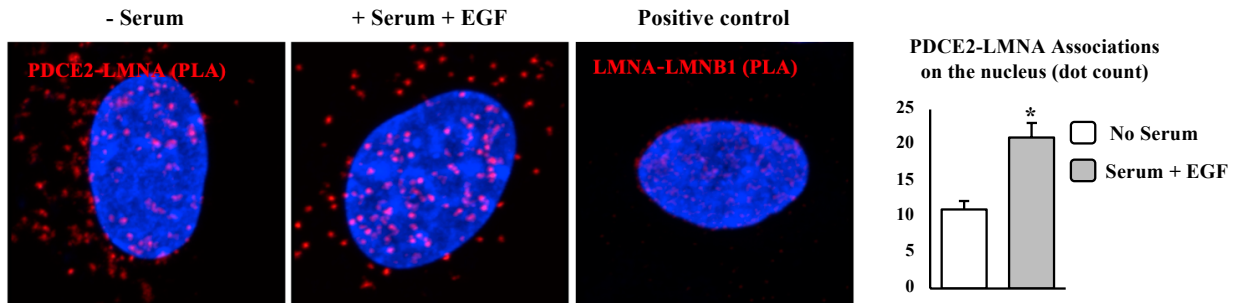


Fig. 3-6 Extramitochondrial PDC colocalizes with LMNA on the NE. Super resolution confocal image of an A549 cell stained for PDCE2 (red), LMNA (green) and mitotracker (magenta). The white squares indicate areas where we obtained high magnification images showing extramitochondrial PDCE2 (red) colocalizing (white arrows) with LMNA (green) after exposure of A549 cells to serum and EGF (500 ng/ml). The nucleus was stained with DAPI (blue). Scale bar is at 5 μ m.

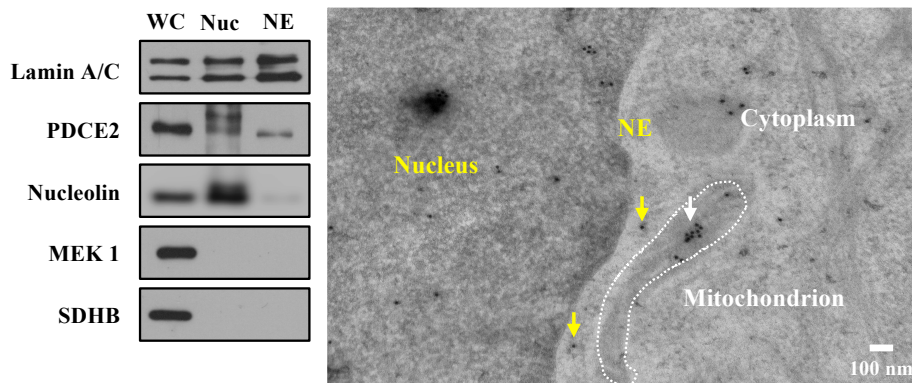
A



B



C



D

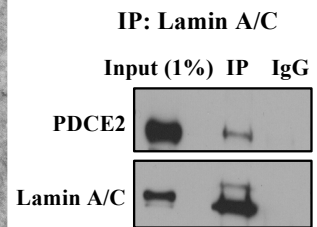


Fig. 3-7 PDC interacts with LMNA. (A) Super resolution image of an A549 cell stained with antibodies against PDCE2 (red), LMNA (green), mitotracker (magenta) and DAPI (blue). The white square indicates an area that we performed a z stack and created a video of a 3D reconstructed model. A still of the video is shown on the right, where extramitochondrial PDC is embedded into the LMNA layer (white arrows), suggesting that the two proteins might interact directly and this interaction is important for the nuclear import of PDC. The video can be seen on <https://bit.ly/34UE14Z> (B) Proximity ligation assay (PLA) between PDCE2 and LMNA (red dots) in A549 cells suggesting that the two proteins come to close proximity and might interact directly. As a positive control we used the known interaction of LMNA and LMNB1. Nuclei were stained with DAPI (blue). n = 150 cells per group in 3 experiments. P value was 0.035 as assessed by a student's t test. Error bars represent SEM. (C) Extramitochondrial PDCE2 can be found on the NE and the nuclear periphery of A549 cells exposed to serum and EGF (500 ng/ml) for 2 hours as seen by immunoblots (extracts from whole cells, nuclei and NE) and immunoTEM (yellow arrows point to extramitochondrial PDCE2, while a white arrow points to PDCE2 within a mitochondrion). (D) A co-immunoprecipitation experiment showing direct interaction between PDCE2 and LMNA in A549 cells.

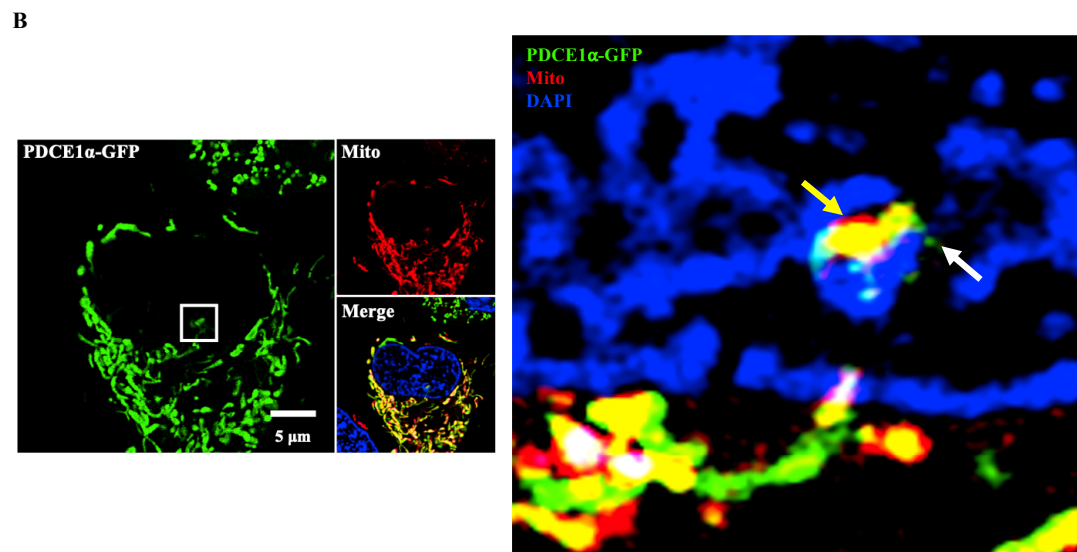
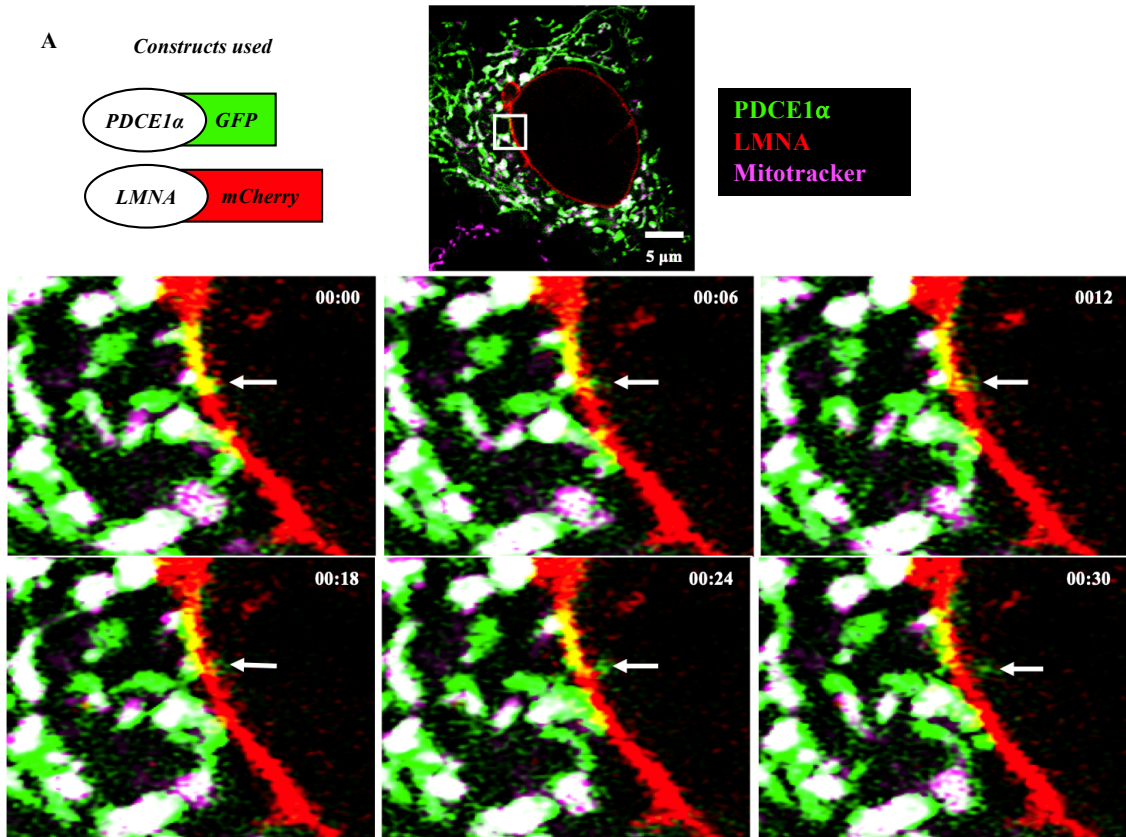


Fig. 3-8 Perinuclear mitochondria release PDC into the nucleoplasm. (A) Super resolution live imaging of A549 cells transfected with constructs expressing PDCE1 α and LMNA coupled to GFP (green) and mCherry (red) respectively. Mitochondria were stained with mitotracker (magenta). (Below) A still of a super resolution live imaging video on the area indicated by the white square (upper image) showing perinuclear mitochondria releasing PDCE1 α (green) into the nucleoplasm (white arrows) in response to serum and EGF (500 ng/ml). Images were obtained every 6 seconds. Scale bar is at 5 μ m. The video can be seen on <https://bit.ly/374amsR> **(B)** Super resolution live imaging of A549 cells transfected with a construct expressing PDCE1 α coupled to GFP (green). Mitochondria were stained with mitotracker (red) and the nucleus with Hoechst (blue). (On the right) A still of a super resolution live imaging video of the area indicated with the white square on the left showing mitochondria (red/yellow arrow) releasing PDC (green) within a nuclear invagination (white arrow). The video can be seen on <https://bit.ly/341UPrP>

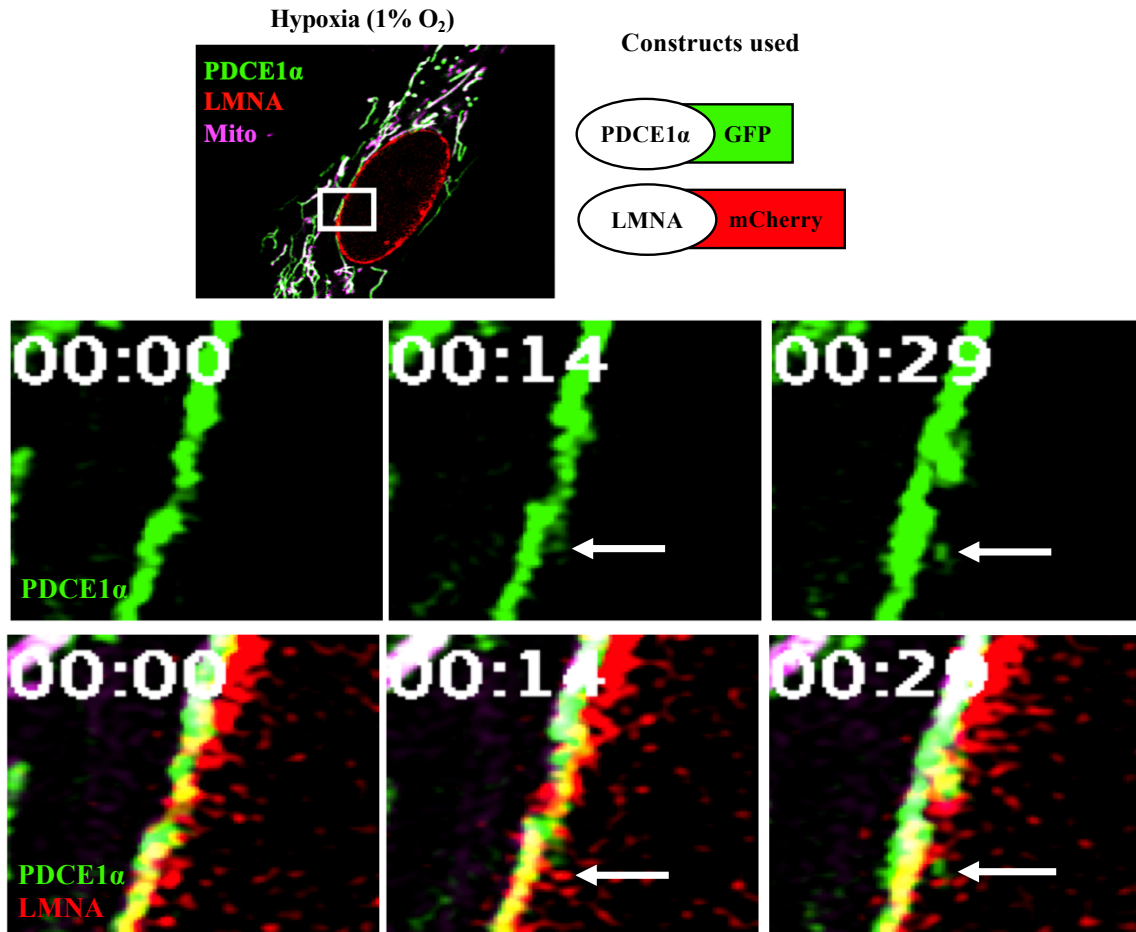


Fig. 3-9 Perinuclear mitochondria release PDC into the nucleoplasm in response to hypoxia. A still of a super resolution live imaging video of an HFF-1 cell under hypoxia (1% O₂) transfected with constructs expressing PDCE1 α and LMNA coupled to GFP (green) and mCherry (red) respectively. (Below) Consecutive time frames of the video from the area indicated by the white square on the upper image showing PDCE1 α being released into the nucleoplasm from perinuclear mitochondria (white arrow). Mitochondria were stained with mitotracker (magenta). The video can be seen at <https://bit.ly/376MrZY>

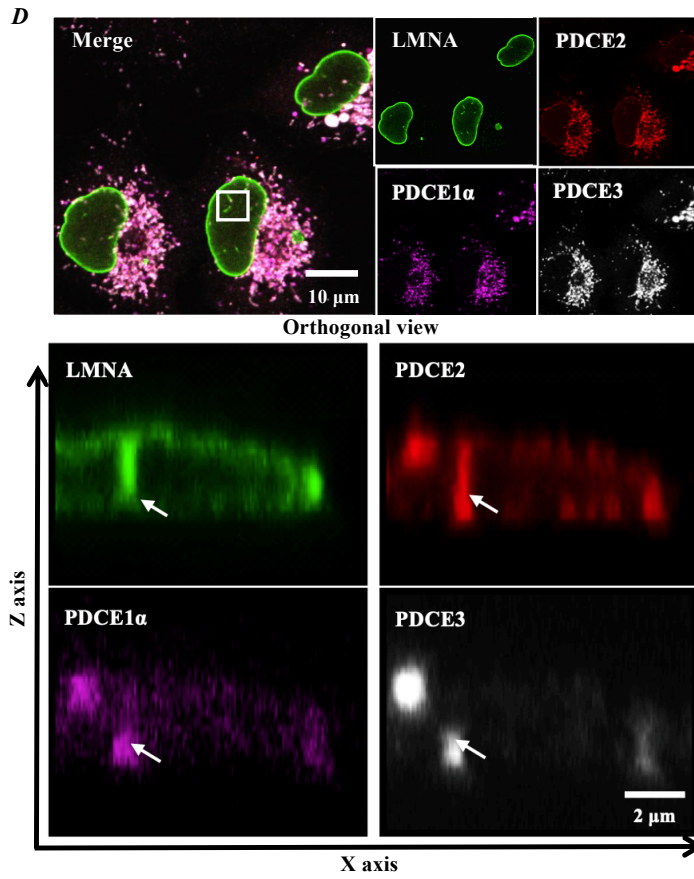
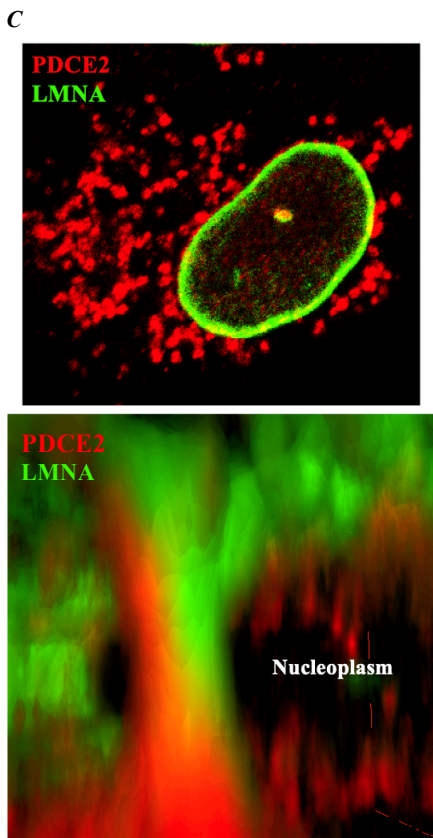
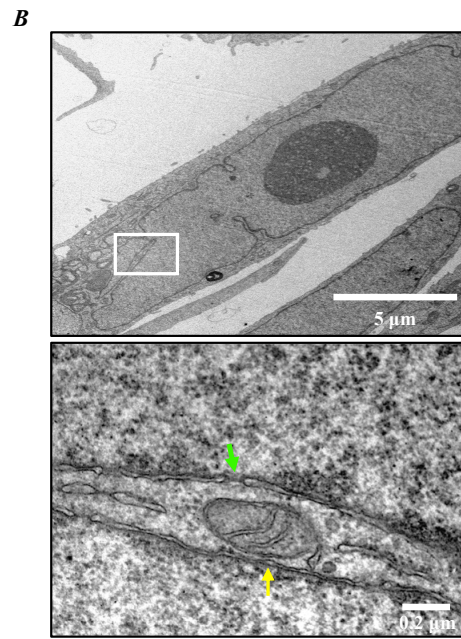
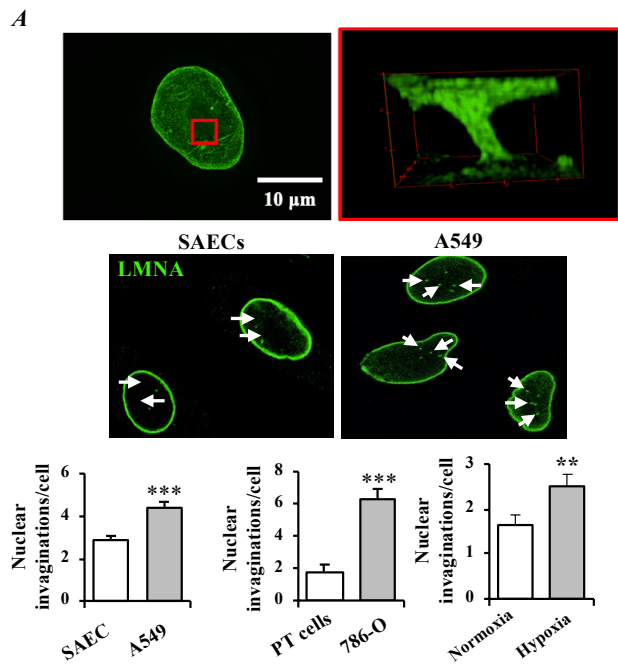


Fig. 3-10 All PDC subunits can be found within nuclear invaginations that are increased after exposure to proliferative stimuli. (A) A super resolution confocal image of an A549 cell stained with LMNA (green) showing a nuclear invagination (red square). On the left, a still from a 3D reconstructed video of the nuclear invagination (indicated by a red square on the left image). The video can be seen at <https://bit.ly/3nR0pVt> Cancer cells (A549 and 786-O cells) have more nuclear invaginations (white arrows) than their healthy controls (small airway epithelial and proximal tubule cells). n = 150 cells per type in 3 experiments with 50 cells. P values were less than 0.001. Scale bar is at 10 μ m. Hypoxia (1% O₂) increases the number of nuclear invaginations in a healthy cell line (proximal tubule cells). n = 180 cells per group in 3 experiments. P value was 0.002. Error bars represent SEM. Statistical significance was assessed by student's t test. **(B)** A TEM image of an A549 cell showing a whole mitochondrion (yellow arrow) within a nuclear invagination (white box). The nuclear pore is indicated by a green arrow. **(C)** PDCE2 (red) colocalizes with LMNA (green) within a nuclear invagination (white arrow) in an A549 cell as seen under a confocal microscope. The lower image is a still from a video of a 3D reconstructed model of the nuclear invagination. The video can be seen at <https://bit.ly/318nutb> **(D)** All PDC subunits (white arrows) can be found within a nuclear invagination of A549 cells stained with LMNA (green), PDCE2 (red), PDCE1 α (magenta) and PDCE3 (grey).

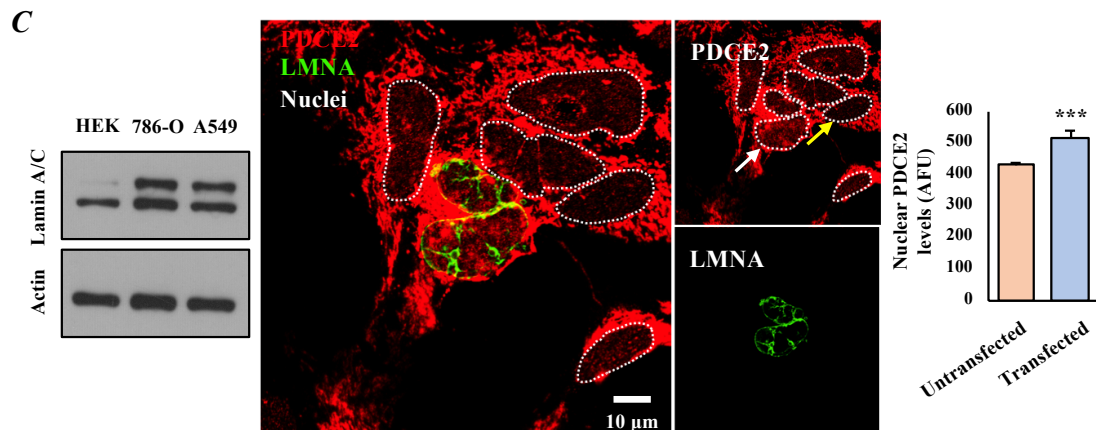
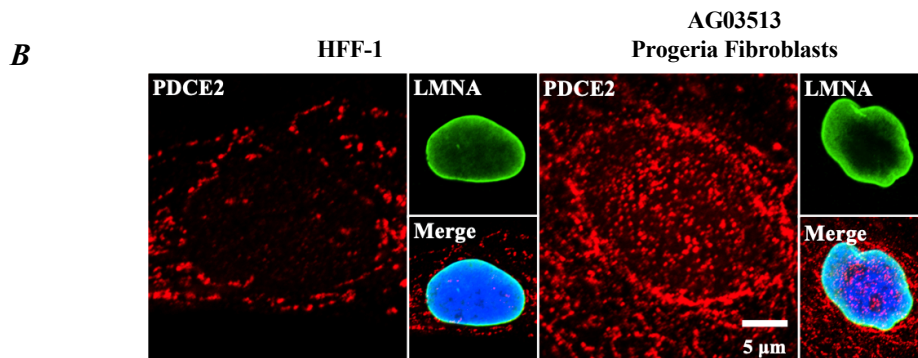
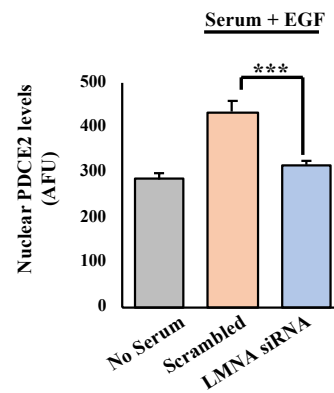
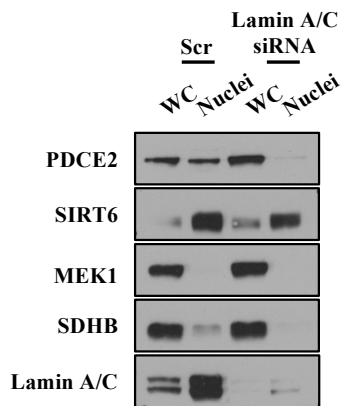
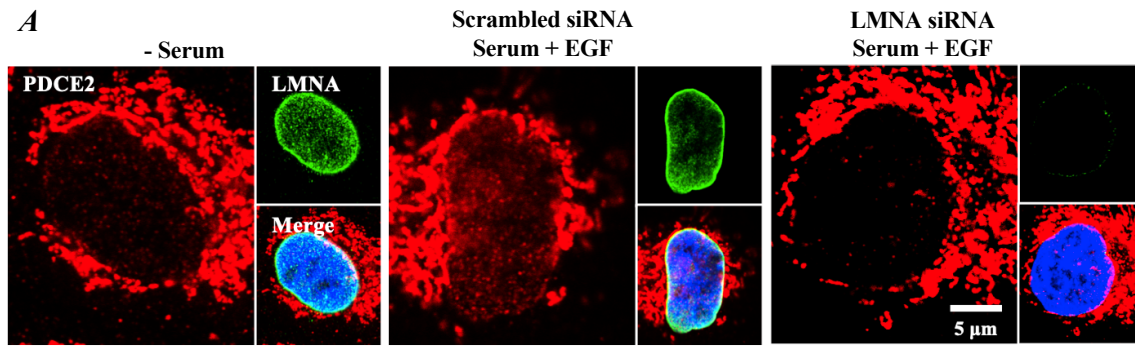


Fig. 3-11 LMNA is necessary for the nuclear entrance of PDC. (A) Loss of LMNA (green) by siRNA decreases nuclear PDCE2 (red) but not SIRT6 levels in A549 cells that were exposed to serum and EGF (500 ng/ml) as assessed by confocal imaging and immunoblots (whole cells and nuclear extracts). Nuclei were stained with DAPI (blue). $n = 150$ cells per group in 3 experiments. P value was less than 0.001 as assessed by one-way ANOVA with Bonferroni post hoc analysis. Error bars represent SEM. Scale bar is at 5 μm . Nuclear purity on immunoblots was assessed by the absence of SDHB (mitochondria) and MEK1 (cytoplasm). (B) Fibroblasts from progeria patients have higher nuclear PDCE2 (red) levels compared to healthy HFF-1 cells. Cells were stained with antibodies against LMNA (green) and DAPI (blue). Scale bar is at 5 μm . (C) Immunoblot showing that HEK cells express lower levels of lamin A (higher band) than 786-O and A549 cells. Overexpression of lamin A (green) on HEK cells by transfecting them with a lamin A-mCherry plasmid results in higher nuclear PDCE2 (red) levels. A nucleus of a transfected cell is indicated by a white arrow, while a yellow arrow points to a cell that did not take up the plasmid. $n = 180$ cells per group in 3 experiments with. P value was 0.024 as assessed by a student's t test. Error bars represent mean. Scale bar is at 10 μm .

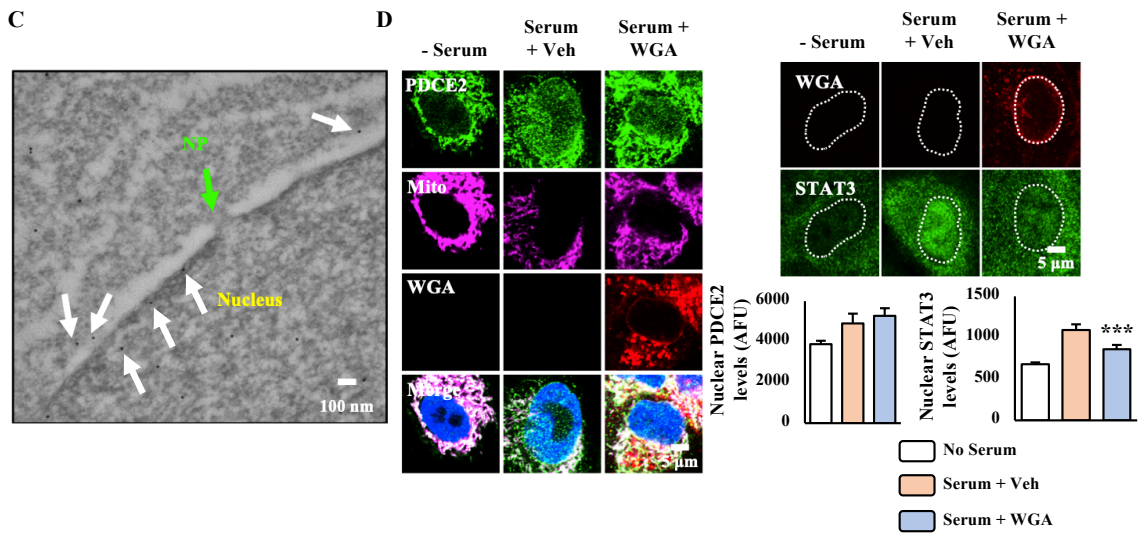
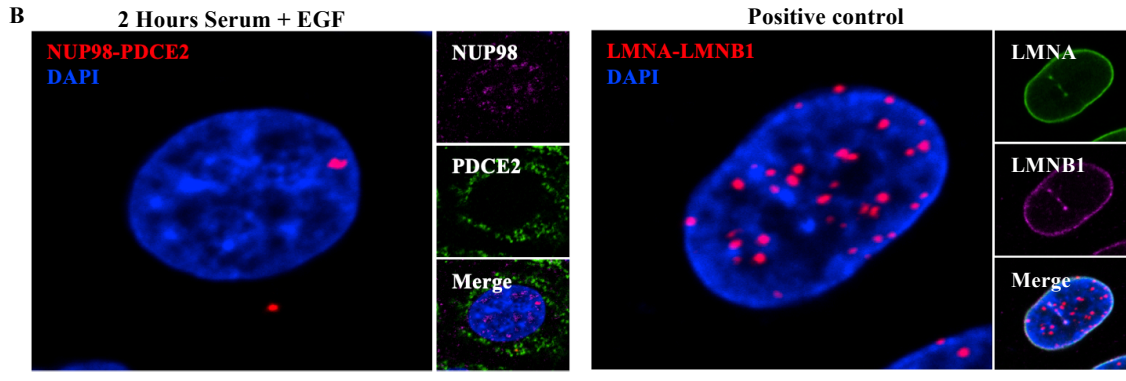
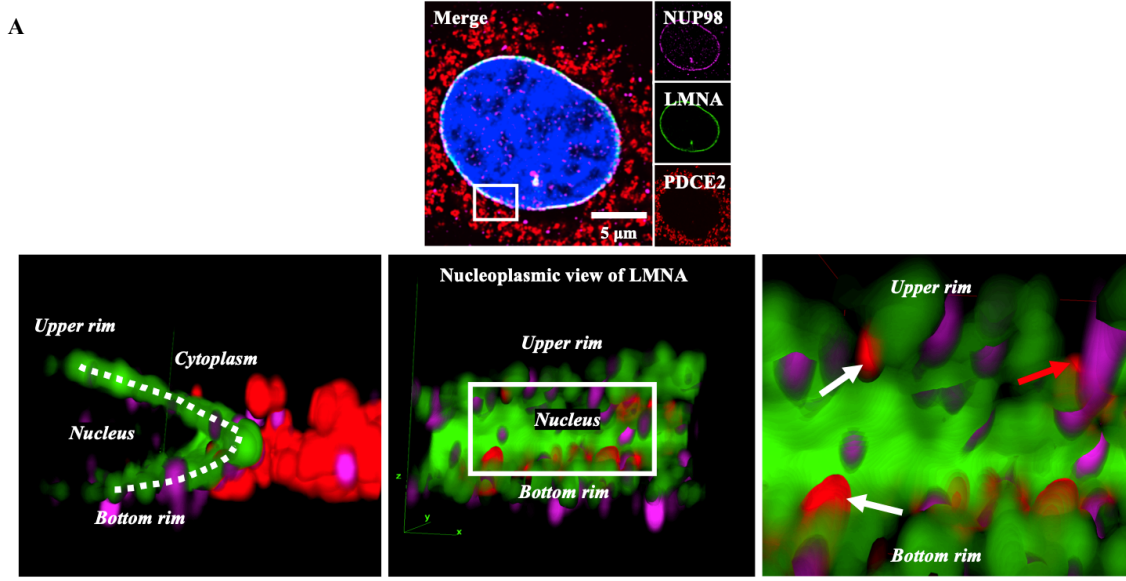


Fig. 3-12 PDC does not enter the nucleus through the nuclear pore. (A) Super resolution confocal image of an A549 cell stained with NUP98 (magenta), LMNA (green) and PDCE2 (red). The white square indicates an area where we performed a z stack and created a 3D reconstruction model. (Below) A still of a video of the 3D reconstructed model showing that most of the PDC does not colocalize with the NP (white arrows). However, a fraction of PDC can be found colocalizing with the NP (red arrow). The video can be seen on <https://bit.ly/3k1BOLt> The nucleus was stained with DAPI (blue). Scale bar is at 5 μ m. **(B)** Proximity ligation assay (red dots) between NUP98 (magenta) and PDCE2 (green) does not show association of the two proteins, suggesting that the majority of PDC does not enter the nucleus through the nuclear pores. The known interaction of LMNA (green) and LMNB1 (magenta) was used as a positive control. The nucleus was stained with DAPI. **(C)** immunoTEM image of an A549 cells showing that PDCE2 (black dots) can be found on the NE (white arrows) and not in close proximity to the NP (green arrow). Scale bar is at 100 nm. **(D)** Microinjection of 450 μ g/ml of wheat germ agglutinin (red) in A549 cells does not alter the levels of nuclear PDCE2 (green) unlike STAT3 (green) that is known to enter the nucleus through the NP after exposure to serum and EGF (500 ng/ml), suggesting that PDC does not enter the nucleus via the canonical pathway (i.e. through the NPs). Mitochondria were stained with mitotracker (magenta) and the nucleus with DAPI (blue). To ensure that we are obtaining the full depth of the nucleus we performed z stacks and summed the intensities before measuring nuclear levels of either PDCE2 or STAT3. n = 150 cells per group in 3 experiments. P value for STAT3 levels was 0.021

as assessed by one-way ANOVA coupled to Bonferroni post-hoc analysis. Error bars represent SEM. Scale bars are at 5 μm .

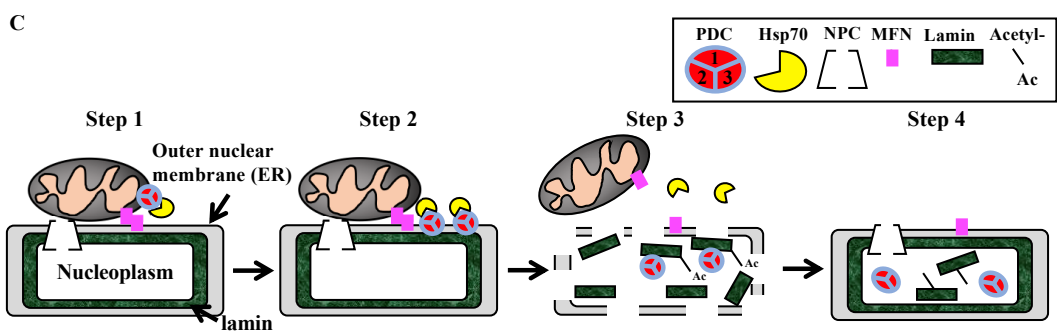
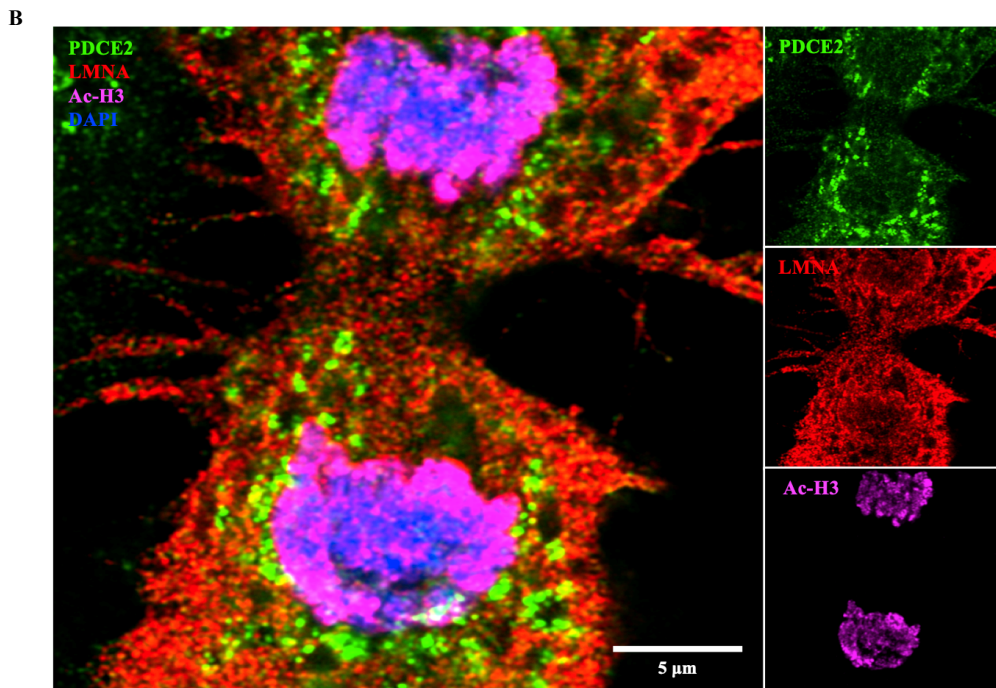
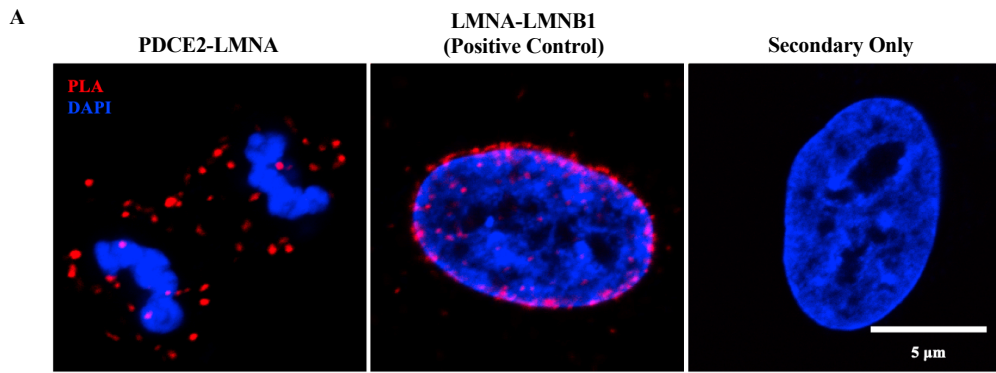


Fig. 3-13 PDC interacts with LMNA during cell division. (A-B) Super resolution confocal imaging and PLA between PDCE2 and LMNA shows interaction of the two proteins during cell division, where LMNA is depolymerized and dispersed throughout the cytoplasm before reforming the NE in the daughter cells, suggesting that lamin-bound PDC can then be released into the nucleoplasm of the daughter nuclei. Scale bars are at 5 μm . **(C)** Proposed mechanism for the nuclear entry of PDC.

References

- 1 Sumegi, B., Liposits, Z., Inman, L., Paull, W. K. & Srere, P. A. Electron microscopic study on the size of pyruvate dehydrogenase complex in situ. *Eur J Biochem* **169**, 223-230, doi:10.1111/j.1432-1033.1987.tb13601.x (1987).
- 2 Zhou, Z. H., McCarthy, D. B., O'Connor, C. M., Reed, L. J. & Stoops, J. K. The remarkable structural and functional organization of the eukaryotic pyruvate dehydrogenase complexes. *Proc Natl Acad Sci U S A* **98**, 14802-14807, doi:10.1073/pnas.011597698 (2001).
- 3 Zhou, Z. H. *et al.* Direct evidence for the size and conformational variability of the pyruvate dehydrogenase complex revealed by three-dimensional electron microscopy. The "breathing" core and its functional relationship to protein dynamics. *J Biol Chem* **276**, 21704-21713, doi:10.1074/jbc.M101765200 (2001).
- 4 Vijayakrishnan, S. *et al.* Solution structure and characterisation of the human pyruvate dehydrogenase complex core assembly. *J Mol Biol* **399**, 71-93, doi:10.1016/j.jmb.2010.03.043 (2010).
- 5 Chacinska, A., Koehler, C. M., Milenkovic, D., Lithgow, T. & Pfanner, N. Importing mitochondrial proteins: machineries and mechanisms. *Cell* **138**, 628-644, doi:10.1016/j.cell.2009.08.005 (2009).
- 6 Sutendra, G. *et al.* A nuclear pyruvate dehydrogenase complex is important for the generation of acetyl-CoA and histone acetylation. *Cell* **158**, 84-97, doi:10.1016/j.cell.2014.04.046 (2014).

- 7 Pante, N. & Kann, M. Nuclear pore complex is able to transport macromolecules with diameters of about 39 nm. *Mol Biol Cell* **13**, 425-434, doi:10.1091/mbc.01-06-0308 (2002).
- 8 Matsuda, S. *et al.* Nuclear pyruvate kinase M2 complex serves as a transcriptional coactivator of arylhydrocarbon receptor. *Nucleic Acids Res* **44**, 636-647, doi:10.1093/nar/gkv967 (2016).
- 9 Nagaraj, R. *et al.* Nuclear Localization of Mitochondrial TCA Cycle Enzymes as a Critical Step in Mammalian Zygotic Genome Activation. *Cell* **168**, 210-223 e211, doi:10.1016/j.cell.2016.12.026 (2017).
- 10 Richard, A. J., Hang, H. & Stephens, J. M. Pyruvate dehydrogenase complex (PDC) subunits moonlight as interaction partners of phosphorylated STAT5 in adipocytes and adipose tissue. *J Biol Chem* **292**, 19733-19742, doi:10.1074/jbc.M117.811794 (2017).
- 11 Chen, J. *et al.* Compartmentalized activities of the pyruvate dehydrogenase complex sustain lipogenesis in prostate cancer. *Nat Genet* **50**, 219-228, doi:10.1038/s41588-017-0026-3 (2018).
- 12 Ferriero, R. *et al.* Pyruvate dehydrogenase complex and lactate dehydrogenase are targets for therapy of acute liver failure. *J Hepatol* **69**, 325-335, doi:10.1016/j.jhep.2018.03.016 (2018).
- 13 Zhou, W. *et al.* Nuclear accumulation of pyruvate dehydrogenase alpha 1 promotes histone acetylation and is essential for zygotic genome activation in

- porcine embryos. *Biochim Biophys Acta Mol Cell Res* **1867**, 118648, doi:10.1016/j.bbamcr.2020.118648 (2020).
- 14 de Brito, O. M. & Scorrano, L. Mitofusin 2 tethers endoplasmic reticulum to mitochondria. *Nature* **456**, 605-610, doi:10.1038/nature07534 (2008).
- 15 Murley, A. & Nunnari, J. The Emerging Network of Mitochondria-Organelle Contacts. *Mol Cell* **61**, 648-653, doi:10.1016/j.molcel.2016.01.031 (2016).
- 16 Gerace, L. & Blobel, G. The nuclear envelope lamina is reversibly depolymerized during mitosis. *Cell* **19**, 277-287, doi:10.1016/0092-8674(80)90409-2 (1980).
- 17 Cohen, S., Au, S. & Pante, N. How viruses access the nucleus. *Biochim Biophys Acta* **1813**, 1634-1645, doi:10.1016/j.bbamcr.2010.12.009 (2011).
- 18 Andersson, S. G. *et al.* The genome sequence of *Rickettsia prowazekii* and the origin of mitochondria. *Nature* **396**, 133-140, doi:10.1038/24094 (1998).
- 19 Burgdorfer, W., Anacker, R. L., Bird, R. G. & Bertram, D. S. Intranuclear growth of *Rickettsia rickettsii*. *J Bacteriol* **96**, 1415-1418 (1968).
- 20 Westermann, B. Mitochondrial fusion and fission in cell life and death. *Nat Rev Mol Cell Biol* **11**, 872-884, doi:10.1038/nrm3013 (2010).
- 21 Schrepfer, E. & Scorrano, L. Mitofusins, from Mitochondria to Metabolism. *Mol Cell* **61**, 683-694, doi:10.1016/j.molcel.2016.02.022 (2016).
- 22 Wilson, K. L. & Foisner, R. Lamin-binding Proteins. *Cold Spring Harb Perspect Biol* **2**, a000554, doi:10.1101/cshperspect.a000554 (2010).

- 23 Alam, M. S. Proximity Ligation Assay (PLA). *Curr Protoc Immunol* **123**, e58, doi:10.1002/cpim.58 (2018).
- 24 Simon, D. N. & Wilson, K. L. Partners and post-translational modifications of nuclear lamins. *Chromosoma* **122**, 13-31, doi:10.1007/s00412-013-0399-8 (2013).
- 25 Ardestani, P. M. & Liang, F. Sub-cellular localization, expression and functions of Sirt6 during the cell cycle in HeLa cells. *Nucleus* **3**, 442-451, doi:10.4161/nucl.21134 (2012).
- 26 Maresca, G. *et al.* LMNA knock-down affects differentiation and progression of human neuroblastoma cells. *PLoS One* **7**, e45513, doi:10.1371/journal.pone.0045513 (2012).
- 27 Yoneda, Y., Imamoto-Sonobe, N., Yamaizumi, M. & Uchida, T. Reversible inhibition of protein import into the nucleus by wheat germ agglutinin injected into cultured cells. *Exp Cell Res* **173**, 586-595, doi:10.1016/0014-4827(87)90297-7 (1987).
- 28 Benavente, R., Dabauvalle, M. C., Scheer, U. & Chaly, N. Functional role of newly formed pore complexes in postmitotic nuclear reorganization. *Chromosoma* **98**, 233-241, doi:10.1007/bf00327308 (1989).
- 29 Park, O. K., Schaefer, T. S. & Nathans, D. In vitro activation of Stat3 by epidermal growth factor receptor kinase. *Proc Natl Acad Sci U S A* **93**, 13704-13708, doi:10.1073/pnas.93.24.13704 (1996).

- 30 Chan, K. S. *et al.* Epidermal growth factor receptor-mediated activation of Stat3 during multistage skin carcinogenesis. *Cancer Res* **64**, 2382-2389, doi:10.1158/0008-5472.can-03-3197 (2004).
- 31 Song, L., Turkson, J., Karras, J. G., Jove, R. & Haura, E. B. Activation of Stat3 by receptor tyrosine kinases and cytokines regulates survival in human non-small cell carcinoma cells. *Oncogene* **22**, 4150-4165, doi:10.1038/sj.onc.1206479 (2003).
- 32 Liu, L., McBride, K. M. & Reich, N. C. STAT3 nuclear import is independent of tyrosine phosphorylation and mediated by importin-alpha3. *Proc Natl Acad Sci U S A* **102**, 8150-8155, doi:10.1073/pnas.0501643102 (2005).
- 33 Cimica, V., Chen, H. C., Iyer, J. K. & Reich, N. C. Dynamics of the STAT3 transcription factor: nuclear import dependent on Ran and importin-beta1. *PLoS One* **6**, e20188, doi:10.1371/journal.pone.0020188 (2011).
- 34 Eisenberg-Bord, M., Shai, N., Schuldiner, M. & Bohnert, M. A Tether Is a Tether Is a Tether: Tethering at Membrane Contact Sites. *Dev Cell* **39**, 395-409, doi:10.1016/j.devcel.2016.10.022 (2016).
- 35 Iwasawa, R., Mahul-Mellier, A. L., Datler, C., Pazarentzos, E. & Grimm, S. Fis1 and Bap31 bridge the mitochondria-ER interface to establish a platform for apoptosis induction. *EMBO J* **30**, 556-568, doi:10.1038/emboj.2010.346 (2011).
- 36 De Vos, K. J. *et al.* VAPB interacts with the mitochondrial protein PTPIP51 to regulate calcium homeostasis. *Hum Mol Genet* **21**, 1299-1311, doi:10.1093/hmg/ddr559 (2012).

- 37 Elbaz, Y. & Schuldiner, M. Staying in touch: the molecular era of organelle contact sites. *Trends Biochem Sci* **36**, 616-623, doi:10.1016/j.tibs.2011.08.004 (2011).
- 38 Kinnaird, A., Zhao, S., Wellen, K. E. & Michelakis, E. D. Metabolic control of epigenetics in cancer. *Nat Rev Cancer* **16**, 694-707, doi:10.1038/nrc.2016.82 (2016).
- 39 Bonnet, S. *et al.* A mitochondria-K⁺ channel axis is suppressed in cancer and its normalization promotes apoptosis and inhibits cancer growth. *Cancer Cell* **11**, 37-51, doi:10.1016/j.ccr.2006.10.020 (2007).
- 40 Schindelin, J. *et al.* Fiji: an open-source platform for biological-image analysis. *Nat Methods* **9**, 676-682, doi:10.1038/nmeth.2019 (2012).
- 41 Schmid, B., Schindelin, J., Cardona, A., Longair, M. & Heisenberg, M. A high-level 3D visualization API for Java and ImageJ. *BMC Bioinformatics* **11**, 274, doi:10.1186/1471-2105-11-274 (2010).
- 42 Frezza, C., Cipolat, S. & Scorrano, L. Organelle isolation: functional mitochondria from mouse liver, muscle and cultured fibroblasts. *Nat Protoc* **2**, 287-295, doi:10.1038/nprot.2006.478 (2007).

Chapter four: Final conclusions and future directions

4.1 Overall conclusions

In this dissertation we expand our previous work on PDC's translocation into the nucleus¹. We provide evidence for the presence of two different pathways that PDC is using to enter the nucleus and speculate that the utilization of each pathway is primarily dependent on the size of the complex, which is regulated by the stoichiometry and organization of its individual subunits².

In the second chapter of this thesis we show that the translocation of PDC into the nucleus depends on tubulin acetylation. We show for the first time that extramitochondrial PDC associates with both Hsp70 and acetylated microtubules and this interaction is enhanced after exposure to proliferative stimuli that also induce the nuclear translocation of PDC (i.e. serum and EGF). This is in agreement with previous observations that highlight the importance of this post translational modification (i.e. tubulin acetylation) in intracellular trafficking, since it facilitates the tethering of carrier proteins like dyneins or heat shock proteins on microtubules³⁻⁵. In the same chapter we show that loss of tubulin acetylation by knocking down the main tubulin acetyltransferase α TAT1 results in decreased levels of nuclear PDC, while pharmacologic inhibition of the main tubulin deacetylase HDAC6 by the small drug inhibitor tubacin, hence increased tubulin acetylation, results in a faster and more efficient translocation of the complex into the nucleus. Moreover, we found that extramitochondrial PDC is directly interacting with acetylated microtubules through its E2 subunit independently of microtubule stability and this interaction is lost upon knockdown of α TAT1 (i.e. decreased tubulin acetylation). We speculate that this interaction provides a secondary binding site and hence a sturdier interaction between the Hsp70-PDC complex with

microtubules while it is translocating into the nucleus similar to the dynein-dynactin complex^{6,7}.

In the same chapter we show that PDC might act as a novel tubulin acetyltransferase since loss of PDC's activity results in decreased tubulin acetylation, something that did not happen when we knocked down ACLY that provides the bulk of cytoplasmic acetyl-CoA by utilizing citrate. This finding, even though provocative, is not surprising since the E2 subunit of PDC has an intrinsic acetyl-transferase activity and it is responsible for the addition of an acetyl-group to a CoA-SH molecule from the oxidation of pyruvate. Our findings suggest that extramitochondrial PDC might be responsible for the remaining tubulin acetylation that has been observed in mice when α TAT1 is knocked out⁸. However, it cannot be excluded that extramitochondrial PDC bound onto the microtubule network might be regulating tubulin acetylation indirectly by providing acetyl-CoA to α TAT1. The elucidation of the role of PDC on tubulin acetylation requires further research. Overall, our work suggests that a certain fraction of extramitochondrial PDC might be using this pathway to reach the nucleus after forming a complex with Hsp70. However, since the entrance of proteins into the nucleus occurs via crossing of the NPs that allow only the entrance of proteins with diameters of ~39 nm we speculate that this pathway is relevant only for the smaller size PDC complexes with diameters of 25 to 39 nm. Once into the nucleus, these complexes can reach deep into the nucleoplasm and produce acetyl-CoA from pyruvate that can be used towards histone acetylation and potentially gene transcription in a localized manner, something that might have implications in the fine-tuning of the cell cycle progression.

In the third chapter of this dissertation, we unveil a novel mechanism for the entrance of PDC into the nucleus that does not involve crossing of the NPs. Direct crossing of the nuclear envelope by proteins is not a new concept as it is a common strategy for certain viruses⁹. We show that proliferative stimuli induce the perinuclear clustering of mitochondria and provide evidence that they tether to the NE via MFN2-rich domains, similar to the MFN2-mediated mitochondria-ER tethering, before releasing PDC into the nucleoplasm. The presence of MFN2 on the nuclear envelope is not surprising since it is a continuation of the rough endoplasmic reticulum and therefore it is reasonable to expect that both compartments will have similarities in their protein composition. We speculate that this is the main pathway that PDC uses to enter the nucleus, especially during states of increased proliferation. Moreover, this pathway might be more relevant to larger size (>39 nm of diameter) PDC complexes (and hence more active as it has been previously suggested¹⁰⁻¹²), since these complexes cannot cross the NP due to its intrinsic size exclusion.

PDC that enters the nucleus through this novel pathway interacts with the underlying lamin A layer, where it remains tethered until cell division that lamin A is depolymerized and dispersed throughout the cytoplasm, until its repolymerization in the nuclear envelope of the daughter cells. Exploitation of the nuclear envelope disassembly during mitosis has also been used as a means of viral entry into the nucleus⁹. The reformation of the NE in the daughter cells will allow the PDC that is bound to lamin to enter the nucleoplasm of the new cells. We speculate that the interaction of PDC with lamin A might be facilitated via acetylation of a lysine residue of the latter in its Ig-like domain (via the E2 subunit of PDC) that has been previously

shown to facilitate tethering of lamin A with a plethora of nuclear proteins. This is also in agreement with the idea that protein acetylation enhances protein – protein interactions.

4.2 Future directions

Overall, our work has new implications for future basic science and translational research:

- The discovery of acetylated microtubules as a means of nuclear translocation of PDC might provide a novel therapeutic target in various states or diseases, e.g. aging or cancer. Pharmacologic regulation of acetyl tubulin levels can result in higher or lower levels of nuclear PDC that might provide a novel approach for controlling cell proliferation.
- The framing of PDC as a potential tubulin acetyltransferase opens a new and exciting field of research. Verification of this idea will expand the role of PDC into the cell and suggest that it can use its intrinsic acetyltransferase activity to directly acetylate proteins.
- The finding that PDC does not enter the nucleus through the nuclear pores can be extended to a plethora of proteins that are known to translocate into the nucleus from different cellular compartments, including mitochondria, but do not have a known nuclear localization sequence. Further work will unveil all the key proteins of this novel pathway and can potentially lead to new therapeutic targets for various diseases.
- The presence of MFN2 on the nuclear envelope, even though not surprising, provides a new way to approach the mitochondria to nucleus communication.

However, MFN2 is not the only protein that facilitates tethering of mitochondria onto the ER, and thus the NE. Future research is necessary to reveal other proteins that might mediate the tethering of mitochondria to the NE and can potentially provide another way to control cell proliferation that has implications in various diseases with altered cellular functions e.g. cancer or aging.

- Little is known regarding the exit of proteins from the mitochondria once they are properly folded. Since PDC resides in the mitochondrial matrix it will have to cross both the inner and outer mitochondrial membranes before it can translocate into the nucleus by any of the two pathways that we propose in this dissertation. Studies involving the fractionation of mitochondrial membranes revealed that fully assembled PDC can be found on both the intermembrane space and the outer mitochondrial membrane¹³, suggesting that the whole complex somehow manages to leave the matrix. Recently, it was found that mitochondria release small vesicles known as mitochondrial-derived vesicles (MDVs) to communicate with other cellular compartments i.e. the lysosome and the late endosome^{14,15}. Interestingly enough, PDCE1 α was found to be present in these vesicles but the authors were not able to verify its final destination¹⁵. The exact mechanism for the MDV formation is not known but it was suggested that it involves mitochondrial molecular chaperones (e.g. Hsp70) and the local oxidation of cardiolipin that results in the outward bending of the mitochondrial membranes before the formation of the vesicle^{15,16}. Therefore, it is reasonable to assume that alterations in mitochondrial membrane curvature due to local lipid oxidations or by the action of molecular chaperones might offer a potential way for PDC to leave the matrix and cross the mitochondrial membranes before exposed to

the cytoplasm, either as a free complex or within an MDV. Even though, further research is needed, elucidation of this pathway might result in a novel therapeutic target that can offer a way to control the mitochondria-to-nucleus communication.

- Nuclear PDC is carrying out its canonical function by producing acetyl-CoA that is necessary to sustain the nuclear pool of acetyl-CoA, where a part of it is used towards histone acetylation facilitating the progression of the cell cycle¹. However, it is reasonable to assume that a fraction of the PDC-derived acetyl-CoA will be used to acetylate other proteins that reside in the nucleoplasm. One example is its interacting partner lamin A that has been recently shown to be acetylated¹⁷. Another example is ANKLE2 the hyperacetylation of which is necessary for the breakdown of the NE prior to cell division¹⁸⁻²⁰. Therefore, it is tempting to speculate that nuclear PDC might have a broader role in the regulation of proliferation by providing the necessary acetyl-CoA for the acetylation of **a)** histones and **b)** other proteins that are fine-tuning cell division. Identification of other interacting partners of nuclear PDC will provide a better insight on its role in cell proliferation.

- Lamin A is the only member of the nuclear lamins family that can reside on both the NE and the nucleoplasm²¹. In the nucleoplasm, lamin A is known to interact with and regulate various proteins that are involved in gene transcription and histone post-translational modifications, e.g. retinoblastoma²² and the polycomb group of proteins²³. Since nuclear PDC can also localize in the nucleoplasm and interacts with lamin A then it is reasonable to assume that nucleoplasmic lamin might provide a scaffold for PDC to bind to and produce acetyl-CoA locally and therefore induce the transcription of certain genes. Even though further research is needed, it is tempting to

speculate that the interaction of PDC with lamin A can also regulate its activity and therefore provide a novel therapeutic target for various diseases where gene transcription is altered, e.g. cancer and aging.

References

- 1 Sutendra, G. *et al.* A nuclear pyruvate dehydrogenase complex is important for the generation of acetyl-CoA and histone acetylation. *Cell* **158**, 84-97, doi:10.1016/j.cell.2014.04.046 (2014).
- 2 Patel, M. S., Nemeria, N. S., Furey, W. & Jordan, F. The pyruvate dehydrogenase complexes: structure-based function and regulation. *J Biol Chem* **289**, 16615-16623, doi:10.1074/jbc.R114.563148 (2014).
- 3 Giustiniani, J. *et al.* Tubulin acetylation favors Hsp90 recruitment to microtubules and stimulates the signaling function of the Hsp90 clients Akt/PKB and p53. *Cell Signal* **21**, 529-539, doi:10.1016/j.cellsig.2008.12.004 (2009).
- 4 Kirschke, E., Goswami, D., Southworth, D., Griffin, P. R. & Agard, D. A. Glucocorticoid receptor function regulated by coordinated action of the Hsp90 and Hsp70 chaperone cycles. *Cell* **157**, 1685-1697, doi:10.1016/j.cell.2014.04.038 (2014).
- 5 Reed, N. A. *et al.* Microtubule acetylation promotes kinesin-1 binding and transport. *Curr Biol* **16**, 2166-2172, doi:10.1016/j.cub.2006.09.014 (2006).
- 6 Kardon, J. R. & Vale, R. D. Regulators of the cytoplasmic dynein motor. *Nat Rev Mol Cell Biol* **10**, 854-865, doi:10.1038/nrm2804 (2009).
- 7 Kincaid, M. M. & King, S. J. Motors and their tethers: the role of secondary binding sites in processive motility. *Cell Cycle* **5**, 2733-2737, doi:10.4161/cc.5.23.3521 (2006).

- 8 Kalebic, N. *et al.* alphaTAT1 is the major alpha-tubulin acetyltransferase in mice. *Nat Commun* **4**, 1962, doi:10.1038/ncomms2962 (2013).
- 9 Cohen, S., Au, S. & Pante, N. How viruses access the nucleus. *Biochim Biophys Acta* **1813**, 1634-1645, doi:10.1016/j.bbamcr.2010.12.009 (2011).
- 10 Sumegi, B., Liposits, Z., Inman, L., Paull, W. K. & Srere, P. A. Electron microscopic study on the size of pyruvate dehydrogenase complex in situ. *Eur J Biochem* **169**, 223-230, doi:10.1111/j.1432-1033.1987.tb13601.x (1987).
- 11 Zhou, Z. H. *et al.* Direct evidence for the size and conformational variability of the pyruvate dehydrogenase complex revealed by three-dimensional electron microscopy. The "breathing" core and its functional relationship to protein dynamics. *J Biol Chem* **276**, 21704-21713, doi:10.1074/jbc.M101765200 (2001).
- 12 Zhou, Z. H., McCarthy, D. B., O'Connor, C. M., Reed, L. J. & Stoops, J. K. The remarkable structural and functional organization of the eukaryotic pyruvate dehydrogenase complexes. *Proc Natl Acad Sci U S A* **98**, 14802-14807, doi:10.1073/pnas.011597698 (2001).
- 13 Hitosugi, T. *et al.* Tyrosine phosphorylation of mitochondrial pyruvate dehydrogenase kinase 1 is important for cancer metabolism. *Mol Cell* **44**, 864-877, doi:10.1016/j.molcel.2011.10.015 (2011).
- 14 Neuspiel, M. *et al.* Cargo-selected transport from the mitochondria to peroxisomes is mediated by vesicular carriers. *Curr Biol* **18**, 102-108, doi:10.1016/j.cub.2007.12.038 (2008).

- 15 Soubannier, V. *et al.* A vesicular transport pathway shuttles cargo from mitochondria to lysosomes. *Curr Biol* **22**, 135-141, doi:10.1016/j.cub.2011.11.057 (2012).
- 16 Sugiura, A., McLelland, G. L., Fon, E. A. & McBride, H. M. A new pathway for mitochondrial quality control: mitochondrial-derived vesicles. *EMBO J* **33**, 2142-2156, doi:10.15252/embj.201488104 (2014).
- 17 Karoutas, A. *et al.* The NSL complex maintains nuclear architecture stability via lamin A/C acetylation. *Nat Cell Biol* **21**, 1248-1260, doi:10.1038/s41556-019-0397-z (2019).
- 18 Kaufmann, T. *et al.* SIRT2 regulates nuclear envelope reassembly through ANKLE2 deacetylation. *J Cell Sci* **129**, 4607-4621, doi:10.1242/jcs.192633 (2016).
- 19 Snyers, L. *et al.* LEM4/ANKLE-2 deficiency impairs post-mitotic re-localization of BAF, LAP2alpha and LaminA to the nucleus, causes nuclear envelope instability in telophase and leads to hyperploidy in HeLa cells. *Eur J Cell Biol* **97**, 63-74, doi:10.1016/j.ejcb.2017.12.001 (2018).
- 20 Asencio, C. *et al.* Coordination of kinase and phosphatase activities by Lem4 enables nuclear envelope reassembly during mitosis. *Cell* **150**, 122-135, doi:10.1016/j.cell.2012.04.043 (2012).
- 21 Naetar, N., Ferraioli, S. & Foisner, R. Lamins in the nuclear interior - life outside the lamina. *J Cell Sci* **130**, 2087-2096, doi:10.1242/jcs.203430 (2017).

22 Johnson, B. R. *et al.* A-type lamins regulate retinoblastoma protein function by promoting subnuclear localization and preventing proteasomal degradation. *Proc Natl Acad Sci U S A* **101**, 9677-9682, doi:10.1073/pnas.0403250101 (2004).

23 Marullo, F. *et al.* Nucleoplasmic Lamin A/C and Polycomb group of proteins: An evolutionarily conserved interplay. *Nucleus* **7**, 103-111, doi:10.1080/19491034.2016.1157675 (2016).

Bibliography

- 1 Boukouris, A. E., Zervopoulos, S. D. & Michelakis, E. D. Metabolic Enzymes Moonlighting in the Nucleus: Metabolic Regulation of Gene Transcription. *Trends Biochem Sci* **41**, 712-730, doi:10.1016/j.tibs.2016.05.013 (2016).
- 2 McEwen, B. S., Allfrey, V. G. & Mirsky, A. E. Studies on Energy-yielding Reactions in Thymus Nuclei : III. PARTICIPATION OF GLYCOLYSIS AND THE CITRIC ACID CYCLE IN NUCLEAR ADENOSINE TRIPHOSPHATE SYNTHESIS. *J Biol Chem* **238**, 2579-2586 (1963).
- 3 Siebert, G. & Humphrey, G. B. Enzymology of the nucleus. *Adv Enzymol Relat Areas Mol Biol* **27**, 239-288 (1965).
- 4 Yang, W. *et al.* PKM2 phosphorylates histone H3 and promotes gene transcription and tumorigenesis. *Cell* **150**, 685-696, doi:10.1016/j.cell.2012.07.018 (2012).
- 5 Dayton, T. L., Jacks, T. & Vander Heiden, M. G. PKM2, cancer metabolism, and the road ahead. *EMBO Rep* **17**, 1721-1730, doi:10.15252/embr.201643300 (2016).
- 6 Vander Heiden, M. G. *et al.* Evidence for an alternative glycolytic pathway in rapidly proliferating cells. *Science* **329**, 1492-1499, doi:10.1126/science.1188015 (2010).
- 7 Matsuda, S. *et al.* Nuclear pyruvate kinase M2 complex serves as a transcriptional coactivator of arylhydrocarbon receptor. *Nucleic Acids Res* **44**, 636-647, doi:10.1093/nar/gkv967 (2016).
- 8 Fan, J., Krautkramer, K. A., Feldman, J. L. & Denu, J. M. Metabolic regulation of histone post-translational modifications. *ACS Chem Biol* **10**, 95-108, doi:10.1021/cb500846u (2015).

- 9 Berg, J. M., Tymoczko, J. L., Stryer, L., & Stryer, L. *Biochemistry*. 7th edn, (New York: W.H. Freeman, 2002).
- 10 Sutendra, G. *et al.* A nuclear pyruvate dehydrogenase complex is important for the generation of acetyl-CoA and histone acetylation. *Cell* **158**, 84-97, doi:10.1016/j.cell.2014.04.046 (2014).
- 11 Patel, M. S., Nemeria, N. S., Furey, W. & Jordan, F. The pyruvate dehydrogenase complexes: structure-based function and regulation. *J Biol Chem* **289**, 16615-16623, doi:10.1074/jbc.R114.563148 (2014).
- 12 Patel, M. S. & Roche, T. E. Molecular biology and biochemistry of pyruvate dehydrogenase complexes. *FASEB J* **4**, 3224-3233, doi:10.1096/fasebj.4.14.2227213 (1990).
- 13 Sanderson, S. J., Miller, C. & Lindsay, J. G. Stoichiometry, organisation and catalytic function of protein X of the pyruvate dehydrogenase complex from bovine heart. *Eur J Biochem* **236**, 68-77, doi:10.1111/j.1432-1033.1996.00068.x (1996).
- 14 Hiromasa, Y., Fujisawa, T., Aso, Y. & Roche, T. E. Organization of the cores of the mammalian pyruvate dehydrogenase complex formed by E2 and E2 plus the E3-binding protein and their capacities to bind the E1 and E3 components. *J Biol Chem* **279**, 6921-6933, doi:10.1074/jbc.M308172200 (2004).
- 15 Brautigam, C. A., Wynn, R. M., Chuang, J. L. & Chuang, D. T. Subunit and catalytic component stoichiometries of an in vitro reconstituted human pyruvate dehydrogenase complex. *J Biol Chem* **284**, 13086-13098, doi:10.1074/jbc.M806563200 (2009).

- 16 Sumegi, B., Liposits, Z., Inman, L., Paull, W. K. & Srere, P. A. Electron microscopic study on the size of pyruvate dehydrogenase complex in situ. *Eur J Biochem* **169**, 223-230, doi:10.1111/j.1432-1033.1987.tb13601.x (1987).
- 17 Zhou, Z. H., McCarthy, D. B., O'Connor, C. M., Reed, L. J. & Stoops, J. K. The remarkable structural and functional organization of the eukaryotic pyruvate dehydrogenase complexes. *Proc Natl Acad Sci U S A* **98**, 14802-14807, doi:10.1073/pnas.011597698 (2001).
- 18 Zhou, Z. H. *et al.* Direct evidence for the size and conformational variability of the pyruvate dehydrogenase complex revealed by three-dimensional electron microscopy. The "breathing" core and its functional relationship to protein dynamics. *J Biol Chem* **276**, 21704-21713, doi:10.1074/jbc.M101765200 (2001).
- 19 Korotchkina, L. G. & Patel, M. S. Site specificity of four pyruvate dehydrogenase kinase isoenzymes toward the three phosphorylation sites of human pyruvate dehydrogenase. *J Biol Chem* **276**, 37223-37229, doi:10.1074/jbc.M103069200 (2001).
- 20 Teague, W. M., Pettit, F. H., Wu, T. L., Silberman, S. R. & Reed, L. J. Purification and properties of pyruvate dehydrogenase phosphatase from bovine heart and kidney. *Biochemistry* **21**, 5585-5592, doi:10.1021/bi00265a031 (1982).
- 21 Bowker-Kinley, M. M., Davis, W. I., Wu, P., Harris, R. A. & Popov, K. M. Evidence for existence of tissue-specific regulation of the mammalian pyruvate dehydrogenase complex. *Biochem J* **329 (Pt 1)**, 191-196, doi:10.1042/bj3290191 (1998).

- 22 Denton, R. M. Regulation of mitochondrial dehydrogenases by calcium ions. *Biochim Biophys Acta* **1787**, 1309-1316, doi:10.1016/j.bbabi.2009.01.005 (2009).
- 23 Schmidt, O., Pfanner, N. & Meisinger, C. Mitochondrial protein import: from proteomics to functional mechanisms. *Nat Rev Mol Cell Biol* **11**, 655-667, doi:10.1038/nrm2959 (2010).
- 24 Shi, Y. & Thomas, J. O. The transport of proteins into the nucleus requires the 70-kilodalton heat shock protein or its cytosolic cognate. *Mol Cell Biol* **12**, 2186-2192, doi:10.1128/mcb.12.5.2186 (1992).
- 25 Nagaraj, R. *et al.* Nuclear Localization of Mitochondrial TCA Cycle Enzymes as a Critical Step in Mammalian Zygotic Genome Activation. *Cell* **168**, 210-223 e211, doi:10.1016/j.cell.2016.12.026 (2017).
- 26 Richard, A. J., Hang, H. & Stephens, J. M. Pyruvate dehydrogenase complex (PDC) subunits moonlight as interaction partners of phosphorylated STAT5 in adipocytes and adipose tissue. *J Biol Chem* **292**, 19733-19742, doi:10.1074/jbc.M117.811794 (2017).
- 27 Chen, J. *et al.* Compartmentalized activities of the pyruvate dehydrogenase complex sustain lipogenesis in prostate cancer. *Nat Genet* **50**, 219-228, doi:10.1038/s41588-017-0026-3 (2018).
- 28 Ferriero, R. *et al.* Pyruvate dehydrogenase complex and lactate dehydrogenase are targets for therapy of acute liver failure. *J Hepatol* **69**, 325-335, doi:10.1016/j.jhep.2018.03.016 (2018).
- 29 Brown, G. K., Otero, L. J., LeGris, M. & Brown, R. M. Pyruvate dehydrogenase deficiency. *J Med Genet* **31**, 875-879, doi:10.1136/jmg.31.11.875 (1994).

- 30 Robinson, B. H., MacMillan, H., Petrova-Benedict, R. & Sherwood, W. G. Variable clinical presentation in patients with defective E1 component of pyruvate dehydrogenase complex. *J Pediatr* **111**, 525-533, doi:10.1016/s0022-3476(87)80112-9 (1987).
- 31 Archer, S. L., Weir, E. K. & Wilkins, M. R. Basic science of pulmonary arterial hypertension for clinicians: new concepts and experimental therapies. *Circulation* **121**, 2045-2066, doi:10.1161/CIRCULATIONAHA.108.847707 (2010).
- 32 Michelakis, E. D. *et al.* Inhibition of pyruvate dehydrogenase kinase improves pulmonary arterial hypertension in genetically susceptible patients. *Sci Transl Med* **9**, doi:10.1126/scitranslmed.aao4583 (2017).
- 33 Pastorino, J. G., Hoek, J. B. & Shulga, N. Activation of glycogen synthase kinase 3beta disrupts the binding of hexokinase II to mitochondria by phosphorylating voltage-dependent anion channel and potentiates chemotherapy-induced cytotoxicity. *Cancer Res* **65**, 10545-10554, doi:10.1158/0008-5472.CAN-05-1925 (2005).
- 34 McFate, T. *et al.* Pyruvate dehydrogenase complex activity controls metabolic and malignant phenotype in cancer cells. *J Biol Chem* **283**, 22700-22708, doi:10.1074/jbc.M801765200 (2008).
- 35 Dunbar, E. M. *et al.* Phase 1 trial of dichloroacetate (DCA) in adults with recurrent malignant brain tumors. *Invest New Drugs* **32**, 452-464, doi:10.1007/s10637-013-0047-4 (2014).

- 36 Michelakis, E. D. *et al.* Metabolic modulation of glioblastoma with dichloroacetate. *Sci Transl Med* **2**, 31ra34, doi:10.1126/scitranslmed.3000677 (2010).
- 37 Ahrens, E. H., Jr., Payne, M. A., Kunkel, H. G., Eisenmenger, W. J. & Blondheim, S. H. Primary biliary cirrhosis. *Medicine (Baltimore)* **29**, 299-364, doi:10.1097/00005792-195012000-00002 (1950).
- 38 Baum, H. & Palmer, C. The PBC-specific antigen. *Mol Aspects Med* **8**, 201-234, doi:10.1016/0098-2997(85)90007-x (1985).
- 39 Frazer, I. H., Mackay, I. R., Jordan, T. W., Whittingham, S. & Marzuki, S. Reactivity of anti-mitochondrial autoantibodies in primary biliary cirrhosis: definition of two novel mitochondrial polypeptide autoantigens. *J Immunol* **135**, 1739-1745 (1985).
- 40 Caviston, J. P. & Holzbaur, E. L. Microtubule motors at the intersection of trafficking and transport. *Trends Cell Biol* **16**, 530-537, doi:10.1016/j.tcb.2006.08.002 (2006).
- 41 Akhmanova, A. & Steinmetz, M. O. Control of microtubule organization and dynamics: two ends in the limelight. *Nat Rev Mol Cell Biol* **16**, 711-726, doi:10.1038/nrm4084 (2015).
- 42 Roberts, A. J., Kon, T., Knight, P. J., Sutoh, K. & Burgess, S. A. Functions and mechanics of dynein motor proteins. *Nat Rev Mol Cell Biol* **14**, 713-726, doi:10.1038/nrm3667 (2013).

- 43 Hirokawa, N., Noda, Y., Tanaka, Y. & Niwa, S. Kinesin superfamily motor proteins and intracellular transport. *Nat Rev Mol Cell Biol* **10**, 682-696, doi:10.1038/nrm2774 (2009).
- 44 Reck-Peterson, S. L., Redwine, W. B., Vale, R. D. & Carter, A. P. The cytoplasmic dynein transport machinery and its many cargoes. *Nat Rev Mol Cell Biol* **19**, 382-398, doi:10.1038/s41580-018-0004-3 (2018).
- 45 Lindquist, S. The heat-shock response. *Annu Rev Biochem* **55**, 1151-1191, doi:10.1146/annurev.bi.55.070186.005443 (1986).
- 46 Hache, R. J., Tse, R., Reich, T., Savory, J. G. & Lefebvre, Y. A. Nucleocytoplasmic trafficking of steroid-free glucocorticoid receptor. *J Biol Chem* **274**, 1432-1439, doi:10.1074/jbc.274.3.1432 (1999).
- 47 Kanno, Y., Miyama, Y., Ando, M. & Inouye, Y. Dependence on the microtubule network and 90-kDa heat shock protein of phenobarbital-induced nuclear translocation of the rat constitutive androstane receptor. *Mol Pharmacol* **77**, 311-316, doi:10.1124/mol.109.060434 (2010).
- 48 Reed, N. A. *et al.* Microtubule acetylation promotes kinesin-1 binding and transport. *Curr Biol* **16**, 2166-2172, doi:10.1016/j.cub.2006.09.014 (2006).
- 49 Alper, J. D., Decker, F., Agana, B. & Howard, J. The motility of axonemal dynein is regulated by the tubulin code. *Biophys J* **107**, 2872-2880, doi:10.1016/j.bpj.2014.10.061 (2014).
- 50 Friedman, J. R., Webster, B. M., Mastronarde, D. N., Verhey, K. J. & Voeltz, G. K. ER sliding dynamics and ER-mitochondrial contacts occur on acetylated microtubules. *J Cell Biol* **190**, 363-375, doi:10.1083/jcb.200911024 (2010).

- 51 Howard, J. & Hyman, A. A. Dynamics and mechanics of the microtubule plus end. *Nature* **422**, 753-758, doi:10.1038/nature01600 (2003).
- 52 Kardon, J. R. & Vale, R. D. Regulators of the cytoplasmic dynein motor. *Nat Rev Mol Cell Biol* **10**, 854-865, doi:10.1038/nrm2804 (2009).
- 53 Carbonaro, M., Escuin, D., O'Brate, A., Thadani-Mulero, M. & Giannakakou, P. Microtubules regulate hypoxia-inducible factor-1alpha protein trafficking and activity: implications for taxane therapy. *J Biol Chem* **287**, 11859-11869, doi:10.1074/jbc.M112.345587 (2012).
- 54 Giannakakou, P. *et al.* Enhanced microtubule-dependent trafficking and p53 nuclear accumulation by suppression of microtubule dynamics. *Proc Natl Acad Sci U S A* **99**, 10855-10860, doi:10.1073/pnas.132275599 (2002).
- 55 Wu, Y. *et al.* Herpesvirus acts with the cytoskeleton and promotes cancer progression. *J Cancer* **10**, 2185-2193, doi:10.7150/jca.30222 (2019).
- 56 Iwamoto, M. *et al.* Functional association of cellular microtubules with viral capsid assembly supports efficient hepatitis B virus replication. *Sci Rep* **7**, 10620, doi:10.1038/s41598-017-11015-4 (2017).
- 57 Neuspiel, M. *et al.* Cargo-selected transport from the mitochondria to peroxisomes is mediated by vesicular carriers. *Curr Biol* **18**, 102-108, doi:10.1016/j.cub.2007.12.038 (2008).
- 58 Soubannier, V. *et al.* A vesicular transport pathway shuttles cargo from mitochondria to lysosomes. *Curr Biol* **22**, 135-141, doi:10.1016/j.cub.2011.11.057 (2012).

- 59 Fahrenkrog, B. & Aebi, U. The nuclear pore complex: nucleocytoplasmic transport and beyond. *Nat Rev Mol Cell Biol* **4**, 757-766, doi:10.1038/nrm1230 (2003).
- 60 Fahrenkrog, B. & Aebi, U. The vertebrate nuclear pore complex: from structure to function. *Results Probl Cell Differ* **35**, 25-48 (2002).
- 61 Stoffler, D., Fahrenkrog, B. & Aebi, U. The nuclear pore complex: from molecular architecture to functional dynamics. *Curr Opin Cell Biol* **11**, 391-401, doi:10.1016/S0955-0674(99)80055-6 (1999).
- 62 Fahrenkrog, B. *et al.* Domain-specific antibodies reveal multiple-site topology of Nup153 within the nuclear pore complex. *J Struct Biol* **140**, 254-267 (2002).
- 63 Bayliss, R., Littlewood, T. & Stewart, M. Structural basis for the interaction between FxFG nucleoporin repeats and importin-beta in nuclear trafficking. *Cell* **102**, 99-108, doi:10.1016/s0092-8674(00)00014-3 (2000).
- 64 Guo, Y. & Zheng, Y. Lamins position the nuclear pores and centrosomes by modulating dynein. *Mol Biol Cell* **26**, 3379-3389, doi:10.1091/mbc.E15-07-0482 (2015).
- 65 Wentz, S. R. & Rout, M. P. The nuclear pore complex and nuclear transport. *Cold Spring Harb Perspect Biol* **2**, a000562, doi:10.1101/cshperspect.a000562 (2010).
- 66 Pante, N. & Kann, M. Nuclear pore complex is able to transport macromolecules with diameters of about 39 nm. *Mol Biol Cell* **13**, 425-434, doi:10.1091/mbc.01-06-0308 (2002).
- 67 Nigg, E. A. Nucleocytoplasmic transport: signals, mechanisms and regulation. *Nature* **386**, 779-787, doi:10.1038/386779a0 (1997).

- 68 Lange, A. *et al.* Classical nuclear localization signals: definition, function, and interaction with importin alpha. *J Biol Chem* **282**, 5101-5105, doi:10.1074/jbc.R600026200 (2007).
- 69 Stewart, M. Molecular mechanism of the nuclear protein import cycle. *Nat Rev Mol Cell Biol* **8**, 195-208, doi:10.1038/nrm2114 (2007).
- 70 Fagotto, F., Gluck, U. & Gumbiner, B. M. Nuclear localization signal-independent and importin/karyopherin-independent nuclear import of beta-catenin. *Curr Biol* **8**, 181-190, doi:10.1016/s0960-9822(98)70082-x (1998).
- 71 De Magistris, P. & Antonin, W. The Dynamic Nature of the Nuclear Envelope. *Curr Biol* **28**, R487-R497, doi:10.1016/j.cub.2018.01.073 (2018).
- 72 Watson, M. L. The nuclear envelope; its structure and relation to cytoplasmic membranes. *J Biophys Biochem Cytol* **1**, 257-270, doi:10.1083/jcb.1.3.257 (1955).
- 73 Wilson, K. L. & Berk, J. M. The nuclear envelope at a glance. *J Cell Sci* **123**, 1973-1978, doi:10.1242/jcs.019042 (2010).
- 74 Gruenbaum, Y., Margalit, A., Goldman, R. D., Shumaker, D. K. & Wilson, K. L. The nuclear lamina comes of age. *Nat Rev Mol Cell Biol* **6**, 21-31, doi:10.1038/nrm1550 (2005).
- 75 Goldman, A. E., Maul, G., Steinert, P. M., Yang, H. Y. & Goldman, R. D. Keratin-like proteins that coisolate with intermediate filaments of BHK-21 cells are nuclear lamins. *Proc Natl Acad Sci U S A* **83**, 3839-3843, doi:10.1073/pnas.83.11.3839 (1986).

- 76 Nakajima, N. & Abe, K. Genomic structure of the mouse A-type lamin gene locus encoding somatic and germ cell-specific lamins. *FEBS Lett* **365**, 108-114, doi:10.1016/0014-5793(95)00453-g (1995).
- 77 Machiels, B. M. *et al.* Subcellular localization of proteasomes in apoptotic lung tumor cells and persistence as compared to intermediate filaments. *Eur J Cell Biol* **70**, 250-259 (1996).
- 78 Burke, B. & Stewart, C. L. The nuclear lamins: flexibility in function. *Nat Rev Mol Cell Biol* **14**, 13-24, doi:10.1038/nrm3488 (2013).
- 79 Furukawa, K. & Hotta, Y. cDNA cloning of a germ cell specific lamin B3 from mouse spermatocytes and analysis of its function by ectopic expression in somatic cells. *EMBO J* **12**, 97-106 (1993).
- 80 Beck, L. A., Hosick, T. J. & Sinensky, M. Isoprenylation is required for the processing of the lamin A precursor. *J Cell Biol* **110**, 1489-1499, doi:10.1083/jcb.110.5.1489 (1990).
- 81 Kitten, G. T. & Nigg, E. A. The CaaX motif is required for isoprenylation, carboxyl methylation, and nuclear membrane association of lamin B2. *J Cell Biol* **113**, 13-23, doi:10.1083/jcb.113.1.13 (1991).
- 82 Sinensky, M. *et al.* The processing pathway of prelamin A. *J Cell Sci* **107 (Pt 1)**, 61-67 (1994).
- 83 Holtz, D., Tanaka, R. A., Hartwig, J. & McKeon, F. The CaaX motif of lamin A functions in conjunction with the nuclear localization signal to target assembly to the nuclear envelope. *Cell* **59**, 969-977, doi:10.1016/0092-8674(89)90753-8 (1989).

- 84 Weber, K., Plessmann, U. & Traub, P. Maturation of nuclear lamin A involves a specific carboxy-terminal trimming, which removes the polyisoprenylation site from the precursor; implications for the structure of the nuclear lamina. *FEBS Lett* **257**, 411-414, doi:10.1016/0014-5793(89)81584-4 (1989).
- 85 Fisher, D. Z., Chaudhary, N. & Blobel, G. cDNA sequencing of nuclear lamins A and C reveals primary and secondary structural homology to intermediate filament proteins. *Proc Natl Acad Sci U S A* **83**, 6450-6454, doi:10.1073/pnas.83.17.6450 (1986).
- 86 McKeon, F. D., Kirschner, M. W. & Caput, D. Homologies in both primary and secondary structure between nuclear envelope and intermediate filament proteins. *Nature* **319**, 463-468, doi:10.1038/319463a0 (1986).
- 87 Dhe-Paganon, S., Werner, E. D., Chi, Y. I. & Shoelson, S. E. Structure of the globular tail of nuclear lamin. *J Biol Chem* **277**, 17381-17384, doi:10.1074/jbc.C200038200 (2002).
- 88 Williams, A. F. & Barclay, A. N. The immunoglobulin superfamily--domains for cell surface recognition. *Annu Rev Immunol* **6**, 381-405, doi:10.1146/annurev.iy.06.040188.002121 (1988).
- 89 Wilson, K. L. & Foisner, R. Lamin-binding Proteins. *Cold Spring Harb Perspect Biol* **2**, a000554, doi:10.1101/cshperspect.a000554 (2010).
- 90 Harada, T. *et al.* Nuclear lamin stiffness is a barrier to 3D migration, but softness can limit survival. *J Cell Biol* **204**, 669-682, doi:10.1083/jcb.201308029 (2014).
- 91 Simon, D. N. & Wilson, K. L. Partners and post-translational modifications of nuclear lamins. *Chromosoma* **122**, 13-31, doi:10.1007/s00412-013-0399-8 (2013).

- 92 Heald, R. & McKeon, F. Mutations of phosphorylation sites in lamin A that prevent nuclear lamina disassembly in mitosis. *Cell* **61**, 579-589, doi:10.1016/0092-8674(90)90470-y (1990).
- 93 Peter, M., Nakagawa, J., Doree, M., Labbe, J. C. & Nigg, E. A. In vitro disassembly of the nuclear lamina and M phase-specific phosphorylation of lamins by cdc2 kinase. *Cell* **61**, 591-602, doi:10.1016/0092-8674(90)90471-p (1990).
- 94 Gerace, L. & Blobel, G. The nuclear envelope lamina is reversibly depolymerized during mitosis. *Cell* **19**, 277-287, doi:10.1016/0092-8674(80)90409-2 (1980).
- 95 Karoutas, A. *et al.* The NSL complex maintains nuclear architecture stability via lamin A/C acetylation. *Nat Cell Biol* **21**, 1248-1260, doi:10.1038/s41556-019-0397-z (2019).
- 96 Murray, L. A., Sheng, X. & Cristea, I. M. Orchestration of protein acetylation as a toggle for cellular defense and virus replication. *Nat Commun* **9**, 4967, doi:10.1038/s41467-018-07179-w (2018).
- 97 Xie, W. *et al.* A-type Lamins Form Distinct Filamentous Networks with Differential Nuclear Pore Complex Associations. *Curr Biol* **26**, 2651-2658, doi:10.1016/j.cub.2016.07.049 (2016).
- 98 Schirmer, E. C., Guan, T. & Gerace, L. Involvement of the lamin rod domain in heterotypic lamin interactions important for nuclear organization. *J Cell Biol* **153**, 479-489, doi:10.1083/jcb.153.3.479 (2001).
- 99 Laguri, C. *et al.* Structural characterization of the LEM motif common to three human inner nuclear membrane proteins. *Structure* **9**, 503-511, doi:10.1016/s0969-2126(01)00611-6 (2001).

- 100 Margalit, A., Brachner, A., Gotzmann, J., Foisner, R. & Gruenbaum, Y. Barrier-to-autointegration factor--a BAFfling little protein. *Trends Cell Biol* **17**, 202-208, doi:10.1016/j.tcb.2007.02.004 (2007).
- 101 Taniura, H., Glass, C. & Gerace, L. A chromatin binding site in the tail domain of nuclear lamins that interacts with core histones. *J Cell Biol* **131**, 33-44, doi:10.1083/jcb.131.1.33 (1995).
- 102 Mattout, A., Goldberg, M., Tzur, Y., Margalit, A. & Gruenbaum, Y. Specific and conserved sequences in *D. melanogaster* and *C. elegans* lamins and histone H2A mediate the attachment of lamins to chromosomes. *J Cell Sci* **120**, 77-85, doi:10.1242/jcs.03325 (2007).
- 103 Dorner, D. *et al.* Lamina-associated polypeptide 2alpha regulates cell cycle progression and differentiation via the retinoblastoma-E2F pathway. *J Cell Biol* **173**, 83-93, doi:10.1083/jcb.200511149 (2006).
- 104 Kumaran, R. I., Muralikrishna, B. & Parnaik, V. K. Lamin A/C speckles mediate spatial organization of splicing factor compartments and RNA polymerase II transcription. *J Cell Biol* **159**, 783-793, doi:10.1083/jcb.200204149 (2002).
- 105 Giacinti, C. & Giordano, A. RB and cell cycle progression. *Oncogene* **25**, 5220-5227, doi:10.1038/sj.onc.1209615 (2006).
- 106 Cesarini, E. *et al.* Lamin A/C sustains PcG protein architecture, maintaining transcriptional repression at target genes. *J Cell Biol* **211**, 533-551, doi:10.1083/jcb.201504035 (2015).

- 107 Marullo, F. *et al.* Nucleoplasmic Lamin A/C and Polycomb group of proteins: An evolutionarily conserved interplay. *Nucleus* **7**, 103-111, doi:10.1080/19491034.2016.1157675 (2016).
- 108 Hozak, P., Sasseville, A. M., Raymond, Y. & Cook, P. R. Lamin proteins form an internal nucleoskeleton as well as a peripheral lamina in human cells. *J Cell Sci* **108 (Pt 2)**, 635-644 (1995).
- 109 Bridger, J. M., Kill, I. R., O'Farrell, M. & Hutchison, C. J. Internal lamin structures within G1 nuclei of human dermal fibroblasts. *J Cell Sci* **104 (Pt 2)**, 297-306 (1993).
- 110 Shimi, T. *et al.* The A- and B-type nuclear lamin networks: microdomains involved in chromatin organization and transcription. *Genes Dev* **22**, 3409-3421, doi:10.1101/gad.1735208 (2008).
- 111 Schreiber, K. H. & Kennedy, B. K. When lamins go bad: nuclear structure and disease. *Cell* **152**, 1365-1375, doi:10.1016/j.cell.2013.02.015 (2013).
- 112 Eriksson, M. *et al.* Recurrent de novo point mutations in lamin A cause Hutchinson-Gilford progeria syndrome. *Nature* **423**, 293-298, doi:10.1038/nature01629 (2003).
- 113 Hennekam, R. C. Hutchinson-Gilford progeria syndrome: review of the phenotype. *Am J Med Genet A* **140**, 2603-2624, doi:10.1002/ajmg.a.31346 (2006).
- 114 Foster, C. R., Przyborski, S. A., Wilson, R. G. & Hutchison, C. J. Lamins as cancer biomarkers. *Biochem Soc Trans* **38**, 297-300, doi:10.1042/BST0380297 (2010).

- 115 Irianto, J., Pfeifer, C. R., Ivanovska, I. L., Swift, J. & Discher, D. E. Nuclear lamins in cancer. *Cell Mol Bioeng* **9**, 258-267, doi:10.1007/s12195-016-0437-8 (2016).
- 116 Simon, D. N., Zastrow, M. S. & Wilson, K. L. Direct actin binding to A- and B-type lamin tails and actin filament bundling by the lamin A tail. *Nucleus* **1**, 264-272, doi:10.4161/nucl.1.3.11799 (2010).
- 117 Zastrow, M. S., Flaherty, D. B., Benian, G. M. & Wilson, K. L. Nuclear titin interacts with A- and B-type lamins in vitro and in vivo. *J Cell Sci* **119**, 239-249, doi:10.1242/jcs.02728 (2006).
- 118 Libotte, T. *et al.* Lamin A/C-dependent localization of Nesprin-2, a giant scaffold at the nuclear envelope. *Mol Biol Cell* **16**, 3411-3424, doi:10.1091/mbc.e04-11-1009 (2005).
- 119 Mislow, J. M. *et al.* Nesprin-1alpha self-associates and binds directly to emerin and lamin A in vitro. *FEBS Lett* **525**, 135-140, doi:10.1016/s0014-5793(02)03105-8 (2002).
- 120 Vlcek, S., Foisner, R. & Wilson, K. L. Lco1 is a novel widely expressed lamin-binding protein in the nuclear interior. *Exp Cell Res* **298**, 499-511, doi:10.1016/j.yexcr.2004.04.028 (2004).
- 121 Haque, F. *et al.* SUN1 interacts with nuclear lamin A and cytoplasmic nesprins to provide a physical connection between the nuclear lamina and the cytoskeleton. *Mol Cell Biol* **26**, 3738-3751, doi:10.1128/MCB.26.10.3738-3751.2006 (2006).

- 122 Crisp, M. *et al.* Coupling of the nucleus and cytoplasm: role of the LINC complex. *J Cell Biol* **172**, 41-53, doi:10.1083/jcb.200509124 (2006).
- 123 Al-Haboubi, T., Shumaker, D. K., Koser, J., Wehnert, M. & Fahrenkrog, B. Distinct association of the nuclear pore protein Nup153 with A- and B-type lamins. *Nucleus* **2**, 500-509, doi:10.4161/nucl.2.5.17913 (2011).
- 124 Lussi, Y. C., Hugi, I., Laurell, E., Kutay, U. & Fahrenkrog, B. The nucleoporin Nup88 is interacting with nuclear lamin A. *Mol Biol Cell* **22**, 1080-1090, doi:10.1091/mbc.E10-05-0463 (2011).
- 125 Dechat, T. *et al.* Lamina-associated polypeptide 2alpha binds intranuclear A-type lamins. *J Cell Sci* **113 Pt 19**, 3473-3484 (2000).
- 126 Mansharamani, M. & Wilson, K. L. Direct binding of nuclear membrane protein MAN1 to emerin in vitro and two modes of binding to barrier-to-autointegration factor. *J Biol Chem* **280**, 13863-13870, doi:10.1074/jbc.M413020200 (2005).
- 127 Brachner, A., Reipert, S., Foisner, R. & Gotzmann, J. LEM2 is a novel MAN1-related inner nuclear membrane protein associated with A-type lamins. *J Cell Sci* **118**, 5797-5810, doi:10.1242/jcs.02701 (2005).
- 128 Sakaki, M. *et al.* Interaction between emerin and nuclear lamins. *J Biochem* **129**, 321-327, doi:10.1093/oxfordjournals.jbchem.a002860 (2001).
- 129 Lee, K. K. *et al.* Distinct functional domains in emerin bind lamin A and DNA-bridging protein BAF. *J Cell Sci* **114**, 4567-4573 (2001).

- 130 Shumaker, D. K. *et al.* The highly conserved nuclear lamin Ig-fold binds to PCNA: its role in DNA replication. *J Cell Biol* **181**, 269-280, doi:10.1083/jcb.200708155 (2008).
- 131 Stierle, V. *et al.* The carboxyl-terminal region common to lamins A and C contains a DNA binding domain. *Biochemistry* **42**, 4819-4828, doi:10.1021/bi020704g (2003).
- 132 Lloyd, D. J., Trembath, R. C. & Shackleton, S. A novel interaction between lamin A and SREBP1: implications for partial lipodystrophy and other laminopathies. *Hum Mol Genet* **11**, 769-777, doi:10.1093/hmg/11.7.769 (2002).
- 133 Martelli, A. M. *et al.* Molecular characterization of protein kinase C-alpha binding to lamin A. *J Cell Biochem* **86**, 320-330, doi:10.1002/jcb.10227 (2002).
- 134 Barton, R. M. & Worman, H. J. Prenylated prelamin A interacts with Narf, a novel nuclear protein. *J Biol Chem* **274**, 30008-30018, doi:10.1074/jbc.274.42.30008 (1999).
- 135 Vijayakrishnan, S. *et al.* Solution structure and characterisation of the human pyruvate dehydrogenase complex core assembly. *J Mol Biol* **399**, 71-93, doi:10.1016/j.jmb.2010.03.043 (2010).
- 136 Brouhard, G. J. & Rice, L. M. Microtubule dynamics: an interplay of biochemistry and mechanics. *Nat Rev Mol Cell Biol* **19**, 451-463, doi:10.1038/s41580-018-0009-y (2018).
- 137 Wloga, D. & Gaertig, J. Post-translational modifications of microtubules. *J Cell Sci* **123**, 3447-3455, doi:10.1242/jcs.063727 (2010).

- 138 Maruta, H., Greer, K. & Rosenbaum, J. L. The acetylation of alpha-tubulin and its relationship to the assembly and disassembly of microtubules. *J Cell Biol* **103**, 571-579, doi:10.1083/jcb.103.2.571 (1986).
- 139 Piperno, G., LeDizet, M. & Chang, X. J. Microtubules containing acetylated alpha-tubulin in mammalian cells in culture. *J Cell Biol* **104**, 289-302, doi:10.1083/jcb.104.2.289 (1987).
- 140 Balabanian, L., Berger, C. L. & Hendricks, A. G. Acetylated Microtubules Are Preferentially Bundled Leading to Enhanced Kinesin-1 Motility. *Biophys J* **113**, 1551-1560, doi:10.1016/j.bpj.2017.08.009 (2017).
- 141 Giustiniani, J. *et al.* Tubulin acetylation favors Hsp90 recruitment to microtubules and stimulates the signaling function of the Hsp90 clients Akt/PKB and p53. *Cell Signal* **21**, 529-539, doi:10.1016/j.cellsig.2008.12.004 (2009).
- 142 Husain, M. & Harrod, K. S. Enhanced acetylation of alpha-tubulin in influenza A virus infected epithelial cells. *FEBS Lett* **585**, 128-132, doi:10.1016/j.febslet.2010.11.023 (2011).
- 143 Kirschke, E., Goswami, D., Southworth, D., Griffin, P. R. & Agard, D. A. Glucocorticoid receptor function regulated by coordinated action of the Hsp90 and Hsp70 chaperone cycles. *Cell* **157**, 1685-1697, doi:10.1016/j.cell.2014.04.038 (2014).
- 144 Trebble, P. J. *et al.* A ligand-specific kinetic switch regulates glucocorticoid receptor trafficking and function. *J Cell Sci* **126**, 3159-3169, doi:10.1242/jcs.124784 (2013).

- 145 Chen, M. *et al.* Serum starvation induced cell cycle synchronization facilitates human somatic cells reprogramming. *PLoS One* **7**, e28203, doi:10.1371/journal.pone.0028203 (2012).
- 146 Akella, J. S. *et al.* MEC-17 is an alpha-tubulin acetyltransferase. *Nature* **467**, 218-222, doi:10.1038/nature09324 (2010).
- 147 Li, L. & Yang, X. J. Tubulin acetylation: responsible enzymes, biological functions and human diseases. *Cell Mol Life Sci* **72**, 4237-4255, doi:10.1007/s00018-015-2000-5 (2015).
- 148 Kinnaird, A., Zhao, S., Wellen, K. E. & Michelakis, E. D. Metabolic control of epigenetics in cancer. *Nat Rev Cancer* **16**, 694-707, doi:10.1038/nrc.2016.82 (2016).
- 149 Anastasiou, D. & Cantley, L. C. Breathless cancer cells get fat on glutamine. *Cell Res* **22**, 443-446, doi:10.1038/cr.2012.5 (2012).
- 150 Wellen, K. E. *et al.* ATP-citrate lyase links cellular metabolism to histone acetylation. *Science* **324**, 1076-1080, doi:10.1126/science.1164097 (2009).
- 151 Kalebic, N. *et al.* alphaTAT1 is the major alpha-tubulin acetyltransferase in mice. *Nat Commun* **4**, 1962, doi:10.1038/ncomms2962 (2013).
- 152 Hubbert, C. *et al.* HDAC6 is a microtubule-associated deacetylase. *Nature* **417**, 455-458, doi:10.1038/417455a (2002).
- 153 Matsuyama, A. *et al.* In vivo destabilization of dynamic microtubules by HDAC6-mediated deacetylation. *EMBO J* **21**, 6820-6831, doi:10.1093/emboj/cdf682 (2002).

- 154 Haggarty, S. J., Koeller, K. M., Wong, J. C., Grozinger, C. M. & Schreiber, S. L. Domain-selective small-molecule inhibitor of histone deacetylase 6 (HDAC6)-mediated tubulin deacetylation. *Proc Natl Acad Sci U S A* **100**, 4389-4394, doi:10.1073/pnas.0430973100 (2003).
- 155 Zhang, X. *et al.* HDAC6 modulates cell motility by altering the acetylation level of cortactin. *Mol Cell* **27**, 197-213, doi:10.1016/j.molcel.2007.05.033 (2007).
- 156 Kovacs, J. J. *et al.* HDAC6 regulates Hsp90 acetylation and chaperone-dependent activation of glucocorticoid receptor. *Mol Cell* **18**, 601-607, doi:10.1016/j.molcel.2005.04.021 (2005).
- 157 Yoshida, N. *et al.* Prediction of prognosis of estrogen receptor-positive breast cancer with combination of selected estrogen-regulated genes. *Cancer Sci* **95**, 496-502, doi:10.1111/j.1349-7006.2004.tb03239.x (2004).
- 158 Knockenhauer, K. E. & Schwartz, T. U. The Nuclear Pore Complex as a Flexible and Dynamic Gate. *Cell* **164**, 1162-1171, doi:10.1016/j.cell.2016.01.034 (2016).
- 159 Chu, D. T. & Klymkowsky, M. W. The appearance of acetylated alpha-tubulin during early development and cellular differentiation in *Xenopus*. *Dev Biol* **136**, 104-117, doi:10.1016/0012-1606(89)90134-6 (1989).
- 160 Almouzni, G., Khochbin, S., Dimitrov, S. & Wolffe, A. P. Histone acetylation influences both gene expression and development of *Xenopus laevis*. *Dev Biol* **165**, 654-669, doi:10.1006/dbio.1994.1283 (1994).

- 161 Vogelauer, M., Rubbi, L., Lucas, I., Brewer, B. J. & Grunstein, M. Histone acetylation regulates the time of replication origin firing. *Mol Cell* **10**, 1223-1233, doi:10.1016/s1097-2765(02)00702-5 (2002).
- 162 Moussaieff, A. *et al.* Glycolysis-mediated changes in acetyl-CoA and histone acetylation control the early differentiation of embryonic stem cells. *Cell Metab* **21**, 392-402, doi:10.1016/j.cmet.2015.02.002 (2015).
- 163 Schindelin, J. *et al.* Fiji: an open-source platform for biological-image analysis. *Nat Methods* **9**, 676-682, doi:10.1038/nmeth.2019 (2012).
- 164 Schmid, B., Schindelin, J., Cardona, A., Longair, M. & Heisenberg, M. A high-level 3D visualization API for Java and ImageJ. *BMC Bioinformatics* **11**, 274, doi:10.1186/1471-2105-11-274 (2010).
- 165 Bonnet, S. *et al.* A mitochondria-K⁺ channel axis is suppressed in cancer and its normalization promotes apoptosis and inhibits cancer growth. *Cancer Cell* **11**, 37-51, doi:10.1016/j.ccr.2006.10.020 (2007).
- 166 Chacinska, A., Koehler, C. M., Milenkovic, D., Lithgow, T. & Pfanner, N. Importing mitochondrial proteins: machineries and mechanisms. *Cell* **138**, 628-644, doi:10.1016/j.cell.2009.08.005 (2009).
- 167 de Brito, O. M. & Scorrano, L. Mitofusin 2 tethers endoplasmic reticulum to mitochondria. *Nature* **456**, 605-610, doi:10.1038/nature07534 (2008).
- 168 Murley, A. & Nunnari, J. The Emerging Network of Mitochondria-Organelle Contacts. *Mol Cell* **61**, 648-653, doi:10.1016/j.molcel.2016.01.031 (2016).
- 169 Cohen, S., Au, S. & Pante, N. How viruses access the nucleus. *Biochim Biophys Acta* **1813**, 1634-1645, doi:10.1016/j.bbamcr.2010.12.009 (2011).

- 170 Andersson, S. G. *et al.* The genome sequence of *Rickettsia prowazekii* and the origin of mitochondria. *Nature* **396**, 133-140, doi:10.1038/24094 (1998).
- 171 Burgdorfer, W., Anacker, R. L., Bird, R. G. & Bertram, D. S. Intranuclear growth of *Rickettsia rickettsii*. *J Bacteriol* **96**, 1415-1418 (1968).
- 172 Westermann, B. Mitochondrial fusion and fission in cell life and death. *Nat Rev Mol Cell Biol* **11**, 872-884, doi:10.1038/nrm3013 (2010).
- 173 Schrepfer, E. & Scorrano, L. Mitofusins, from Mitochondria to Metabolism. *Mol Cell* **61**, 683-694, doi:10.1016/j.molcel.2016.02.022 (2016).
- 174 Alam, M. S. Proximity Ligation Assay (PLA). *Curr Protoc Immunol* **123**, e58, doi:10.1002/cpim.58 (2018).
- 175 Ardestani, P. M. & Liang, F. Sub-cellular localization, expression and functions of Sirt6 during the cell cycle in HeLa cells. *Nucleus* **3**, 442-451, doi:10.4161/nucl.21134 (2012).
- 176 Maresca, G. *et al.* LMNA knock-down affects differentiation and progression of human neuroblastoma cells. *PLoS One* **7**, e45513, doi:10.1371/journal.pone.0045513 (2012).
- 177 Yoneda, Y., Imamoto-Sonobe, N., Yamaizumi, M. & Uchida, T. Reversible inhibition of protein import into the nucleus by wheat germ agglutinin injected into cultured cells. *Exp Cell Res* **173**, 586-595, doi:10.1016/0014-4827(87)90297-7 (1987).
- 178 Benavente, R., Dabauvalle, M. C., Scheer, U. & Chaly, N. Functional role of newly formed pore complexes in postmitotic nuclear reorganization. *Chromosoma* **98**, 233-241, doi:10.1007/bf00327308 (1989).

- 179 Park, O. K., Schaefer, T. S. & Nathans, D. In vitro activation of Stat3 by epidermal growth factor receptor kinase. *Proc Natl Acad Sci U S A* **93**, 13704-13708, doi:10.1073/pnas.93.24.13704 (1996).
- 180 Chan, K. S. *et al.* Epidermal growth factor receptor-mediated activation of Stat3 during multistage skin carcinogenesis. *Cancer Res* **64**, 2382-2389, doi:10.1158/0008-5472.can-03-3197 (2004).
- 181 Song, L., Turkson, J., Karras, J. G., Jove, R. & Haura, E. B. Activation of Stat3 by receptor tyrosine kinases and cytokines regulates survival in human non-small cell carcinoma cells. *Oncogene* **22**, 4150-4165, doi:10.1038/sj.onc.1206479 (2003).
- 182 Liu, L., McBride, K. M. & Reich, N. C. STAT3 nuclear import is independent of tyrosine phosphorylation and mediated by importin-alpha3. *Proc Natl Acad Sci U S A* **102**, 8150-8155, doi:10.1073/pnas.0501643102 (2005).
- 183 Cimica, V., Chen, H. C., Iyer, J. K. & Reich, N. C. Dynamics of the STAT3 transcription factor: nuclear import dependent on Ran and importin-beta1. *PLoS One* **6**, e20188, doi:10.1371/journal.pone.0020188 (2011).
- 184 Eisenberg-Bord, M., Shai, N., Schuldiner, M. & Bohnert, M. A Tether Is a Tether Is a Tether: Tethering at Membrane Contact Sites. *Dev Cell* **39**, 395-409, doi:10.1016/j.devcel.2016.10.022 (2016).
- 185 Iwasawa, R., Mahul-Mellier, A. L., Datler, C., Pazarentzos, E. & Grimm, S. Fis1 and Bap31 bridge the mitochondria-ER interface to establish a platform for apoptosis induction. *EMBO J* **30**, 556-568, doi:10.1038/emboj.2010.346 (2011).

- 186 De Vos, K. J. *et al.* VAPB interacts with the mitochondrial protein PTPIP51 to regulate calcium homeostasis. *Hum Mol Genet* **21**, 1299-1311, doi:10.1093/hmg/ddr559 (2012).
- 187 Elbaz, Y. & Schuldiner, M. Staying in touch: the molecular era of organelle contact sites. *Trends Biochem Sci* **36**, 616-623, doi:10.1016/j.tibs.2011.08.004 (2011).
- 188 Frezza, C., Cipolat, S. & Scorrano, L. Organelle isolation: functional mitochondria from mouse liver, muscle and cultured fibroblasts. *Nat Protoc* **2**, 287-295, doi:10.1038/nprot.2006.478 (2007).

Appendix I: Antibodies used in this dissertation

Antibody	Company	Catalogue number	Immunofluorescence/ PLA dilution	TEM dilution	Western Blot dilution
PDHA1	Santa Cruz Biotechnology	sc-377092	1:50	N/A	1:1000
PDCE2	Abcam	ab126224	1:200	1:20	1:5000
PDCE2	Cell signaling technology	12362	N/A	N/A	1:1000
PDCE3	Abcam	ab133551	1:100	N/A	N/A
LMNA	Cell signaling technology	4777S	1:100	N/A	1:1000
LMNB1	Abcam	ab16048	1:100	N/A	1:1000
SDHB	Abcam	ab14714	1:100	N/A	1:1000
MEK1	Cell signaling technology	2352S	N/A	N/A	1:1000
Actin	Abcam	ab3280	N/A	N/A	1:10,000
Tubulin	Sigma Aldrich	T6199	1:1000	N/A	1:10,000
Acetyl-Tubulin	Sigma Aldrich	T6793	1:2000	N/A	1:20,000
Acetyl-Tubulin	Cell signaling technology	5335	1:800	N/A	1:1000
Detyrosinated-Tubulin	Abcam	ab48389	N/A	N/A	1:1000
Hsp70	Santa Cruz Biotechnology	sc-27	1:50	N/A	N/A
Citrate synthase	Abcam	ab96600	1:200	N/A	N/A
Sirt6	Cell signaling technology	12486S	N/A	N/A	1:1000
MFN2	Cell signaling technology	11925S	1:100	1:10	1:1000
STAT3	Cell signaling technology	9139S	1:1600	N/A	N/A
PKM2	Cell signaling technology	sc-292640	1:50	N/A	N/A
TOM20	Santa Cruz Biotechnology	sc-11415	1:50	N/A	N/A
Histone 3	Cell signaling technology	9715S	N/A	N/A	1:50,000
Acetyl-Histone 3	Sigma Millipore	06-599	1:500	N/A	1:20,000
Nucleolin	Cell signaling technology	14574S	1:50	N/A	1:1000

Nup98	Cell signaling technology	2598S	1:100	N/A	N/A
ACLY	Cell signaling technology	13390	N/A	N/A	1:1000

Appendix II: Macros for image analysis with FIJI

Measuring extramitochondrial PDC and its colocalization with acetyl- tubulin.

Fig. 2-2 and Fig. 2-3

```
image=getTitle();
run("Duplicate...", " ");
run("Subtract Background...", "rolling=100");
run("Gaussian Blur...", "sigma=1");
setAutoThreshold("Triangle dark");
setOption("BlackBackground", true);
run("Convert to Mask");
run("Create Selection");
roiManager("Add");
close();
selectWindow(image);
run("Next Slice [>]");
run("Next Slice [>]");
run("Next Slice [>]");
run("Duplicate...", " ");
rename("DAPI " + image);
run("Gaussian Blur...", "sigma=1");
setAutoThreshold("Otsu dark");
//run("Threshold...");
run("Convert to Mask");
run("Fill Holes");
waitForUser("Select the Nucleus");
roiManager("Add");
selectWindow(image);
run("Previous Slice [<]");
run("Previous Slice [<]");
run("Duplicate...", " ");
rename("PDCE2 " + image);
run("Subtract Background...", "rolling=100");
run("Gaussian Blur...", "sigma=1");
setAutoThreshold("Otsu dark");
//run("Threshold...");
run("Convert to Mask");
roiManager("Select", 0);
setBackground(0, 0, 0);
run("Clear", "slice");
run("Select None");
roiManager("Select", 1);
setBackground(0, 0, 0);
run("Clear", "slice");
run("Create Selection");
run("Select None");
run("Find Maxima...", "prominence=10 output=Count");
```

```

run("Select None");
run("Create Selection");
roiManager("Add");
selectWindow(image);
run("Next Slice [>]");
run("Duplicate...", " ");
rename("actub");
run("Subtract Background...", "rolling=100");
run("Gaussian Blur...", "sigma=1");
setAutoThreshold("Triangle dark");
//run("Threshold...");
run("Convert to Mask");
run("Create Selection");
run("Make Inverse");
roiManager("Add");
run("Select None");
selectWindow("PDCE2 " + image);
roiManager("Select", 3);
run("Clear", "slice");
run("Select None");
selectWindow("actub");
run("Create Selection");
roiManager("Add");
selectWindow("PDCE2 " + image);
roiManager("Select", 4);
run("Find Maxima...", "prominence=10 output=Count");
run("Select None");
run("Create Selection");
roiManager("Add");
selectWindow(image);
roiManager("Select", 5);
waitForUser("Should I close the image?");
roiManager("Deselect");
roiManager("Delete");
run("Close All");

```

Measuring mitochondrial distance from the nucleus written in IJ1 Macro language for Fiji. This code allows measurement of mitochondria on top of the nucleus and then every 175 nm. (Fig. 3-1A)

```
image1=getTitle();
waitForUser("Ready?");
run("Out [-]");
run("Out [-]");
run("Out [-]");
run("Enhance Contrast", "saturated=0.35");
run("Next Slice [>]");
run("Enhance Contrast", "saturated=0.35");
run("Next Slice [>]");
run("Enhance Contrast", "saturated=0.35");
run("Next Slice [>]");
run("Enhance Contrast", "saturated=0.35");
waitForUser("Ready?");
close();
waitForUser("Ready?");
run("Out [-]");
run("Out [-]");
run("Out [-]");
run("Enhance Contrast", "saturated=0.35");
run("Next Slice [>]");
run("Enhance Contrast", "saturated=0.35");
run("Next Slice [>]");
run("Enhance Contrast", "saturated=0.35");
run("Next Slice [>]");
run("Enhance Contrast", "saturated=0.35");
run("Duplicate...", "duplicate");
run("Out [-]");
run("Out [-]");
run("Out [-]");
selectWindow("Montage-1");
run("Split Channels");
selectWindow("C4-Montage-1");
run("Out [-]");
run("Out [-]");
run("Out [-]");
selectWindow("C3-Montage-1");
run("Out [-]");
run("Out [-]");
run("Out [-]");
selectWindow("C2-Montage-1");
run("Out [-]");
run("Out [-]");
run("Out [-]");
```

```

selectWindow("C1-Montage-1");
run("Out [-]");
run("Out [-]");
run("Out [-]");
selectWindow("C1-Montage-1");
run("Duplicate...", " ");
run("Out [-]");
run("Out [-]");
run("Out [-]");
setAutoThreshold("Triangle dark");
setOption("BlackBackground", true);
run("Convert to Mask");
run("Dilate");
run("Dilate");
run("Dilate");
run("Create Selection");
roiManager("Add");
selectWindow("C1-Montage-1");
run("32-bit");
roiManager("Select", 0);
run("Make Inverse");
setBackground(0, 0, 0);
run("Clear", "slice");
run("Divide...", "value=0");
run("Select None");
selectWindow("C3-Montage-1");
run("Duplicate...", " ");
run("Out [-]");
run("Out [-]");
run("Out [-]");
run("Gaussian Blur...", "sigma=10");
setAutoThreshold("Otsu dark");
run("Convert to Mask");
run("Fill Holes");
waitForUser("Ready?");
roiManager("Add");
run("Clear Outside");
run("Select None");
run("Dilate");
run("Dilate");
run("Dilate");
run("Dilate");
run("Dilate");
waitForUser("Ready?");
run("Create Selection");
roiManager("Add");

```

```
run("Select None");
run("Dilate");
run("Dilate");
run("Dilate");
run("Dilate");
run("Dilate");
waitForUser("Ready?");
run("Create Selection");
roiManager("Add");
selectWindow("C1-Montage-1");
rename(image1);
roiManager("Select", 1);
waitForUser("Ready?");
run("Measure");
run("Clear", "slice");
run("Divide...", "value=0.000");
roiManager("Select", 2);
waitForUser("Ready?");
run("Measure");
run("Clear", "slice");
run("Divide...", "value=0.000");
roiManager("Select", 3);
waitForUser("Ready?");
run("Measure");
roiManager("Deselect");
roiManager("Delete");
run("Close All");
```

This macro measures the intensity of a MFN2 on the nuclear envelope. Moreover, it can also give you the ratio of the intensity of the protein of interest on the nuclear envelope over the nucleoplasm. It can also save images of the protein of interest on the nuclear envelope and the nucleoplasm in your preferred folder. Fig. 3-4C

```
image1=getTitle();
Dialog.create("What do you want to do?");
Dialog.addCheckbox("Measure MFN2 on the NE", false);
Dialog.addCheckbox("Get ratio for MFN2 on the NE over nuclear MFN2", false);
Dialog.addCheckbox("Create MFN2 image on the NE", false);
Dialog.show();
choice1=Dialog.getCheckbox();
choice2=Dialog.getCheckbox();
choice3=Dialog.getCheckbox();
if (choice1==true) {
    run("Duplicate...", "duplicate channels=3");
run("Make Montage...", "columns=7 rows=5 scale=0.25");
run("Enhance Contrast", "saturated=0.35");
waitForUser("Action Required", "Write down the boxes from montage that you want
to analyze");
Dialog.create("What boxes do you want to keep?");
Dialog.addNumber("First image", 0);
Dialog.addNumber("Last image", 0);
Dialog.show();
number1=Dialog.getNumber();
number2=Dialog.getNumber();
close();
run("Duplicate...", "duplicate range=number1-number2");
run("Make Montage...", "columns=7 rows=5 scale=0.25");
rename("LMNA");
run("Enhance Contrast", "saturated=0.35");
run("Gaussian Blur...", "sigma=2");
setAutoThreshold("Otsu dark");
run("Convert to Mask");
run("Fill Holes");
run("Erode");
run("Create Selection");
roiManager("Add");
roiManager("Select", 0);
roiManager("Rename", "LMNA");
selectWindow(image1);
run("Duplicate...", "duplicate channels=4 slices=number1-number2");
run("Make Montage...", "columns=7 rows=5 scale=0.25");
rename("DAPI");
run("Gaussian Blur...", "sigma=2");
setAutoThreshold("Otsu dark");
run("Convert to Mask");
```

```

run("Fill Holes");
run("Erode");
run("Erode");
run("Erode");
run("Create Selection");
roiManager("Add");
roiManager("Select", 1);
roiManager("Rename", "Nuclei");
selectWindow("LMNA");
roiManager("Select", 1);
setBackground(0, 0, 0);
run("Clear", "slice");
run("Select None");
run("Create Selection");
run("Make Inverse");
roiManager("Add");
roiManager("Select", 2);
roiManager("Rename", "NE");
selectWindow(image1);
run("Duplicate...", "duplicate channels=2 slices=number1-number2");
run("Make Montage...", "columns=7 rows=5 scale=0.25");
run("Enhance Contrast", "saturated=0.35");
rename(image1);
roiManager("Select", 2);
run("Measure");
roiManager("Deselect");
roiManager("Delete");
run("Close All");
print(image1, "First Image - " + number1, "Last Image - " + number2);
}
if (choice2==true) {
    run("Duplicate...", "duplicate channels=3");
run("Make Montage...", "columns=7 rows=5 scale=0.25");
run("Enhance Contrast", "saturated=0.35");
waitForUser("Action Required", "Write down the boxes from montage that you want
to analyze");
Dialog.create("What boxes do you want to keep?");
Dialog.addNumber("First image", 0);
Dialog.addNumber("Last image", 0);
Dialog.show();
number1=Dialog.getNumber();
number2=Dialog.getNumber();
close();
run("Duplicate...", "duplicate range=number1-number2");
run("Make Montage...", "columns=7 rows=5 scale=0.25");
rename("LMNA");

```



```

run("Enhance Contrast", "saturated=0.35");
run("Gaussian Blur...", "sigma=2");
setAutoThreshold("Otsu dark");
run("Convert to Mask");
run("Fill Holes");
run("Erode");
run("Create Selection");
roiManager("Add");
roiManager("Select", 0);
roiManager("Rename", "LMNA");
selectWindow(image1);
run("Duplicate...", "duplicate channels=4 slices=number1-number2");
run("Make Montage...", "columns=7 rows=5 scale=0.25");
rename("DAPI");
run("Gaussian Blur...", "sigma=2");
setAutoThreshold("Otsu dark");
run("Convert to Mask");
run("Fill Holes");
run("Erode");
run("Erode");
run("Erode");
run("Create Selection");
roiManager("Add");
roiManager("Select", 1);
roiManager("Rename", "Nuclei");
selectWindow("LMNA");
roiManager("Select", 1);
setBackground(0, 0, 0);
run("Clear", "slice");
run("Select None");
run("Create Selection");
run("Make Inverse");
roiManager("Add");
roiManager("Select", 2);
roiManager("Rename", "NE");
selectWindow(image1);
run("Duplicate...", "duplicate channels=2 slices=number1-number2");
run("Make Montage...", "columns=7 rows=5 scale=0.25");
run("Enhance Contrast", "saturated=0.35");
rename(image1);
roiManager("Select", 2);
run("Measure");
roiManager("Select", 1);
run("Measure");
roiManager("Deselect");
roiManager("Delete");

```

```

run("Close All");
print(image1, "First Image - " + number1, "Last Image - " + number2);
}
if (choice3==true) {
    run("Duplicate...", "duplicate channels=3");
run("Make Montage...", "columns=7 rows=5 scale=0.25");
run("Enhance Contrast", "saturated=0.35");
waitForUser("Action Required", "Write down the boxes from montage that you want
to analyze");
Dialog.create("What boxes do you want to keep?");
Dialog.addNumber("First image", 0);
Dialog.addNumber("Last image", 0);
Dialog.show();
number1=Dialog.getNumber();
number2=Dialog.getNumber();
close();
run("Duplicate...", "duplicate range=number1-number2");
run("Make Montage...", "columns=3 rows=2 scale=0.25");
rename("LMNA");
run("Enhance Contrast", "saturated=0.35");
run("Gaussian Blur...", "sigma=2");
setAutoThreshold("Otsu dark");
run("Convert to Mask");
run("Fill Holes");
run("Erode");
run("Create Selection");
roiManager("Add");
roiManager("Select", 0);
roiManager("Rename", "LMNA");
selectWindow(image1);
run("Duplicate...", "duplicate channels=4 slices=number1-number2");
run("Make Montage...", "columns=3 rows=2 scale=0.25");
rename("DAPI");
run("Gaussian Blur...", "sigma=2");
setAutoThreshold("Otsu dark");
run("Convert to Mask");
run("Fill Holes");
run("Erode");
run("Erode");
run("Erode");
run("Create Selection");
roiManager("Add");
roiManager("Select", 1);
roiManager("Rename", "Nuclei");
selectWindow("LMNA");
roiManager("Select", 1);

```

```
setBackgroundColor(0, 0, 0);
run("Clear", "slice");
run("Select None");
run("Create Selection");
run("Make Inverse");
roiManager("Add");
roiManager("Select", 2);
roiManager("Rename", "NE");
selectWindow(image1);
run("Duplicate...", "duplicate channels=2 slices=number1-number2");
run("Make Montage...", "columns=3 rows=2 scale=0.25");
run("Enhance Contrast", "saturated=0.35");
roiManager("Select", 2);
run("Clear Outside");
roiManager("Deselect");
roiManager("Delete");
dir=getDirectory("Choose Destination Directory");
saveAs("Tiff", dir+image1);
run("Close All");
}
```